Aus dem Institut für Chirurgische Forschung

Im Walter Brendel Zentrum für Experimentelle Medizin

Direktor: Prof. Dr. U. Pohl

Molecularly targeted therapy on a new preclinical mouse model for gastric neuroendocrine tumors

Dissertation

zum Erwerb des Doktorgrades der Humanbiologie

an der Medizinischen Fakultät der

Ludwig-Maximilians-Universität zu München

vorgelegt von

Jie Pan

Aus Zhejiang, China

2013

Mit Genehmigung der medizinischen Fakultät

der Universität München

Berichterstatterin:	Prof. Dr. med. Georg Enders
Mitberichterstatter:	Prof. Dr. Andreas Jung
	Priv. Doz. Dr. Lars Lindner
	Prof. Dr. Max Schnurr
Dekan:	Prof. Dr. med. Dr. h.c. Maximilian Reiser FACR, FRCR
Tag der mündlichen Prüfung:	18.07.2013

Amicus Plato

Amicus Aristotle

sed Magis Amicus VERITAS

Declaration

I hereby declare that the thesis is my original work and I have not received outside assistance. All the work and results presented in the thesis were performed independently. Anything from the literature was cited and listed in the reference. Part of the results have been published in the paper Ihler F, Vetter EV, Pan J, Kammerer R, Debey-Pascher S, Schultze JL, Zimmermann W, Enders G. Expression of neuroendocrine gene signature in gastric tumor cells from CEA424-SV40 large T antigen-transgenic mice depends on SV40 large T antigen. PLoS One. 2012; 7(1):e29846. No unauthorized data was included.

All the data presented in the thesis will not be used in any other thesis for scientific degree application.

The work for the thesis began from Oct. 2010 with the supervision from Prof. Dr. med. Enders G in Walter Brendel Centre of Experimental Medicine, Ludwig-Maximilians University Munich, Germany.

Munich, on 20.07.2013

(Jie Pan)

CONTENTS

1 ABSTRACT

Neuroendocrine tumors are a heterogeneous group of malignancies with an increasing prevalence. Since there is not much progress in therapy, model systems are urgently needed. We have a CEA424-SV40 TAg transgenic mouse model which develops spontaneous tumors in the antral region of the stomach. In addition, several cell lines derived from the tumor were established. Gene expression analysis of the tumor tissue as well as cell lines revealed neuroendocrine markers. Therefore we further characterized this model with special emphasis on the cells of origin and used it for testing new targeted treatment protocols.

To analyze CEA424-SV40 TAg mouse model in more detail, tumor tissue as well as the cell lines derived from the primary tumor were investigated by immunohistochemistry, immunofluorescence, western blot, and ELISA. Antibodies used were directed at SV40 TAg, Ki-67, chromogranin A, chromogranin B, secretin, H^+-K^+-ATPase, glucagon, and transcription factors NeuroD1 and Nkx2.2. Plasma hormone levels of serotonin and secretin were measured by ELISA. Immunostainings of SV40 TAg and Ki-67 revealed highly proliferative tumors cells. The tumors stained intensively for the neuroendocrine markers chromogranin A, chromogranin B, secretin and glucagon. The tumor tissue as well as the cell lines expressed transcription factors NeuroD and Nkx2.2, which are involved in the differentiation of the neuroendocrine lineage. Hormone levels of serotonin and secretin in the plasma of the transgenic mice were dramatically elevated when compared with normal littermates, thus supporting the neuroendocrine phenotype.

As the neuroendocrine phenotype of CEA424-SV40 TAg transgenic mouse was confirmed, molecularly targeted therapies were tested in this model system both in vitro and in vivo. Cell lines were tested for drug sensitivity with mTOR inhibitors (RAD001, NVP-BEZ235), paclitaxel, E2F inhibitor, HSP90 inhibitor, and p53 stabilizer Nutlin-3a. All the drugs tested in vitro could efficiently inhibit cell proliferation in a dose dependent manner. From these drugs the mTOR inhibitor

RAD001 was chosen for the in vivo experiment. Daily feeding of 10 mg/kg RAD001 inhibited the tumor development and prolonged the survival time of the CEA424-SV40 TAg transgenic mice dramatically. The effects of the RAD001 treatment on tumor cells were achieved mainly through inactivating mTOR-p70S6K and mTOR-4EBP1 signaling as proven by western blot and immunohistochemistry. Still, some cells must develop escape mechanisms, since the tumor tend to grow.

To gain a better understanding of the T antigen transforming mechanisms as well as the possible escape mechanisms, some efforts were made on the tumor originating cells in the CEA424-SV40 Tag transgenic mouse model. Possible candidates for these tumor originating cells in the stomach are the newly described epithelial as well as mesenchymal stem cells. In a first attempt, the expression feature of epithelial and mesenchymal stem cell markers were analyzed. Established cell lines as well as tumor tissue from the tumor bearing mice were investigated by reverse transcription PCR (RT-PCR), immunohistochemistry, immunofluorescence, western blot, and microarray analysis. From several markers analyzed, the tumor cell lines showed a high expression level of the potential epithelial stem cell marker Bmi1 in RT-PCR and cDNA expression array. This could be further substantiated by western-blotting and immunostaining. Consequently, Bmi1 message could also be found in the growing tumors both in mRNA and protein levels. Experiments using siRNA to knock down the SV40-TAg expression showed that the Bmi1 expression went down in the cell lines thus showing the interrelationship. On the other hand, the mesenchymal stem cell marker Etv1 was also found to be expressed in the tumor tissue and cell lines derived from the tumor. More interestingly, Etv1 expression level was up-regulated over the time course of the tumor development. From these, an Etv1 positive mesenchymal cell could be a possible candidate for transformation. Since the CEA-promoter used for the generation of the T-antigen transgenic animals contains Etv1 binding sites, it is tempting to speculate, that this may drive the transcription of the T antigen.

In conclusion, our data provide convincing evidence that CEA424-SV40 TAg mice

are a clinically relevant model for neuroendocrine tumor. Testing of molecularly targeted therapies both in vitro and in vivo offered promising candidates for further clinical evaluation. Thus, this new model system could be of great value not only for studies on the mechanisms of how SV40 TAg induces neuroendocrine tumors but also for exploring novel targeted therapy in a preclinical setting.

2 ZUSAMMENFASSUNG

Neuroendokrine Tumore stellen heterogene Tumore mit ansteigender Prävalenz dar. Da es nur geringe Verbesserungen in der Therapie gibt, besteht ein Bedarf an neuen Modellsystemen.

In unserer Arbeitsgruppe wurde das CEA424-SV40-T-Antigen transgene Mausmodell entwickelt, in welchem sich spontan Tumore im Bereich des Magenantrums bilden. Gleichzeitig wurden Zelllinien aus diesem Tumor etabliert. Die Analyse der Genexpression im Tumor und in den Zelllinien ergaben Hinweise auf einen neuroendokrinen Tumortyp. Deshalb wurde der Phänotyp des Tumors auch mit Blick auf den Ursprung der Tumore analysiert und für die Testung von Therapieoptionen eingesetzt.

Die Analyse der CEA-424-SV40-TAg-Mäuse sowie der Tumorlinien wurden mittels Immunhistochemie, Immunfluoreszenz, Westernblot und ELISA untersucht. Dazu wurden Antikörper gegen das SV40-T-Antigen, den Proliferationsmarker Ki-67, Chromogranin A, Chromogranin B, Sekretin, die H-K-ATPase, Glukagon und die Transkriptionsfaktoren NeuroD und Nkx2.2 eingesetzt. Die Plasma Hormonkonzentrationen von Serotonin und Sekretin wurden mittels ELISA bestimmt. Die Färbung für das SV40-T-Antigen und Ki-67 zeigte einen hoch proliferierenden Tumor. Dieser war hoch positiv für die neuroendokrinen Marker Chromogranin A, Chromogranin B, Sekretin und Glukagon. Sowohl der Tumor als auch die Tumorzelllinien exprimierten die Transkriptionsfaktoren NeuroD und Nkx2.2, welche an der Differenzierung von neuroendokrinen Zellen beteiligt sind. Die Hormonkonzentrationen von Serotonin und Sekretin waren im Plasma der transgenen Mäuse deutlich erhöht. Dies ergab das Gesamtbild eines neuroendokrinen Karzinoms.

In diesem Modell wurden nun verschiedene molekular begründete Therapien in vitro und in vivo getestet. So wurde an den Zelllinien die Empfindlichkeit von mTOR Inhibitoren (RAD001, NVP-BEZ235), Paclitaxel, E2F -Inhibitor, Hsp90-Inhibitor und

dem p53 Inhibitor Nutlin3 getestet. Alle verwendeten Substanzen konnten die Proliferation der Tumorzellen dosisabhängig hemmen. Von diesen wurde dann der mTOR Inhibitor RAD001 für die in vivo Anwendung ausgewählt.

RAD001 konnte dabei die Entwicklung der Tumore signifikant hemmen und verlängerte das Überleben der Tiere dramatisch. Der Effekt der mTOR Inhibition bestand dabei vor allem in der Hemmung des mTOR-p70S6K und mTOR-4EBP1 Pathways, was im Westernblot und der Immunhistochemie gezeigt werden konnte. Trotzdem muss festgehalten werden, dass einige Tumorzellen der Therapie entkommen konnten.

Um nun Informationen über den Transformations- und den Escape-Mechanismus zu bekommen, wurde versucht die Tumorursprungszelle zu beschreiben. Mögliche Kandidaten dafür sind sowohl die jüngst beschriebenen intestinalen Epithelstammzellen als auch mesenchymale Stammzellen. Dazu wurden Marker-Gene an den etablierten Zelllinien und den Tumoren mit Hilfe von RT-PCR, Immunhistochemie, Immunfluoreszenz, Westernblot und Microarray untersucht. Dabei fand sich in den Tumorzellen eine hohe Expression des möglichen epithelialen Stammzellmarkers Bmi1. Dies konnte auch im Westernblot und in der Immunfärbung bestätigt werden. Folgerichtig fand sich dieser Marker auch in den wachsenden Tumoren. Experimente, in denen mit siRNA die Expression des SV40-T- Antigen blockiert wurde, ergaben eine Reduktion der Bmi1-Expression und weisen damit auf einen engen Zusammenhang hin. Gleichzeitig fand sich allerdings auch eine hohe Expression des mesenchymalen Stammzell-Markergenes Etv1 im Tumor und in den etablierten Zelllinien. Etv1 stieg dabei im Verlauf der Tumorentwicklung im Gewebe deutlich an. Deshalb könnte es sich bei der ursprünglich transformierten Zelle auch um eine mesenchymale Stammzelle handeln. Da der CEA Promotor, der die Expression des SV40-T-Antigens in den transgenen Mäusen regulieren soll, einige Bindungsstellen für den Transkriptionsfaktor Etv1 hat, liegt die Möglichkeit der Induktion des T-Antigens über Etv1 nahe. Dazu stehen aber noch weitere Experimente aus.

Zusammenfassend zeigen die hier präsentierten Daten, dass es sich bei dem CEA424-SV40 Tag-Mausmodell um ein klinisch relevantes Modell für einen neuroendokrinen Tumor handelt. Zusammen mit den etablierten Tumorzelllinien können daran neue Therapieansätze getestet werden. Damit bietet es die Möglichkeit sowohl den Zusammenhang zwischen dem T-Antigen und der Entwicklung des neuroendokrinen Phänotyps als auch neue Therapieformen zu untersuchen.

3 INTRODUCTION

3.1 Preclinical mouse model systems for the translational research of human cancer

3.1.1 General

As George D. Snell said, “Of all the laboratory mammals, probably none has contributed more to the advancement of knowledge than the common mouse.”[1] For the whole century, laboratory mice played a central role in the study of cancer biology and novel drug screening. Their use has been expanded over the past three decades since the first genetic model of cancer, termed “oncomice”, was developed in 1980s[2]. These mouse models not only offer unique opportunities to investigate the molecular mechanisms of cancer development and progression in genetically modified and environmentally controlled mammalian systems, but also provide platforms for testing therapeutic approaches in conditions that may more precisely mimic the real in vivo environment, including various tumor microenvironments which have attracted more and more interests of scientists recently.

3.1.2 The use of cultured tumor cell lines and xenograft mouse models for cancer research

Before the development of genetically engineered cancer-prone mice, preclinical cancer research was relied to a large extent upon the use of cultured tumor cell lines and xenograft mouse models. Cell based tests are designed to determine if the drugs can induce anti-tumor effects like apoptosis or cytostasis, and whether these desired responses can be achieved at a reasonably low concentration. Although these cell lines do help a lot in selecting promising agents from millions of candidate compounds, their ability to mimic tumor cells in a native in vivo environment is challenged. These cell lines are usually from particularly aggressive tumors and have been selected for

optimal proliferation under in vitro culture conditions. They may also acquire additional mutations during the long term cultivation[3]. As pure populations, they can not provide further information about the impact from supporting cells inside and around the tumors and the stress from ongoing immune surveillance[4]. It is also impossible to evaluate the interactions between the drugs and the host in a culture flask. That is why in vivo animal model systems are essential for novel drug screening.

Currently, xenograft mouse models are still the most commonly used animal models for human cancer research[5]. In this case, tumor cell lines or small tumor masses are injected or transplanted into immunodeficient mice[5]. Although these models conserve some molecular pathways and can provide valuable information missed in cell/tissue culture systems, their predictive abilities are still being debated. Essentially, xenograft mouse model based experiments still focus on cell lines. These propagated cells may behave quite differently from the original malignant cells. Even carefully designed xenograft models may still fail to fully represent the behavior of an in situ developed tumor in its native in vivo environment[5]. The complex interaction between the host and the tumor are interrupted and the prognostic usefulness of these testing systems for human clinical trials has been limited[5, 6]. According to a broad study of in vitro and xenografts models from the National Cancer Institute, the predictive ability of these testing systems for drug responses in phase II clinical trials is not as optimistic[5, 7]. Still, these highly imperfect tumor cell lines and xenograft models are valuable testing systems available and are unlikely to be completely replaced by the improved animal models of human cancer in the near future.

3.1.3 The contribution of genetically engineered mouse models for human cancer research

With the improved tools for genomic analysis, especially the gene expression array technologies, and the increasingly refined methods of genetic manipulation, a dramatic progress of genetically engineered mouse models in recent years provided

key insights into the complexity of human cancers. Despite more expensive and time-consuming, the use of genetically engineered mouse models can overcome many shortcomings of cell based and xenografts models. These mouse models develop in situ tumors in an intact host immune system as well as in the context of the tumor microenvironment, which can better mimic the oncogenesis of human cancer and may provide more valuable information regarding safety and efficacy of novel drugs for clinical evaluation.

The main principles for genetic modeling of human malignancy include the expression of oncogenes like the SV40 T antigen, the knock-in of genetic point mutations, or the knock-out of tumor suppressor genes like Trp53[8]. Nowadays, as a consequence of advanced gene targeting technology, the conditional induced alterations of the genome in tissue specific compartments have become more common[9]. It is hoped that these genetically engineered mouse models can be powerful translational tools for human cancer research.

3.2 Established CEA424-SV40 T antigen transgenic mouse model

3.2.1 SV40 T Ag induced transformation

Simian virus 40 (SV40) is a DNA polyomavirus. Under certain conditions, it has the potential to be oncogenic in animals and capable of inducing transformation of various cell lines in vitro[10, 11]. SV40 is also found to be associated with several human tumors, like lymphoma, osteosarcomas, ependymomas, choroid plexus tumors, and mesotheliomas[12-16]. Two proteins, the large T antigen (T Ag) and the small t antigen (t Ag) are encoded by SV40 for its transforming ability. The large T antigen (T Ag) contains 708 amino acids, and is a product of an early gene transcribed during SV40 infection[10]. The T Ag, which is involved in multiple activities for the replication of the virus and the regulation of the host cellular processes[17], is necessary and in most

cases sufficient for tumorigenesis[10, 14-16, 18, 19]. The SV40 T Ag interacts with host cellular proteins through several folding domains/regions[10, 18, 20]. The tumor suppressor protein p53, which is found to be mutated or deleted in most of human cancers, can be inactivated by the C-terminus of T Ag[10, 21-24]. On the other hand, the N-terminus of TAg, where the LXCXE motif and the J domain reside, is involved in the inactivation of Rb family members[10, 25, 26]. The E2F, which takes an important role in cell-cycle progression and oncogenesis, is then set free from Rb and this subsequently leads to the progression of cells into the S phase[27-29]. It has also been reported that T Ag binds to some other cellular factors like p300 and CBP, which may contribute to its powerful oncoprotein function[20].

3.2.2 CEA424-SV40 T antigen transgenic mice

Since SV40 T antigen gene is such a potent oncogene, it has widely been used to generate tumors in transgenic mice. Certain tissue-specific gene promoters are often used to regulate the expression of SV40 T antigen gene so as to generate tumors in targeted organs.

About 10 years ago, Thompson et al successfully established a transgenic C57BL/6 mouse model based on the SV40 T Ag transgene controlled by a small 424 bp promoter of the human carcinoembryonic antigen (CEA) gene[30]. One transgenic line (L5496), which was later named as CEA424-SV40 T antigen transgenic mouse, spontaneously developed gastric tumors in the pyloric region in 100% of the offspring. Tumors can already be observed in the stomach of 37 days old CEA424-SV40 T antigen transgenic mice as small multi-focal tumor areas. Around day-90, these mice start to lose weight and gradually become moribund before finally die probably of undernourishment due to pyloric stenosis by the tumor mass. Several cell lines were also established from the primary tumors of these transgenic mice, like 424GC, mGC3, mGC5 and mGC8[31]. This model system has been used for testing anti-tumor strategy since then[32-35].

3.2.3 Preliminarily detected neuroendocrine signature in CEA424-SV40 T antigen transgenic mouse

When the CEA424-SV40 T antigen transgenic mouse model was established, the tumors developed in the stomach were tentatively identified as adenocarcinomas for several reasons. First, CEA has been used as a marker for adenocarcinomas in many organs, including almost all colorectal adenocarcinomas, as well as lung, breast and pancreatic carcinomas[36]. Second, the cell lines derived from the tumor express mucin and some cell adhesion molecules like EpCAM and CEACAM1, which indicated a possible epithelial origin[31].

In an attempt to further characterize these tumors, RNA from the antral region of 30, 60 and 90 days old CEA424-SV40 TAg transgenic mice and normal littermates was used for genome-wide expression analysis[37]. Interestingly and surprisingly, a neuroendocrine gene signature was revealed. The expression levels of 4, 27 and 329 probe sets/genes were more than 5 folds up-regulated in 30, 60 and 90 days old tumor-bearing mice, respectively, when compared with normal mice[37]. Among them, the majority of the most strongly up-regulated genes were found to be typical for the neuroendocrine lineage[37]. Knock down of the SV40-T Ag expression by siRNA also led to down-regulation of neuroendocrine gene expression in 424GC cell line (cell line derived from the primary tumor). In addition, transmission electron microscopic analysis of a typical tumor cell in a tumor from a 90 days old CEA424-SV40 TAg mouse revealed numerous electron-dense secretory granules which are characteristic for a neuroendocrine phenotype[37]. All these information indicated that the gastric tumors developed in the CEA424-SV40 TAg mouse may be a neuroendocrine tumor and this model system could be of grate value not only for studies on the mechanisms of how SV40 TAg induces neuroendocrine tumors but also for testing new targeted therapy in a preclinical setting. Nonetheless, additional evidence should be provided to make this conclusion solid and many open questions like where the tumor cells come from and how this neuroendocrine phenotype is obtained are to be answered.

3.3 Neuroendocrine tumor model system for better understanding of disease biology and preclinical testing

3.3.1 General introduction and epidemiology of neuroendocrine tumors

Neuroendocrine tumors (NETs) are a highly heterogeneous group of tumors that can arise from neuroendocrine cells throughout the body[38]. These tumors are characterized by distinct clinical syndromes caused by various secreted peptides and neuroamines[3]. The term "carcinoid" was used to describe these tumors for the first time by Siegfried Oberndofer in 1907. Although these tumors were considered to be benign and indolent at that time, it has now become apparent that tumors of this group also consist of a spectrum of malignancies which can be aggressive and resistant to therapy.

Recent data indicated that the incidence and prevalence of gastroenteropancreatic neuroendocrine tumors (GEP-NETs) has been increasing substantially over the last three decades, with carcinoids arising from gastrointestinal tract making up the majority[38-41]. An analysis of the Surveillance, Epidemiology, and End Results (SEER) database reported that the incidence of NETs in the United States was 5.25 per 100000 in 2004 and the prevalence of individuals with NETs may exceed 100000 in this country (NCCN Guidelines Version 1.2011)[38]. GEP-NETs represent up to 2% of all malignancies and are the second most common gastrointestinal malignancy after colorectal cancer[3, 42]. Among these, gastric carcinoids comprise 23% of all digestive neuroendocrine neoplasms with a yearly age-adjusted incidence of around 0.2 per 100,000 population[43]. The five year survival of the patients with carcinoid tumors arising from stomach is the lowest comparing to small intestine, rectum, and appendix[44]. The tendency of the increasing incidence may partly reflect the improvement in disease awareness and diagnostic techniques including the increased availability of advanced endoscopic and radiologic imaging[3, 38, 42], although the number of the patients with NETs is still believed to be underestimated.

A study in the USA based on over 13000 neuroendocrine tumor patients showed that approximately 20% of these patients were associated with other neoplasms, one third of which belong to the gastrointestinal tract[44, 45]. The complexity and heterogeneity of the disease itself usually results in long terms of misdiagnosis with metastases evident at presentation in 60-80% of the patients[42, 46]. The 5-year overall survival from carcinoids at all sites has not changed since 1973 according to the SEER database (US National Cancer Institute. SEER Database. http://seer.cancer.gov/). A better understanding of the disease biology with emphasis on molecular genetics and disease modeling is therefore urgently needed to improve the clinical management for GEP-NETs.

3.3.2 Shortage of in vitro and animal model systems for neuroendocrine tumors

One major limit for the progress in gastroenteropancreatic neuroendocrine tumors includes limited understanding of the cellular biology of neuroendocrine cells and the molecular mechanisms of tumorigenesis[47]. Thus model systems for studying disease pathogenesis and screening novel treatment approach are needed.

The two most frequently used neuroendocrine tumor cell lines are BON1 and GOT1. BON1 is derived from a human pancreatic carcinoid and GOT1 is from liver metastasis of a midgut carcinoid[3]. There are few well characterized neuroendocrine tumor cell lines from the gastrointestinal system. The use of xenograft models are also hampered by the lack of such cell lines. There are now some genetically engineered murine models available for neuroendocrine tumors in pancrease [48, 49], prostate[50-52] and colon[53], while there are few well described model for NETs in stomach, like Apt4b-SV40 TAg transgenic mouse[54]. The shortage of in vitro and animal model systems in general is one of the considerable impediments for further studies on the molecular biology of this disease as well as preclinical evaluation of new therapeutic approach.

3.4 Emerging molecularly targeted therapy for neuroendocrine tumors

3.4.1 Targeting the PI3K-Akt-mTOR Pathway

mTOR is an atypical intracellular serine/threonine protein kinase which takes a key role in several physiological processes, including protein translation, cell growth, proliferation, survival, metabolism, angiogenesis and autophagy[55-57]. mTOR has drawn much attention recently because of its involvement in human tumorigenesis. Aberrant activation of PI3K-Akt-mTOR pathway has also been reported in a significant proportion of patients with NETs, for example, multiple endocrine neoplasia type 1 (MEN1), neurofibromatosis-1 (NF-1), tuberous sclerosis 2 (TSC2), and von Hippel-Lindau (VHL) disease[58-60]. A decreased expression of tumor suppressors and inhibitors of mTOR like TSC2 and phosphatase tensin homologue (PTEN) is also found in pancreatic NETs[58]. The importance of the PI3K-Akt-mTOR pathway in the tumorigenesis of NETs makes it a promising target for novel anti-tumor management. There have been more than one thousand clinical trails for mTOR inhibitors alone or in combination with other agents. In a phase III study on pancreatic NET (RAD001 In Advanced Neuroendocrine Tumors; RADIANT-3), patients treated with everolimus (10 mg/day orally) achieved significant clinical benefit and improvement of progression free survival (11 months for patients treated with everolimus plus best supportive care compared to 4 months for patients received placebo plus best supportive care). In a Japanese subgroup analysis, Ito et al also reported a significant prolonged progression free survival (PFS) by almost 17 months[61, 62].

3.4.2 Targeting angiogenesis

The role of angiogenesis in tumor development has been well described and inspiring results from clinical trails with antiangiogenic therapies have been reported in a variety of tumor types[63]. NETs are among the most vascularized tumors with high

expression of proangiogenic factors, such as the vascular endothelial growth factor (VEGF) and platelet-derived growth factor (PDGF)[58, 64]. It has been reported that the expression level of VEGF was correlated with progression free survival (PFS) in low-grade neuroendocrine tumors[65], and a high expression of PDGFRA was significantly correlated with shorter patients' survival and could serve as a prognostic marker[66]. There are now many antiangiogenic compounds available, including the VEGF monoclonal antibody bevacizumab and the newer compound, VEGF-trap, which target the circulating VEGF, and the compounds which target the receptor tyrosine kinase domains of VEGFR and PDGFR, such as sunitinib, sorafenib and valatanib[58]. There are also endogenous angiogenesis inhibitors such as thalidomide or endostatin[58, 67]. In a phase II trial for patients with advanced, well-differentiated GI-NETs, treatment with bevacizumab (15 mg/kg every 3 weeks) in combination with octreotide LAR resulted in partial tumor remission in 18% of patients, and stable disease was achieved in 77% of the patients[68]. 18 weeks of monotherapy with bevacizumab achieved 30% higher progression free rates than on the PEG interferon arm[68]. In a multinational, randomized, double-blind, placebo-controlled phase III trial of sunitinib in patients with advanced, well-differentiated pancreatic neuroendocrine tumors, patients treated with sunitinib (37.5 mg per day) achieved better progression-free survival, overall survival, and the objective response rate[69].

3.4.3 Targeting growth factor receptors and other parthways

The expression level of EGFR in NET varies among different tumor types[70-75]. One study showed that the expression of EGFR and activated EGFR (p-EGFR) is more common in gastrointestinal carcinoid tumors compared to pancreatic endocrine tumors, and p-EGFR expression in the primary tumor of pancreatic NET indicated a worse prognosis [73]. A small molecule inhibitor of the EGFR tyrosine kinase, gefitinib, has been tested in a single phase II study which included 39 pancreatic NET and 57 carcinoids. Although tumor remissions were rare (6.5% for pancreatic NET and 2.5% for carcinoids), the treatment achieved minor responses and the progression-free rate

at 6 months were 30% and 60% respectively[58]. Furthermore, as EGFR is one of the upstream activators of Akt/mTOR signaling pathways, EGFR inhibitors may yield synergistic effects and interfere with the drug resistance in the mTOR inhibitor therapy. Several preclinical studies using NET cell lines and animal models have already shown this effect[59, 76] which provided a rationale for clinical trails of erlotinib and everolimus[58].

IGF-1 and its receptor is frequently expressed in NETs including gastric NETs[71, 77, 78]. Despite a compelling preclinical rationale and promising data from a phase I trial with AMG 479 (a human monoclonal antibody to IGFR-1)[79], no partial or complete respons was observed in a phase II study for MK-0646 (another human monoclonal antibody to IGFR-1)[80]. Further investigation for IGF-1R antibodies is needed and the combination of IGF-1R antibodies with mTOR inhibitors is currently under clinical trails[58].

Several other drugs like LX1606 (peripheral tryptophan hydroxylase inhibitor), and atiprimod, which targets STAT3, IL-6 and VEGF signaling pathways, are under investigation in clinical trails and may be promising candidates for the management of NETs[58].

3.5 Tumor initiating cells of neuroendocrine tumors in the gastrointestinal system

Despite these many attempts for a potent therapy as described above, the response rate is not compelling. One explanation might be that putative tumor stem cells escape the treatment.

The origin of the cells from which GEP-NETs arise is not well understood. Looking for the tumor initiating cells is helpful for gaining a better understanding of the molecular mechanisms of tumorigenesis and establishing more targeted therapies. Possible candidates for these tumor originating cells are the newly described epithelial

as well as mesenchymal stem cells.

3.5.1 Epithelial stem cells in the gastrointestinal system

"Stem cell" research has been a highlight since 1960s. These small populations of resident stem cells, which are characteristic for their "self-renewal" and "multi-potency", are responsible for the maintenance and repair of adult tissues[81]. The ability to identify the stem cell populations and a better concept of their biology could accelerate our understanding of their role in tissue homeostasis and various diseases including cancer. Much effort has been invested in searching for reliable stem cell markers for different organs and great progress has been achieved in the gastrointestinal system.

3.5.1.1 Adult epithelial stem cells in the stomach

The first evidence of the existence of multipotent, self-renewing stem cells in the stomach from in vivo lineage tracing study was provided by Bjerknes and Cheng in 2002 [82]. By labelling random epithelial cells in adult hemizygous ROSA26 mice, they were able to show the existence of functional multi-potential stem cells in the adult mouse gastric epithelium. The observation of LACZ-negative clones in a single-cell lineage also indicated the possible presence of long-lived progenitors. McDonald et al also demonstrated the existence of multiple adult stem cells in human gastric units in another separate study[83]. However, the definitive identification of these cells has been hampered by the lack of stem cell markers.

In 2010[84], Nick Barker et al reported that $Lgr5^{+ve}$ cells, which are predominantly restricted to the base of adult pyloric glands, are multi-potent, self-renewing stem cells responsible for the long-term renewal of the gastric epithelium[84]. In their newly described in vitro culture system, these single $Lgr5^{+ve}$ cells could efficiently generate long-lived organoids resembling the mature pyloric epithelium. These results indicated that Lgr5 had an important function in gastric epithelial homeostasis as it did in intestine and might be regarded as a unique marker of adult stem cells in the

distal stomach. However, the location of the Lgr5^{+ve} cells was in contrast to the "isthmus model", which favors that the gastric stem cells may reside between the gland and the pit. This opposing view is largely based on the detection of immature, granule-free cells in this region and that cellular proliferation is most predominant in this location[85-89]. It is difficult to reconcile these two models due to the lack of specific markers for the isthmus population. One possible explanation could be that the immediate progeny of the Lgr5^{+ve} cells rapidly migrate from the base of the crypt to the isthmus and undergo transit amplification before the terminal differentiation[90].

3.5.1.2 Adult epithelial stem cells in the intestine

The adult stem cells have been much better investigated in the intestine than in the stomach. Early genetic labelling studies in 1990s demonstrated that individual adult crypts originated from a single multi-potent stem cell, which is active during early intestinal development[81, 91, 92]. However, even today, there is still an intense debate on the identity of the stem cells in the intestine. The two most popular models are the "+4" model and the stem cell zone model. In 1965, cell tracking experiments from Cairnie et al predicted an epithelial stem cell pool at position 4–5, just above the differentiated Paneth cell compartment[93]. Later, Potten et al reported that cells at positions ranging from +2 to +7, but on average at +4, are radiation-sensitive and DNA label-retaining[94]. Later lineage tracing experiment showed that Bmi1 was specifically expressed in these "+4" cells [95]. These "+4" cells are slower-cycling and crucial for crypt maintenance[95-97]. Molecular markers for this cell pool include Bmi1[95], mTert[97, 98], Hopx[99], Lrig1[100], Sox4[101], sFrp5[102, 103] and Dcamkl-1[104-107]. Another stem cell zone model represents Lgr5-expressing cells, also known as crypt base columnar cells (CBCs) [108], which cycle rapidly and are confined between Paneth cells at the crypt base [109]. Lineage tracing demonstrated that these Lgr5^{hi} cells can generate all cell lineages of the small intestinal epithelium throughout life[109-111]. Single Lgr5^{hi} cells cultured in vitro can also give rise to ever-growing crypt–villus organoids, which possess all characteristics of the epithelial tissue in living mice[112]. Prom1/CD133[113,

[114], Olfm4[115], Sox9[116, 117], Ascl2[118] are also considered as molecular markers for the CBCs and similar data from the lineage tracing based on Prom1/CD133 expression were published[113]. $Lgr5^+$ stem cells were also regarded as the cell-of-origin for intestinal cancer[119]. There is still quite a big debate about which cell pool represents the real stem cell populations. Recently there have been some studies which made efforts to describe the functional distinction and the interrelationship between these two potential "ISCs" cell pools. Tian et al showed that Bmi1-expressing cells can give rise to Lgr5-expressing cells after ablation of Lgr5-expressing cells, indicating a hierarchy of stem cells in the small intestine[96]. However, in 2012, Munoz et al reported that the proposed quiescent/"+4" stem cell markers Bmi1, Tert, Hopx and Lrig1 are robustly expressed in CBC cells[120]. Wong et al also showed in an independent study that Lrig1 is most highly expressed in CBC cells[121]. So the $Lgr5^+$ cells are responsible for the self-renewal of the small intestine, while another population of quiescent $Lgr5^-$ stem cells may exist above the crypt base and serve as an alternative stem cell pool[96, 122]. Since it has been shown that $Lgr5^+$ cells can give rise to chromogranin A positive cells[96, 123], they may be candidates for the tumor originating cells of the neuroendocrine tumor described in the CEA424-SV40 TAg transgenic mouse model.

3.5.2 Mesenchymal stem cells

Beside epithelial stem cells, there are other cell types, mesenchymal stem cells, which could give rise to tumors. Mesenchymal stem cells (MSCs) are a heterogeneous multipotent population of nonhematopoietic progenitor cells that can be isolated from almost all kinds of supportive stromal tissue compartments, like adipose tissue, umbilical cord and bone marrow[124, 125]. They can be distinguished from other cell types by their fibroblast like morphology, plastic adherent ability and potential of differentiating into adipocyte, osteoblast and chondrocyte of mesodermal lineage[125] as well as cells of endodermal[126] and neuroectodermal lineage[125]. The criterias for MSCs definition are still controversial due to the lack of specific markers. However, the

International Society for Cellular Therapy has proposed a phenotype definition for MSCs. As a general consensus, CD73, CD90 and CD105 should be positively expressed in MSCs while the expression of CD11b and CD14 (markers for monocyte and macrophage), CD34 (a marker for haematopoietic progenitor and endothelial cell), CD45 (a marker for leukocyte), CD19 and CD79a (markers for B cell) and HLA-DR should be negative[124, 125].

Recent investigations of the immunoregulatory and regenerative properties of MSCs have highlighted the clinical benefit of including MSCs in the therapeutic management. Meanwhile, more detailed studies with the purpose of identifying MSCs have revealed new molecular markers and led to fresh insight into the role of MSCs in oncogenesis. For example, ETV1, a member of the PEA3 subfamily of ETS transcription factors[127], has been shown to be important for the self-renewal capacity of MSCs[128]. ETV1 is also found to be highly expressed in gastrointestinal stromal tumors (GISTs) and functions as a crucial regulator during the tumorigenesis in cooperation with KIT[129, 130]. These new findings revealed the possible role of MSCs in oncogenesis which may promote the study for tumor initiating issue.

Thus, epithelial as well as mesenchymal stem cells could be the source of tumor originating cells in the tumor mouse model presented here.

4 AIM OF THE WORK

Neuroendocrine tumors are a heterogeneous group of malignancies with an increasing incidence and prevalence over the past decades. Neuroendocrine phenotypes frequently indicate poor prognosis in some tumor types, for example prostate cancer and breast cancer. Since there is no real break through in the management of this kind of tumors, model systems are urgently needed. We have a transgenic mouse model where a minimal CEA promoter drives the expression of the SV40 large T Antigen. One mouse strain developed solid tumors in the antral region of the stomach spontaneously with 100% penetrance [30]. These tumors were tentatively classified as adenocarcinomas when the mouse model was established. Surprisingly, gene expression analysis of the tumor tissue as well as cell lines derived from the tumor revealed neuroendocrine markers[37]. These information directing neuroendocrine signatures prompted us to further characterize this model with special emphasis on the cells of origin and test it for screening of new treatment protocols. Therefore, several questions were put forward:

4.1 Is the gastric tumor developed in CEA424-SV40 T Ag transgenic mouse a neuroendocrine tumor?

To confirm the neuroendocrine phenotype of the CEA424-SV40 T Ag transgenic mouse, further characterization of the gastric tumors developed in these mice as well as the established cell lines derived from the primary tumors should be performed. This analysis includes a more detailed characterization of neuroendocrine marker genes as well as hormone concentration in plasma. In addition, the expression of transcription factors with a role in the differentiation of neuroendocrine lineage should be checked both in the tumor tissue and the cell lines from the tumor. Further more, the proliferation status of the tumor should also be determined which is essential for the grading of the tumor.

4.2 Can the tumor cell lines derived from the CEA424-SV40 T Ag gastric tumors be used for screening novel drugs? Are these selected novel therapies applicable in vivo? How is the efficiency and safety of these treatment?

For testing novel molecularly targeted therapies, it makes sense to use the cell lines first to select promising candidates for in vivo study. Drugs inducing efficient responses will be further tested in vivo to see whether they can hamper the tumorigenic process, improve the survival of the tumor bearing mice and whether they are well tolerated.

For testing novel therapies in a preclinical setting, the following molecular-targets were chosen for the work in this thesis: the molecular markers for NETs like mTOR and HSP90, and the targets related to the tumorigenic pathways activated by T antigen which induced tumor in our transgenic mice, like E2F and p53.

4.3 Are there any candidates for the tumor originating cells of the gastric tumors developed in CEA424-SV40 T Ag transgenic mouse?

SV40 T antigen has long been used to generate tumors under the regulation of tissue specific gene promoters in transgenic mice. However, the intriguing question about where these tumor cells come from still remains unanswered in most of these models. Looking for the origin of the tumor cells is not only crucial for a better understanding of the basic transformation steps induced by the SV40-T antigen, but also on a wider view for understanding the reason why the change to a neuroendocrine phenotype is frequently an indicator of poor prognosis in several tumors. Possible candidates for these tumor originating cells in the stomach are the newly described epithelial as well as mesenchymal stem cells.

5 MATERIALS AND METHODS

5.1 Cell culture

5.1.1 Reagents and buffers

Reagents / Buffer	**Manufacturers**
RPMI 1640 with L-Glutamine 500 ml	Lonza, Köln, Germany
Fetal Bovine Serum gold 500 ml	PAA, Cölbe, Germany
L-Glutamin	Lonza, Köln, Germany
Nonessential amino acids (NEAA)	Lonza, Köln, Germany
Sodium pyruvate	Lonza, Köln, Germany
β-mercaptoethanol	SERVA, Heidelberg, Germany
Trypsin0.05%/EDTA0.02 % in PBS	PAN Biotech GmbH, Germany
Lipofectamine® 2000 Reagent	Life Technologies/Invitrogen, Darmstadt, Germany
Opti-MEM Reduced Serum Medium, GlutaMAX	Life Technologies, Darmstadt, Germany
PBS	Biochrom AG, Berlin, Germany
DMSO (Dimethylsµlphoxide)	Sigma-Aldrich, Taufkirchen, Germany
Trypan Blue (0.4%)	Sigma-Aldrich, Taufkirchen, Germany
Crystal violet	Merck, Darmstadt, Germany
Methanol	Merck, Darmstadt, Germany
Cell proliferation reagent WST-1	Roche, Germany
Annexin V-FITC Kit	Miltenyi Biotec, Germany
siRNA-TAg	Life Technologies/Invitrogen, Darmstadt, Germany
esiRNA-Bmi1	Sigma-Aldrich, Taufkirchen, Germany
Cell culture medium	RPMI 1640 with L-Glutamine 500 ml +

	Fetal Bovine Serum gold 50 ml + Glutamin 15 ml + Nonessential amino acids (NEAA) 5 ml + Sodium pyruvate 5 ml + β-mercaptoethanol 3 ul
Cell frozen stock solution	Cell culture medium 27.5 ml + DMSO 5 ml + Fetal Bovine Serum gold 15 ml

5.1.2 Agents

Agents	**Manufacturers**
RAD001	Novartis Pharma, Basel, Switzland
NVP-BEZ235	Novartis Pharma, Basel, Switzland
Paclitaxel	Apotheke Klinikum Grosshadern, Germany
Nutlin-3a	Cayman Chemical, USA
E2F inhibitor (HLM006474)	Calbiochem, Germany
HSP90 inhibitor (NW457)	Calbiochem, Germany

5.1.3 Cell lines

Three cell lines, 424GC, mGC3, mGC8, originally established by Robert Kammerer, were kindly provided by Prof. Zimmermann. These cell lines were derived from spontaneously developing tumors of three different, 13 weeks old CEA424 SV40 TAg transgenic mice (C57BL/6-Tg(CEACAM5-TAg)L5496Wzm), which have been described previously[30, 31].

5.1.4 Methods

5.1.4.1 Cultivation of cells

Cell lines were cultured in 75-cm^2 or 175-cm^2 flasks in an incubator at 37 ℃ with 5% CO_2. The humidity of the incubator was 98%. Culture medium was changed every 2-3 days. Upon reaching 70-80% confluence, the cells were washed with sterile PBS for 2 times and detached by typsin-EDTA solution. The cells were then resuspended with fresh medium and an appropriate number of cells were seeded into a new flask.

5.1.4.2 Determination of cell number

Cell suspension was mixed with an equal volume of 0.4% Trypan Blue to identify dead cells. The number of viable (unstained) cells was then counted in a hemacytometer (Neubauer advanced).

5.1.4.3 Storage and recultivation of the cells

5.1.4.3.1 Cell freezing

Cell culture medium was removed from the cells. The cells were washed with PBS for 2 times before trypsin/EDTA was added. The cells were resuspended with fresh medium and the cell number was determined. The cell suspension was centrifuged at 300g for 5min and the supernatant was removed. The cell pellet was resuspended in freezing medium (10% DMSO, 35% FCS, 55% culture medium) at a concentration of 1-6 million/ml. This suspension was aliquoted into cryo-vials (1 ml/vial). The vials were kept in a -80 ℃ freezer for at least 24 hours before being moved to a liquid nitrogen tank for long-time storage.

5.1.4.3.2 Cell recultivation

Cells in the cryo-vials were shortly warmed in the 37 ℃ water bath for 1-2 minutes and then immediately transfered into to flasks filled with fresh medium prewarmed to

37 ℃ . The medium was changed the next day to avoid toxic effect of the remaining DMSO.

5.1.4.4 Cell proliferation assay

Cells were seeded into 96-well plate at an appropriate concentration (424GC: 2×10^4, mGC3: 1.5×10^4, mGC8: 1.5×10^4) in 100 µl culture medium and incubated overnight at 37 ℃ to allow adherance of the cells. Drugs were suspended at twice the test concentrations and added in 100 µl aliquots. The cells were then further incubated at 37 ℃ for 72 h. At the end of the experiment, supernatant was removed and 100 µl fresh medium was added into each well. For the cell proliferation assay, 10 µl WST-1 reagent (Roche, Germany) was added into each well. The plate was incubated at 37 ℃ with 5% CO_2 for 4 h. The amount of formazen dye formed directly correlated with the number of metabolically active cells in the culture. The absorbance of the dye solution was measured with a microplate ELISA reader. The wave length for measuring the absorbance of the formazan product was 460 nm. The reference wavelength was set to 690 nm.

5.1.4.5 Colony formation assay

Cells treated for 24 or 72 h in 12-well plate were washed with PBS twice and detached by typsin-EDTA solution. Then, cells were resuspended with fresh medium and the cell number was determined. For 424GC, cells were seeded into 6-well plate at a concentration of 1000 cells/well, while for mGC3 and mGC8, at 800 cells/well. Cultivation was performed for 3 weeks and medium was changed every 4 days during this time. The clones were then washed carefully with PBS twice, fixed with methanol for 30 minutes and stained with 0.1% crystal violet in distilled water for 30 minutes. Subsequently, the plates were washed with tap water twice before they were photographed. The clone number was counted using Image J (NIH.GOV).

5.1.4.6 Flow cytometry analysis for cell apoptosis

Cells treated with 100 nM RAD001 or 100 nM NVP-BEZ235 for 72 h were analyzed by FACS. Cells incubated with culture medium were used as control. Cells were washed in 1× Binding Buffer and centrifuged at 300g for 10 minutes. The supernatant was completely removed. The cell pellet was resuspended in 100 µl of 1× Binding Buffer and 10 µl of Annexin V-FITC was then added per 10^6 cells. After careful mixing, the cells were incubated in the dark for 15 minutes at room temperature. Thereafter, 5 µl of PI solution (100 µg/ml) was added immediately prior to analysis.

5.1.4.7 siRNA/esiRNA transfection assay

Appropriate number of cells were seeded into 12 well plates one day before transfection. On the next day, cell cultured medium was removed and 800 µl fresh medium was added into each well. siRNA/esiRNA was diluted in 100 µl Opti-MEM I and mixed gently. In a separate vial, 2 µl Lipofectamine® 2000 Reagent was mixed gently with 100 µl Opti-MEM I and incubated at room temperature for 5 minutes. Then the diluted siRNA/esiRNA was combined with the diluted Lipofectamine® 2000 Reagent. The mixture was incubated at room temperature for another 20 minutes. After this incubation, 200 µl siRNA/esiRNA- Lipofectamine® 2000 complexes were added into each well. The plate was gently rocked back and forth for several times to allow even distribution. The cells were then incubated at 37 ℃ in a CO_2 incubator for 48 and 96 hours respectively before being harvested for RNA or protein samples.

5.2 Animal experiments

5.2.1 Reagents and buffers

Reagents / Agents	Manufacturers
Isoflurane	Abbott, Wiesbaden, Germany
RAD001/Placebo	Novartis Pharma, Basel, Switzerland

5.2.2 Animals

50 days old CEA424-SV40 TAg mice were used for the in vivo experiment. The CEA424-SV40 TAg transgenic mice were kept and bred in Walter Brendel Centre of Experimental Medicine. Animals were housed under conventional conditions with free access to food and water. All animal work has been conducted according to relevant national and international guidelines. Animal studies within this work were registered with and accredited by the local regulatory agency (Reg. Oberbayern 55.2-1-54-2532-47-11).

5.2.3 Methods

5.2.3.1 General experimental setting

All mice were randomized into the respective experimental groups.

Experiment A: To study the effect of the treatment, animals receiving RAD001 or placebo were sacrificed when they lost 20% of their peak weight. This was the end point according to the legal restriction by animal right (Reg. Oberbayern 55.2-1-54-2532-47-11).

Experiment B: In this experiment, animals were treated as above. In contrast to experiment A, all animals were sacrificed when the first control mouse started to lose weight.

5.2.3.2 Dosing

Treated group: RAD001 was fed by gavage daily from day1 to day5 every week, with two days intervals until the end of the experiment. The dose used was 10 mg/kg (10 ml/kg).

Control group: Placebo was fed by gavage daily from day1 to day5 every week, with two days intervals until the end of the experiment. The dose used was 10 mg/kg (10 ml/kg).

5.2.3.3 Feeding

5.2.3.3.1 Drug preparation

RAD001 stock solution and placebo was aliquoted and stored at -20 ℃ in dark. Before feeding, one aliquot of RAD001 stock solution was thawed at room temperature and then diluted with distilled water to a final concentration of 1 mg/ml. After careful mixing on a vortex, the drug was given to mice by gavage within 1 hour according to the datasheet provided by Novartis. RAD001 was fed in a final volume of 10 µl diluted solution per gram body weight.

5.2.3.3.2 Oral gavage procedure

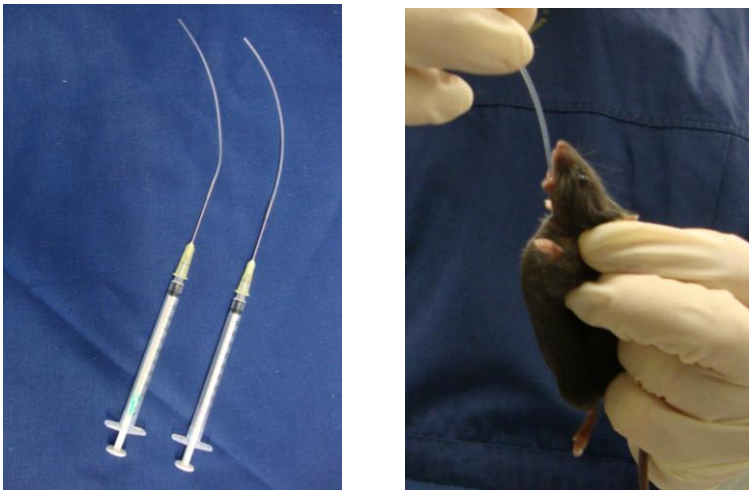

Figure 1. The feeding tubes and the oral gavage procedure

For feeding, a plastic tube was connected with a 0.9×0.4 cm syringe needle which was then fixed onto a 1 ml syringe. The length of the tube was adapted to the distance between the mouth and the last rib of the mouse, which indicated the position of the stomach. The tube was then marked at the incisors of the mouse as the point which should not be past during the procedure to avoid perforating the stomach. Before feeding, mice were lightly anesthetized with isoflurane in a covered beaker for about one minute to avoid violent struggle which might cause trauma to the esophagus. The loose skin of the neck and back of the mouse was grasped so that the mouse could not move its head. The tail was fixed between ring finger and little finger. The head of the mouse was held in vertical alignment with the esophagus. The tube was inserted behind the incisors in either side of the mouth and directed towards the back of the throat before finally went through the esophagus. Appropriate volume of the prepared drug was injected slowly. The color of the mouse's mucosa was monitored during the procedure. The tube was then pulled out gently after dosing. The mouse was put back into the cage and monitored for 5-10 minutes for any sign of labored breathing or distress. This gavage procedure was performed daily from day 1 to day 5 every week.

5.2.3.4 Weight monitoring

Before feeding, the weight of each mice was determined every day.

5.3 RNA isolation and reverse transcription PCR

5.3.1 Reagents and buffers

Reagents / Buffer	**Manufacturers**
NucleoSpin RNA II kit	Macherey-Nagel, Düren, Germany
RNALater	SIGMA, Missouri, USA
Tris(2-carboxyethyl)phosphine hydrochloride (TCEP-HCl)	Thermo scientific, Rockford, USA

50 × TAE Buffer	5 PRIME, Hamburg, Germany
45 µM Oligo (dT)15	Roche, Mannheim, Germany
5 × First Strand Buffer	Life Technologies/Invitrogen, Darmstadt, Germany
10 mM dNTP-Mix	Fermentas, Canada
RNAse Inhibitor	5 PRIME, Hamburg, Germany
M-MLV-RT	Life Technologies/Invitrogen, Darmstadt, Germany
10 × PCR Buffer	PAN Biotech, Germany
50 mM $MgCl_2$	PAN Biotech, Germany
PAN-DNA-Polymerase	PAN Biotech, Germany
6 × MassRuler™ DNA Loading Dye	Fermentas, Canada
MassRuler™ Express DNA Ladder, LR Forward, 28ng/µl	Fermentas, Canada
Agurose	Promega corporation, Madison, USA
GelRed	Bio Trend, Germany

5.3.2 Primers

Primer	Sequences	Annealing temperature
Ahr-f	5’-GCGCAAGCCGGTGCAGAAAACA-3’	62 ℃
Ahr-r	5’-ACCAGCACAAAGCCATTCAGCGCC-3’	
Bmi1-f	5’-AGATGGCCGCTTGGCTCGCATT-3’	56 ℃
Bmi1-r	5’-GCCATTGGCAGCATCAGCTGACG-3’	
Dclk1-f	5’-CCGCTGGGAAGACGTCAGCCTT-3’	62 ℃
Dclk1-r	5’-TTGGTGACTTGCCCGAGCGTGG-3’	
Gapdh-f	5’-TGCCATTTGCAGTGGCAAAGTGG -3’	58 ℃
Gapdh-r	5’-TTGTCATGGATGACCTTGGCCAGG -3’	
Lgr5-f	5’-ATCAGTCAGCTACCCGCCAGTC -3’	60 ℃
Lgr5-r	5’-CAGGCCGCTGAAACAGCTGGGT -3’	

Olfm4-f	5’-AGCAAGCACTGTGGGCAATTTA-3’	52 ℃
Olfm4-r	5’-GGTTGCCTTCCCTCTCTFTFTT-3’	
Prom1-f	5’-GCGGACCCTCTGAATTTGTTCT-3’	52 ℃
Prom1-r	5’-CGGGCTTGTCATAACAGGATTG-3’	
Sox9-f	5’-GCACAACGCGGAGCTCAGCA -3’	60 ℃
Sox9-r	5’-CTGCTCAGTTCACCGATGTCC -3’	
Tert-f	5’-TGCGCTTCATCCCCAAGCCCAA-3’	62 ℃
Tert-r	5’-AGAGCACGCACACACGGCACAA-3’	
Hopx-f	5’-GCCTGCCCACGCTGCAGGTTTT-3’	64 ℃
Hopx-r	5’-CCTCGGCTGCGATGAGGCACAG-3’	

5.3.3 Methods

5.3.3.1 RNA isolation

5.3.3.1.1 Tissue

Tissue from mice was washed three times with ice cold PBS and cut into small pieces. Extra fluid on the tissue was removed with a piece of absorbent paper before the tisssue was immersed into RNALater. The tissue samples in RNALater were kept at 4 ℃ for 24 hours to allow even diffusion of the solution to the tissue and then stored at -20 ℃ for long-term storage. For RNA isolation, one piece of tissue (10 mg to 30 mg) was homogenized in 600 µl Lysis buffer (RA1 in NucleoSpin RNA II kit) + 24 µl TCEP-HCl with an auto cutting machine. The following RNA isolation steps were performed according to the manufacturer’s instructions of the NucleoSpin RNA II kit.

5.3.3.1.2 Cells

Cells in culture were washed with sterile PBS for 2 times and detached by typsin-EDTA solution. The cells were then resuspended with fresh medium and centrifuged at 300 g for 5 min. The supernatant was aspirated and 350 µl Lysis buffer RA1 (NucleoSpin RNA II kit) + 14 µl TCEP-HCl was added to each sample. The

following RNA isolation steps were performed according to the manufacturer's instructions of the NucleoSpin RNA II kit.

5.3.3.2 Measurement of RNA concentration

A 2 µl RNA sample was mixed with 70 µl Tris-HCl buffer (10 mM, pH 8.0). The RNA concentration was determined by measuring the absorption at 260 nm on a Biophotometer (Eppendorf). 1 OD corresponds to an RNA concentration of 40 µg/ml. OD values at 280 nm were used for measuring protein contamination. A ratio for OD260/280 of 1.8-2.0 was used as an indicator of purity. RNA samples were further characterized on an agarose gel.

5.3.3.3 cDNA synthesis

For cDNA synthesis, 2 µg RNA was mixed with ddH_2O to a final volume of 19.5µl. For denaturation, the samples were heated at 75 ℃ for 3 minutes and then transferred onto ice. The synthesis reaction solution was prepared according to the following recipe:

Synthesis:	**1×Mix** (final volume: 30 µl)
45 µM Oligo $(dT)_{15}$	1.0 µl
5×First Strand Buffer	6.0 µl
10 mM dNTP-Mix	1.5 µl
RNAse Inhibitor	1.0 µl
M-MLV-RT	1.0 µl
Denatured RNA	2 µg in 19.5 µl total volume

The reaction was started by an incubation at 37 ℃ for 60 minutes and stopped by heating the samples to 95 ℃ for 10 minutes. The cDNA samples were spun for some seconds and stored at -80 ℃.

5.3.3.4 Reverse transcription polymerase chain reaction (RT-PCR)

The PCR reaction mixture was prepared according to the following recipe:

PCR stock solution	**1 ×Mix**
10 × complete reaction buffer	5 µl
50 mM $MgCl_2$	1.5 µl
Forward primer (10 mM)	1 µl
Reverse primer (10 mM)	1 µl
10 mM dNTP-Mix	0.5 µl
DNA-Polymerase	0.2 µl
ddH_2O	37.8 µl
Template (cDNA)	3 µl (0.2 µg)
	Final volume: 50 µl

The reaction mixture was prepared in PCR soft tubes of 0.5 ml. Subsequently, the amplification of the target sequence was carried out in a Stratagene Robocycler Gradient 40. The amplification was carried out for 23-35 cycles depending on the primers. Each cycle consists of the following individual steps:

1. Denaturation: melting of the deoxyribonucleic acid (DNA) duplexes for 45 seconds at 95 ℃.

2. Primer hybridization: annealing of primers to the DNA single strands for 45 seconds at the appropriate temperature.

3. Elongation: synthesis of the complementary strand at 72 ℃ for 60 seconds.

Before the first cycle, there was an initial 60 seconds denaturation at 95 ℃. At the end, the reaction was kept at 72 ℃ for 10 min to allow completion of the reactions. Then the PCR products were kept at 4 ℃.

5.3.3.5 Agarose gel electrophoresis

The fragments of the PCR products were separated on a 2% agarose gel by electrophoresis. The agarose gel was prepared by dissolving 2 g agarose in 100 ml 1×TAE buffer on a heating plate. 4 µl GelRed was added per 100 ml agarose gel . The comb was kept standing in the agarose-TAE solution until the gel was solid. 10 µl PCR products were mixed with 2 µl 6× MassRuler™ DNA Loading Dye and loaded onto the gel. Electrophoresis was performed at 90 V, 70mA in 1×TAE buffer for 90 min. At the end, the DNA was visualized under UV light and photografts were taken for densitometry.

5.4 Immunohistochemistry and immunofluorescence

5.4.1 Reagents, buffers and antibodies

Reagents / Buffer	**Manufacturers**
Xylene	Applichem, Darmstadt, Gemany
Ethanol 70%, 80%, 96%, 100%	CLN GmbH, Niederhummel, Germany
Paraplast Plus®	Sigma-Aldrich, Taufkirchen, Germany
Image-iT™ FX Signal Enhancer (I36933)	Life Technologies/Invitrogen, Darmstadt, Germany
PBS	Biochrom AG, Berlin, Germany
Natrum Citrate	Merck, Darmstadt, Gemany
Bovine serum albumin (BSA)	Sigma-Aldrich, Taufkirchen, Germany
Hydrogen peroxide 30% (H_2O_2)	Merck, Darmstadt, Gemany
Triton® X-100	Sigma-Aldrich, Taufkirchen, Germany
Alcian Blue	Sigma-Aldrich, Taufkirchen, Germany
Mayer’s hemalum solution	Merck, Darmstadt, Gemany
Hoechst	Sigma-Aldrich, Taufkirchen, Germany

Gelatin	Merck, Darmstadt, Gemany
Liquid DAB+ substrate chromogen system	Dako, CA, USA
AEC chromogen kit	Sigma-Aldrich, Taufkirchen, Germany
Kaiser's glycerol gelatine	Merck, Darmstadt, Gemany
VectaMount Permanent Mounting Medium	Vector, CA, USA
Immunoselect Antifading Mounting Medium	Dianova, Hamburg, Germany
VECTASTAIN Elite ABC Kit (Rat IgG, Mouse IgG, Goat IgG)	Vector, CA, USA
ImmPRESS™ REAGENT. Anti-Rabbit Ig. Peroxidase kit	Vector, CA, USA
Polyclonal rabbit anti-Glucagon antibody (#2760)	Cell signaling, Frankfurt, Germany
Polyclonal rabbit anti-Bmi1 antibody (ab38295)	Abcam, UK
Polyclonal goat anti-Chr-A (C-20) antibody (sc-1488)	Santa Cruz, USA
Polyclonal rabbit anti-Chr-B (H-300) antibody (sc-20135)	Santa Cruz, USA
Polyclonal rabbit anti-Secretin antibody (ab8495）	Abcam, UK
Monoclonol mouse anti-Hydrogen Potassium ATPase Beta antibody (ab2866)	Abcam, UK
Polyclonal rabbit anti-SV40 T Ag (v-300) antibody (sc-20800)	Santa Cruz, USA
Monoclonol rat anti-Ki67 antibody (M7247)	Dako, UK
Polyclonal rabbit anti-ER81 antibody (ab81086)	Abcam, UK
Monoclonol rabbit anti-Bmi1(D42B3) antibody (#5856)	Cell signaling, Frankfurt, Germany
Phospho-S6 Ribosomal Protein (Ser235/236) (D57.2.2E) Rabbit antibody (#4858P)	Cell signaling, Frankfurt, Germany

Phospho-S6 Ribosomal Protein (Ser240/244) (D68F8) Rabbit antibody (#5364P)	Cell signaling, Frankfurt, Germany
Alexa Fluor 488 Goat-anti-rabbit IgG (H+L)	Life Technologies/Invitrogen, Darmstadt, Germany
Alexa Fluor 546 Goat-anti-mouse IgG (H+L)	Life Technologies/Invitrogen, Darmstadt, Germany
Alexa Fluor 546 Goat-anti-rabbit IgG (H+L)	Life Technologies/Invitrogen, Darmstadt, Germany
Alexa Fluor 647 Chicken-anti-goat IgG (H+L)	Life Technologies/Invitrogen, Darmstadt, Germany
Alexa Fluor 488 Donkey-anti-rat IgG (H+L)	Life Technologies/Invitrogen, Darmstadt, Germany

5.4.2 Methods

5.4.2.1 Preparation for tissue samples

The stomachs taken from mice were opened in the minor curvature and washed thoroughly in PBS. The tissue was then transferred to a cork oriented with the mucosa layer facing up. The crimped margin was smoothed carefully with a needle. The tissue was fixed in 4% formaldehyde for 2 hours followed by 1 hours washing in tap running water. Then the tissue was dehydrated and embedded in paraffin wax. The dehydration protocol was listed below:

Reagent	Time
70% Ethanol I	1 hour
70% Ethanol II	1 hour
96% Ethanol I	1 hour
96% Ethanol II	1 hour
96% Ethanol III	1 hour
100% Ethanol I	1 hour
100% Ethanol II	1 hour

100% Ethanol III	1 hour
Xylene I	1.5 hours
Xylene II	1.5 hours
Paraffin I	1.5 hours
Paraffin II	1.5 hours
	Total time: 14 hours

5.4.2.2 Protocol for immunohistochemistry

Sections of 2-3 µm were generated and mounted onto Superfrost® Plus microscope slides. The slides were dried overnight at room temperature and then heated at 50 °C for 2 hours in an oven. Sections were deparaffinized in xylene, and rehydrated in a graded series of ethanol. Antigen retrieval was performed when necessary in boiling sodium citrate buffer (pH 6.0) on a heating plate for 15 min. After cooling down at room temperature for 30 min in the retrieval buffer, the sections were washed with PBS for 5 min/twice. Endogenous peroxidase was blocked by incubation with 3% hydrogen peroxide (H_2O_2) for 10 min or 0.3% H_2O_2 for 30 min. The sections were further treated with blocking solution (according to the host species of the secondary antibody) for 20-60 min before the primary antibody was applied. For rabbit primary antibodies, sections were incubated in primary antibody for 2 h followed by washing steps and incubation in anti-rabbit secondary antibody (ImmPRESS Anti-Rabbit Ig (peroxidase) Polymer Detection Kit, VECTOR) for 1 h at room temperature. For the other primary antibodies, the VECTASTAIN Elite ABC system (VECTASTAIN Elite ABC Kit: Mouse IgG, Rat IgG) was used. The sections were incubated in primary antibody for 0.5-2 h followed by 0.5 h of incubation with the respective biotinylated secondary antibody. The ABC reagent was then applied for signal amplification at room temperature for 0.5 h. Between the incubation steps, the slides were washed with PBS. Freshly prepared peroxidase substrate solution AEC (SIGMA, Germany) or DAB (Dako, Germany) was then added onto the sections until a desired staining intensity was developed. Finally, the slides were counterstained with hematoxylin and

mounted in Kaiser's glycerol gelatine or VectaMount Permanent Mounting Medium.

5.4.2.3 Protocol for immunofluorescence on tissue paraffin sections

Sections were deparaffinized in xylene, and rehydrated in a graded series of ethanol. Antigen retrieval was the same as for immunohistochemistry. Image-iT ™ FX Signal Enhancer (I36933) was then applied to the sections for blocking (room temperature, 30min). After thoroughly washing with PBS, the sections were incubated with a single primary antibody or two mixed primary antibodies at room temperature for 2 h. After washing with PBS, the sections were incubated with the appropriate secondary antibodies for 1 h at RT. Slides were washed, counterstained with Hoechst 33342 and mounted with Immunoselect Antifading Mounting Medium.

5.4.2.4 Protocol for immunofluorescence on cells

For staining cells, gelatin coated coverslips were used. 13mm coverslips were put into 24-well-plate and incubated with 1.5% gelatin for 20 min at 4 ℃. Appropriate number of cells were seeded into the wells and cultured in medium for 24-48 hours. Prior to staining, cells were fixed with 2% formaldehyde for 2 min followed by 4% formaldehyde for 10 min at room temperature. After the wash step with PBS, cells were permeabilized with 0.25% Triton® X-100 diluted in PBS for 10 min. The coverslips were then washed with PBS, and transferred onto slides wrapped with parafilm. Appropriate serum (according to the species that the secondary antibody was raised in) was used for blocking for 30-60 min at room temperature. Cells were then incubated with the primary antibody diluted in 1% BSA (in PBST) in a humidified chamber for 2 h at room temperature. The excess solution was decanted carefully and the cells were washed three times with PBS for 5 min each. Then, cells were incubated with the secondary antibody in the dark for 1 h at room temperature. The wash step was repeated twice before Hoechst 33342 staining and the cells were finally mounted with Immunoselect Antifading Mounting Medium by putting the

coverslips inversely on new slides.

5.5 ELISA

5.5.1 Materials

ELISA Kit	Manufacturers
Secretin ELISA	USCNK, Wuhan, China
Serotonin ELISA	IBL, Hamburg, Germany

5.5.2 ELISA protocol

5.5.2.1 Plasma preparation

Whole blood from 100-day old CEA424-SV40 TAg mice supplemented with EDTA was centrifuged at 1500 g at 4 ℃ for 15 min. The supernatant was aliquoted and stored at -20 ℃.

5.5.2.2 ELISA for serotonin

Serotonin concentrations were measured in EDTA plasma by a competition ELISA (IBL, Hamburg, Germany) according to the manufacture's protocol. Briefly, the plasma samples were first acylated by mixing 50 µl plasma sample with 100 µl assay buffer in a glass test tube. 25 µl of the acylation reagent was then added and the tube was incubated at 37 ℃ in a waterbath for 15 min. Thereafter, 1 ml assay buffer was added into the tube and all the tubes were centrifuged at 1500 g for 10 min. After acylation, 50 µl of each standard, acylated control and acylated plasma samples were pipetted into the respective wells of the microtiter plate. 50 µl of biotinylated serotonin was added into each well, and 50 µl of serotonin antiserum was then added. The plate was covered with adhesive foil and shaked carefully. Finally, the plate was incubated overnight at 4 ℃. On the second day, the plate was washed three times with

250 µl wash buffer and 150 µl freshly prepared enzyme conjugate was added into each well. The plate was incubated 60 min at room temperature on a shaker. After the washing step, 200 µl freshly prepared PNPP (p-nitrophenyl phosphate) substrate solution was added into each well. The plate was incubated for 30 min at room temperature on a shaker before 50 µl PNPP stop solution was added. Finally, the optical density was measured at 405 nm with a microplate ELISA reader.

5.5.2.3 ELISA for secretin

The ELISA for secretin was performed according to the manufacturer's instructions (USCNK, China) given for a direct ELISA. Briefly, 100 µl of standard, blank and samples were added into the appropriate wells and the plate was incubated at 37 ℃ for 2 h. Then the solution was removed and 100 µl of detection reagent A was added into each well. The plate was incubated at 37 ℃ for 1 h. After the washing step, 100 µl of detection reagent B was added into each well. The plate was incubated for another 0.5 h at 37 ℃. 90 µl of substrate solution was added into each well after the washing step, and plate was incubated for 25 min at 37 ℃ in dark. Finally, 50 µl stop solution was added and the absorption was immediately measured at 450 nm on a microplate ELISA reader.

5.6 Western blot

5.6.1 Reagents and buffers

Reagents	**Manufacturers**
Roti-Load1 4x Konz	Roth, Karlsruhe, Germany
Tris Base	Sigma, USA
HEPES	Applicam, Germany
SDS	SERVA, USA

Methanol	Merck, Darmstadt, Germany
6-aminocaproic acid	Sigma-Aldrich, Taufkirchen, Germany
Tween20	Sigma-Aldrich, Taufkirchen, Germany
Non-fat dry milk	Bio-Rad, München, Germany
Bovine serum albumin (BSA)	Sigma-Aldrich, Taufkirchen, Germany
Supersignal West Femto Maximum Sensitivity Substrate	Thermo Scientific, USA
PageRuler prestained protein ladder	Thermo Scientific, USA
Bio-Rad protein assay dye reagent	Bio-Rad, München, Germany
PhosphoSafe Extraction Reagent	Novagen, Germany
Complete, Mini (protease inhibitor)	Roche, Germany
Monoclonol rabbit anti-Bmi1(D42B3) antibody (#5856)	Cell signaling, Frankfurt, Germany
Polyclonal rabbit anti-actin antibody (sc-1616-R)	Santa Cruz, USA
Monoclonol rabbit anti-NeuroD (D35G2) antibody (#54373)	Cell signaling, Frankfurt, Germany
Polyclonal rabbit anti-NKX2-2 antibody	Aviva Systems Biology, USA
Polyclonal rabbit anti-phospho-Akt(Thr308) antibody (#9275)	Cell signaling, Frankfurt, Germany
Polyclonal rabbit anti-Akt antibody (#9272)	Cell signaling, Frankfurt, Germany
Phospho-p70S6 Kinase (Thr389) (108D2) Rabbit mAb (#9234P)	Cell signaling, Frankfurt, Germany
p70S6 Kinase (49D7) Rabbit mAb (#2708P)	Cell signaling, Frankfurt, Germany
4EBP1 (#9644P)	Cell signaling, Frankfurt, Germany
Phospho-4EBP1(#2855P)	Cell signaling, Frankfurt, Germany
Anti-rabbit IgG, HRP-linked Antibody (#7074)	Cell signaling, Frankfurt, Germany

Buffers	**Manufacturers**	
10× Tris-HEPES-SDS Running buffer	Tris Base	121 g
	HEPES	238 g
	SDS	10 g
	Add H_2O to	1000 ml
Anode Buffer I 300mM Tris, pH 10.4	Tris base	18.15 g
	Methanol	100 ml
	Add water to	500 ml
Anode Buffer II 25mM Tris, pH 10.4	Tris base	1.52 g
	Methanol	100 ml
	Add water to	500 ml
Cathode Buffer 25mM Tris, pH 7.6	6-aminocaproic acid	2.6 g
	Methanol	100 ml
	Add water to	500 ml
PBST	0.1% Tween20 in PBS	
Blocking buffer	5% non-fat milk in PBST	
Primary antibody diluent	5% BSA in PBST	
Secondary antibody diluent	5% non-fat milk in PBST	

5.6.2 Methods

5.6.2.1 Cell lysate preparation

Cells in 10 cm dish were taken from the incubator. The supernatant was discarded and the cells were washed with PBS twice. PBS was then carefully and completely removed. Lysis buffer (PhosphoSafe™ Extraction Reagent) was added directly into the well and the plate was incubated at room temperature for 5 min. Cell lysate was scraped off the plate and transfered to a tube before being incubated on ice for another 30 min. The cell lysate was finally centrifuged at 16,000 g at 4 ℃ for 10 min. The supernatant was aliquoted and stored at -80 ℃.

5.6.2.2 Protein concentration measurement

Protein concentrations were measured with the Bio-Rad Protein Assay (Bradford Assay). A serially diluted ovalbumin solution (10 µg/ml) was used as a standard. 5 µl of protein lysate was mixed with 395 µl PBS and 100 µl Bio-Rad reagent in a clean and dry eppendorf tube. Samples were added in duplicate into a 96-well plate at 200µl per well. The plate was incubated at room temperature for 10 min before the absorbance was measured at 595 nm with a microplate reader.

5.6.2.3 Western-blot protocol

5.6.2.3.1 Gel running

The cell lysates were mixed with loading buffer (3 volumes of sample + 1 volume of Roti-load1), boiled at 95 ℃ for 5 min and centrifuged at 16,000 g at 4 ℃ for 5 min. The samples were then applied on to 8-16% polyacrylamide gels. 6 µl marker (Page Ruler) was loaded as molecular weight standard. The running condition was 20 mA for 120-150 min at RT

5.6.2.3.2 Transfer

After separation, proteins were transferred to a nitrocellulose membrane in a semidry transfer chamber (LKB, Sweden). Before transfer, the membrane was briefly washed in distilled water and then immersed in Anode Buffer II for several minutes. The transfer took place in a semidry transfer unit at a constant flow of 55 mA for 120 min at RT.

Transfer structure:

Cover plate (cathode plate)

Nine layers of gel blotting paper from Cathode Buffer

SDS-polyacrylamide gel

nitrocellulose membrane

Three layers of gel blotting paper from Anode Buffer II

Six layers of gel blotting paper from Anode Buffer I

Bottom plate (anode plate)

5.6.2.3.3 Blotting

After transfer, the nitrocellulose membrane was washed in PBST for 5min on a shaker and then transferred to blocking buffer (5% non-fat milk in PBST). The blocking membrane was rocked on a shaker for 1 hour at room temperature. Subsequently, the membrane was incubated with the primary antibodies overnight at 4 ℃ on a rotating platform. The primary antibodies were diluted with 5% bovine serum albumin in PBST.

The membrane was washed in PBST for 5 min × 3 and then incubated in the corresponding horseradish peroxidase (HRP)-conjugated secondary antibodies for 1 hour at room temperature. Finally, the membrane was washed again three times for 5 min with PBST buffer. The detection of the HRP coupled antibodies was carried out with SuperSignal® West Femto Maximum Sensitivity Substrate. 0.5-1 ml working solution was added to each membrane in a plastic wrap. The signal was detected with a Hamamatsu Aequoria system (Hamamatsu Photonics, Herrsching, Germany).

5.7 Statistical analysis

Statistical significance was assessed by comparing median values using the non-parametric Mann-Whitney-U test for independent samples and t-test for random samples (Sigma plot 10.0). *P* values <0.05 were considered significant. For in vivo experiment, the sample size was calculated for stark effects and a $p < 0.05$ value was calculated with Sigma plot 10.0.

6 RESULTS

6.1 Phenotypical characterization of CEA424-SV40 TAg gastric tumors

6.1.1 Tumor development in the antral region of stomach

The expression of SV40 TAg was detected by immunohistochemistry on sections from the stomachs of CEA424-SV40 TAg mice to identify the tumor cells. As shown in Figure 2, tumor cells can already be observed in the pyloric region in 38 days old CEA424-SV40 TAg transgenic mice. At that time, these tumor lesions are small and multifocal, which then gradually grow into extended tumors invading the whole mucosa layer (Figure 2 and 3).

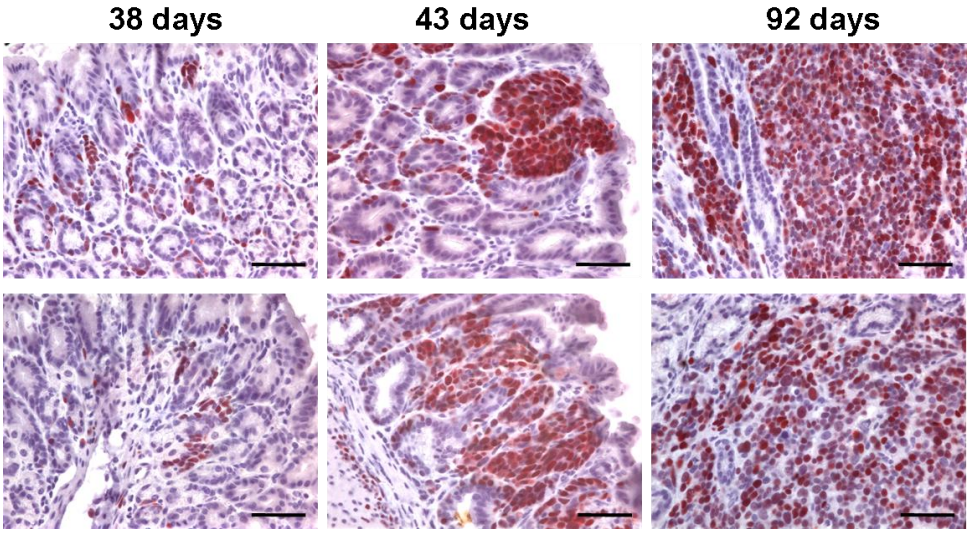

Figure 2. Immunohistochemistry for SV40-TAg in the antral region of the stomach. Tissue sections from day-38, day-43 and day-92 CEA424-SV40 TAg transgenic mice were used for staining. Scale bars: 50 µm.

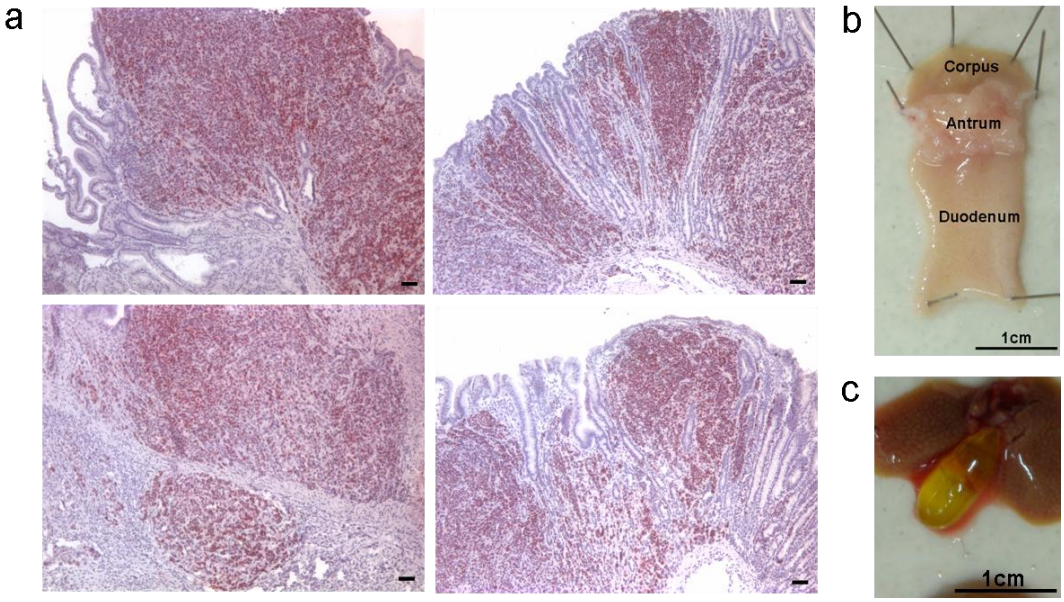

Figure 3. Tumors developed in the antral region of the stomach. a) Anti-SV40 TAg immunohistochemical staining in the stomachs of 90-100 days old CEA424-SV40 TAg transgenic mice. Scale bars: 50 µm. b) Macroscopic picture of the tumor in the antral region of the stomach. c) Enlarged gall bladder.

At an age around 90 days, these CEA424-SV40 TAg mice start to lose weight and become moribund probably because of undernourishment due to pyloric stenosis by the tumor mass. In Figure 4, the weight curves of four CEA424-SV40 TAg mice are shown. The monitoring started on day 50 and ended when the mice lost 20% of their peak weight. At that time, the mice were sacrificed according to the legal restriction. Besides, increased size of the duodenum and cecum, as well as a high frequncy of enlarged gall bladder were also observed in mice over 90 days old (Figure 3).

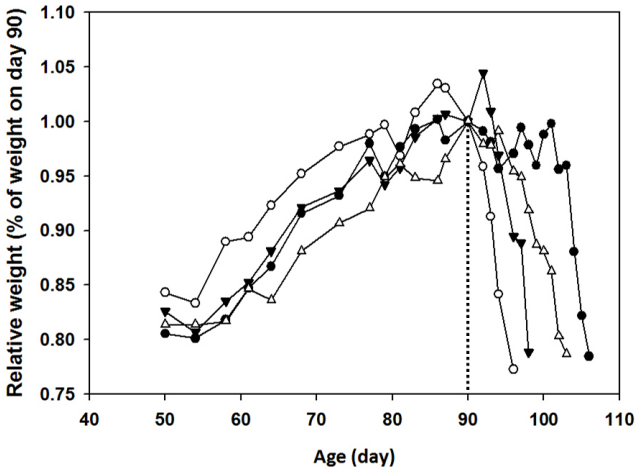

Figure 4. Weight curves of CEA424-SV40 TAg transgenic mice. Weight curves of four individual CEA424-SV40 TAg transgenic mice are shown. Data are given as percentage of the weight on day 90, when most of the animals reached their peak weight.

6.1.2 The proliferative status of CEA424-SV40 TAg gastric tumors

In order to investigate the proliferative status of tumors developing in the stomach of CEA424-SV40 TAg transgenic mouse, double immunofluorescent staining was carried out on stomach sections from 92-95 days old CEA424-SV40 TAg transgenic mice to detect the expression of SV40 TAg together with Ki-67. The Ki-67 protein is present in cells in the active cell cycle and is therefore used as a maker for cellular proliferation. Staining showed a high frequency of Ki-67 positive rate in the tumor area as shown in Figure 5. To further quantify the Ki-67 index of the tumor area, tumor tissue from four CEA424-SV40 TAg transgenic mice was examined for Ki-67 expression by immunohistochemistry (Figure 6). Serial-sections were used for SV40 TAg staining to confirm the tumor area. The Ki-67 index was evaluated in several randomly selected 400× magnification tumor areas for each mouse. The average Ki-67 index (Ki-67 positive nuclei/all nuclei) of the four examined CEA424-SV40 TAg transgenic mice was 59.68±12.27%. This shows a quite impressive proliferation rate, which indicates that the tumors developed in CEA424-SV40 TAg transgenic mice are of high grade proliferation.

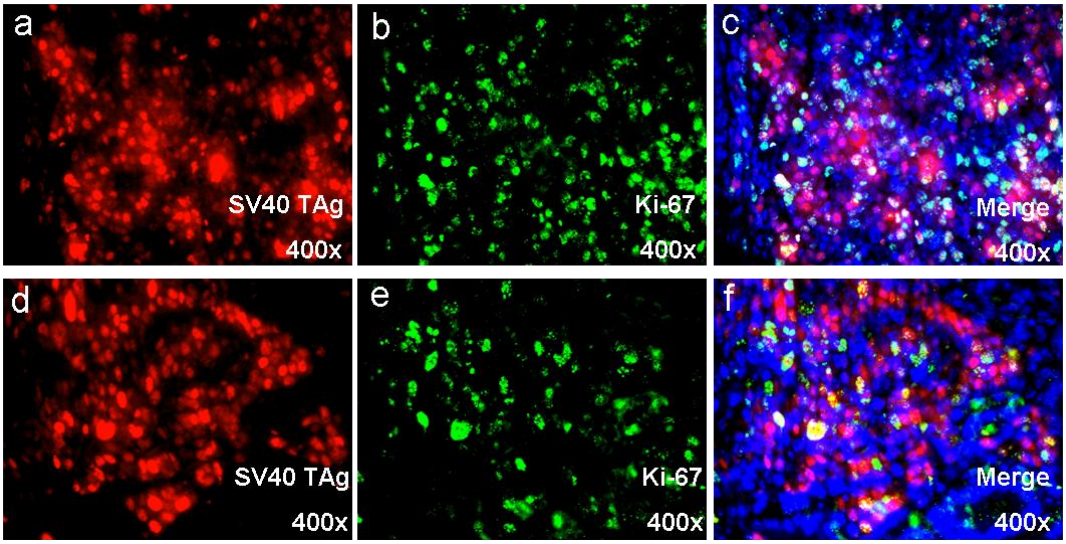

Figure 5. Double staining for SV40 TAg and Ki-67 in the antral region of the stomach. a, d: SV40 TAg: red (Alexa-546); b, e: Ki-67: green (Alexa-488); c, f: Merged images from Alexa-546 + Alexa-488 + Hoechst 33342. Images of 400× magnifications are shown.

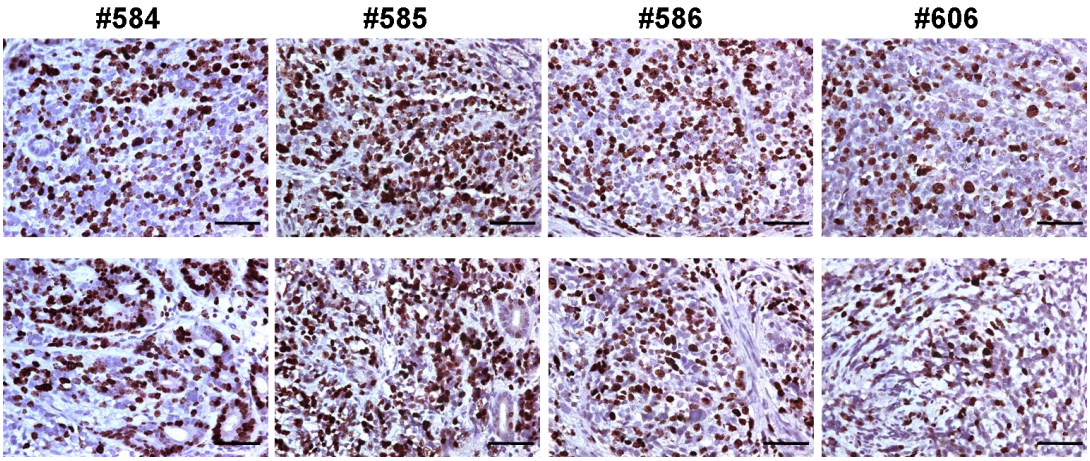

Figure 6. Immunohistochemistry for Ki-67 on stomachs of CEA424-SV40 TAg transgenic mice. The numbers represent individual mice. Scale bars: 50 µm.

6.1.3 Expression analysis of neuroendocrine markers in the CEA424-SV40 TAg gastric tumor

One of the distinct characteristics of neuroendocrine tumors (NETs) is the secretion of various peptides and neuroamines. Molecular markers identified for NETs include the hormones secreted by tumor cells, like serotonin, secretin and glucagon, and the

proteins which have important roles in the biosynthesis or secretion of these hormones, like tryptophan hydroxylase 1 and the chromogranin family.

Previously, transcriptome analysis of RNA from antral tumors of 90 days old CEA424-SV40 TAg transgenic mice was performed. Only probe sets exhibiting a fluorescence of >100 (RFU) were considered as positive in this assay. Genes characteristic for neuroendocrine lineage were found to be highly up-regulated when compared with the normal antral tissue from non-transgenic mice of the same age (Figure 7). Proteins encoded by these genes include tryptophan hydroxylase 1, which is an enzyme involved in the synthesis of the neurotransmitter serotonin, hormones like secretin and glucagon, and proteins from the chromogranin family. Additional transcriptome analysis of RNA from 424GC, one of the cell lines derived from the CEA424-SV40 TAg gastric tumor, was also performed. As shown in Figure 8, the genes mentioned above were also highly expressed. Based on these observations, we asked whether the up-regulation of neuroendocrine gene expression could translate into functional proteins.

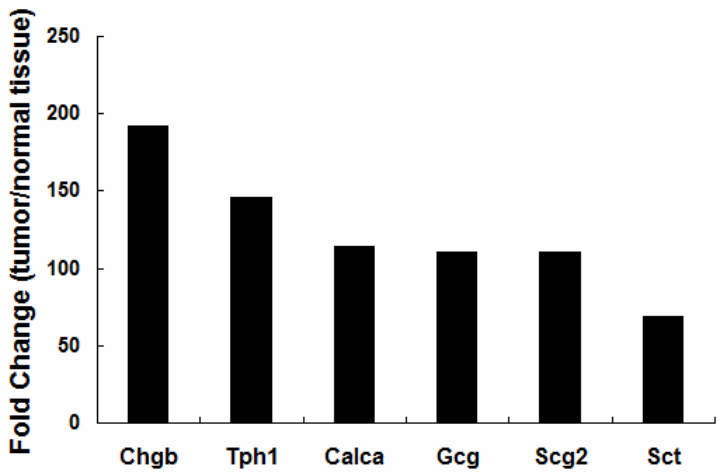

Figure 7. Up-regulation of selected genes in the tumor tissue of 90-day-old CEA424-SV40 TAg mice. A list of highly up-regulated genes characteristic for neuroendocrine lineage is shown. Data are shown as fold change (tumor tissue/ normal antral tissue). Chgb: chromogranin B; Tph1: tryptophan hydroxylase 1; Calca: calcitonin; Gcg: glucagon; Scg2: secretogranin II (chromogranin C); Sct: secretin.

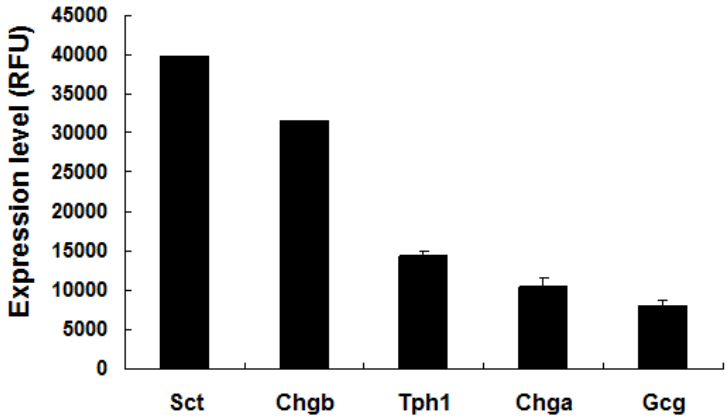

Figure 8. Expression level of selected genes in the cell line 424GC. Sct: secretin; Chgb: chromogranin B; Tph1: tryptophan hydroxylase 1; Chga: chromogranin A; Gcg: glucagon.

6.1.3.1 Immunohistochemistry for chromogranin B in the gastric tumors of 30, 60 and 90 days old CEA424-SV40 TAg transgenic mouse

Chromogranin B, a member of the chromogranin family, is a 33-amino acid neuropeptide derived from Scg-1. The expression of chromogranin B has been documented in various human neuroendocrine tumors from the gastroenteropancreatic system including carcinoid, gastrinoma, glucagonoma and insulinoma[131]. Immunoreactivity for chromogranin B can also be detected in pheochromocytoma, carcinoid of liver and lung, and many types of neuroendocrine tumor from the anterior pituitary[131]. Initially, genome-wide expression analysis was performed with RNA from the antral region of the transgenic mice by microarray. The expression level of chromogranin B was found to be nearly 200 times higher in the tumor tissue than in the tissue from the same region of non-transgenic mice (Figure 7). Thus, we further confirmed the expression of chromogranin B in the tumor area on stomach sections from 30, 60 and 90 days old mice by immunohistochemistry. As shown in Figure 9, intensive cytoplasmic staining could be found in the tumor areas at all three time points. The expression pattern of chromogranin B in the tumor area overlapped with the staining for SV40 TAg, which meant that the tumor cells clearly produced

chromogranin B.

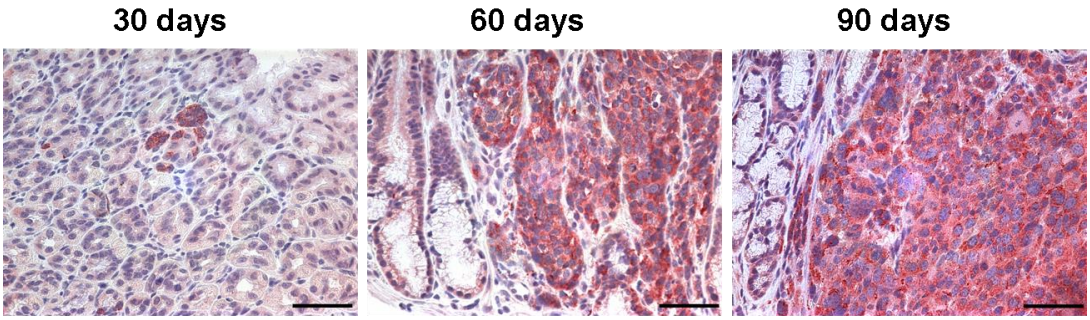

Figure 9. Immunohistochemistry for chromogranin B on stomachs of 30, 60 and 90 days old CEA424-SV40 TAg transgenic mice. Scale bars: 50 µm.

6.1.3.2 Double labeling of chromogranin A and SV40-TAg in the gastric tumors of young CEA424-SV40 TAg transgenic mice

Chromogranin A is another member of the granin family of secretory proteins. Although first being isolated from chromaffin cells of the adrenal medulla, it is now believed to be located in secretory vesicles present throughout the neuroendocrine system and in various neurons[131-133]. Chromogranin A is also considered to be one of the most sensitive markers for biochemical diagnosis and surveillance of gastric neuroendocrine tumors[134] (NCCN guidelines 2011). Thus, the expression of chromogranin A in the tumor area was examined. Double immunofluorescent labeling directed at SV40 TAg and chromogranin A was carried out on stomach sections from young CEA424-SV40 TAg transgenic mice. Co-expression of SV40-T antigen and chromogranin A was observed in some tumor areas. The detection of chromogranin A expression in tumor cells indicated neuroendocrine signature at early time points of the tumor development (Figure 10).

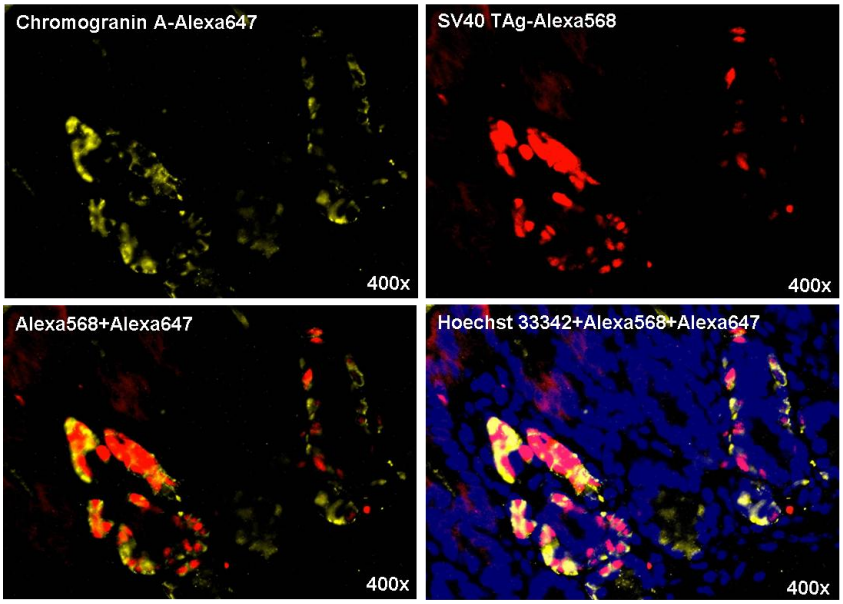

Figure 10. Double staining for SV40 TAg and chromogranin A on stomach of a 38 days old CEA424-SV40 TAg transgenic mouse. Chromogranin A: yellow (Alexa-647); SV40 TAg: red (Alexa-546); DNA: blue (Hoechst 33342). Images of 400× magnifications are shown.

6.1.3.3 Detection of glucagon expression in the gastric tumors of 90 days old CEA424-SV40 TAg transgenic mice

Glucagon is a peptide hormone secreted by A cells in the pancreas which can raise blood glucose levels by promoting gluconeogenesis and glycogenolysis. Abnormally elevated level of glucagon is a predominant clinical sign for glucagonoma which may occur alone or together with multiple endocrine neoplasia type 1. Double staining for SV40 TAg and glucagon was applied to mGC3, a cell line derived from the tumor. As shown in Figure 11, the nuclei of these tumor cells were positively stained by SV40 TAg while glucagon was expressed in the cytoplasm.

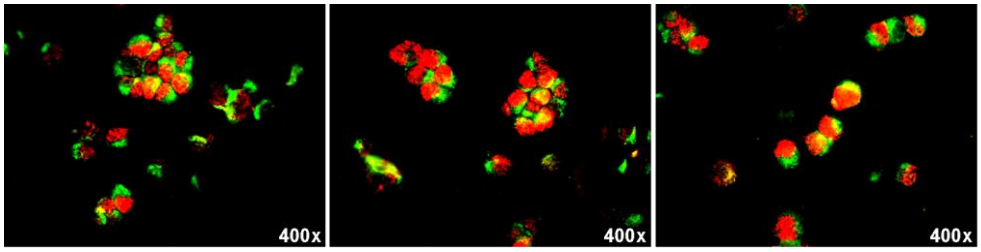

Figure 11. Immunofluorescent staining for SV40 TAg and glucagon in cell line mGC3. SV40 TAg: red (Alexa-546); glucagon: green (Alexa-488). Images of 400× magnifications are shown.

In addition, stomach sections from 90-100 days old CEA424-SV40 TAg transgenic mice (n=7) were used for immunohistochemistry to detect the local distribution of glucagon. As shown in Figure 12, numerous glucagon positive cells were observed in the tumor areas.

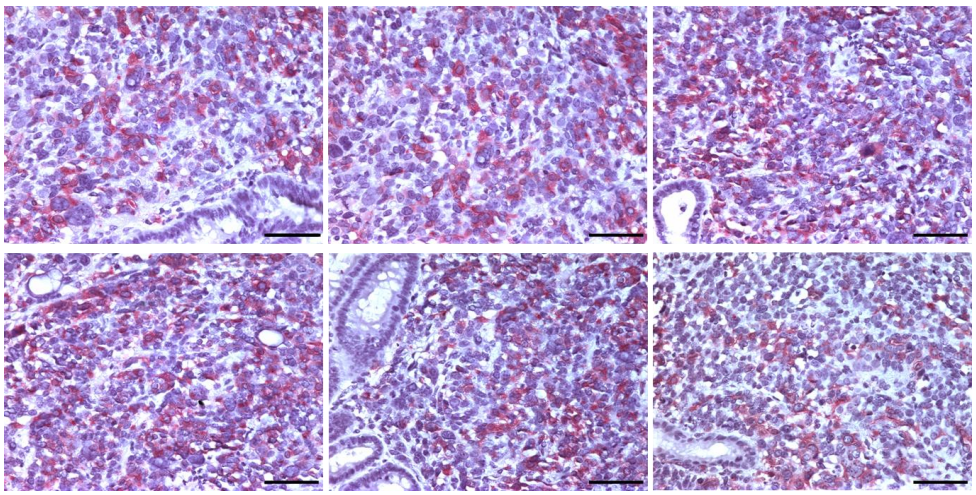

Figure 12. Immunohistochemistry for glucagon in the gastric tumors of CEA424-SV40 TAg transgenic mice. Staining images from three individual mice are shown. Scale bars: 50 μm.

6.1.3.4 Detection of secretin expression in the gastric tumors of CEA424-SV40 TAg transgenic mice

Secretin is a hormone that controls secretions into the duodenum. It is normally produced by the S cells of the duodenum which belong to the diffuse neuroendocrine system of the gut. In the microarray analysis, the expression level of secretin was highly elevated (fold change: 68.9) in the tumor tissue when compared with the normal antral tissue (Figure 7). It was also highly expressed in tumor derived cell line 424GC as shown in Figure 8. To further confirm its overexpression in the CEA424-SV40 TAg gastric tumors, immunohistochemical staining for secretin was applied to stomach sections from transgenic mice over 90 days old. As shown in Figure 13, the tumor areas were intensively stained with the anti-secretin antibody. Double immunofluorescent staining for secretin and SV40 TAg revealed secretin

positive tumor cells (Figure 14).

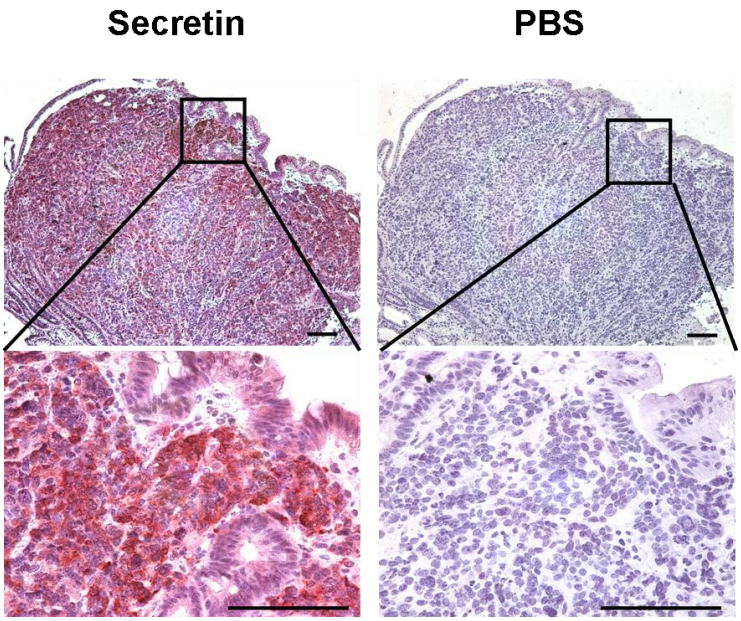

Figure 13. Immunohistochemistry for secretin in stomach of a 92 days old CEA424-SV40 TAg transgenic mouse. Left: secretin; right: negative control. In the lower part, an enlargement of the area from the upper picture is shown. Scale bars: 100 µm.

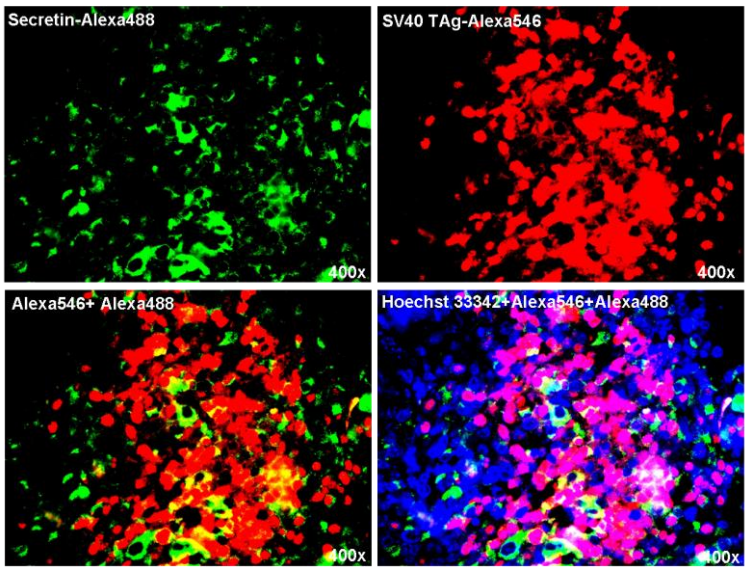

Figure 14. Double staining for SV40 TAg and secretin in stomach of a 92 days old CEA424-SV40 TAg transgenic mouse. SV40 TAg: red (Alexa-546); secretin: green (Alexa-488); DNA: blue (Hoechst33342). Images of 400× magnifications are shown.

Elevated hormone concentration in the blood is typical for patients with functional NETs. As the tumor cells highly expressed secretin, the question was whether this hormone was elevated in the blood of tumor bearing mice. Thus, whole blood was taken from 90 days old CEA424-SV40 TAg transgenic mice and non-transgenic mice, and secretin concentration was measured by a specific ELISA. As shown in Figure 15, the hormone concentration of secretin in CEA424-SV40 TAg transgenic mice was significantly elevated when compared with the normal mice (CEA424-SV40 TAg transgenic mice: 2325±1094 pg/ml, control mice: 186.4±18.9 pg/ml, $p<0.05$).

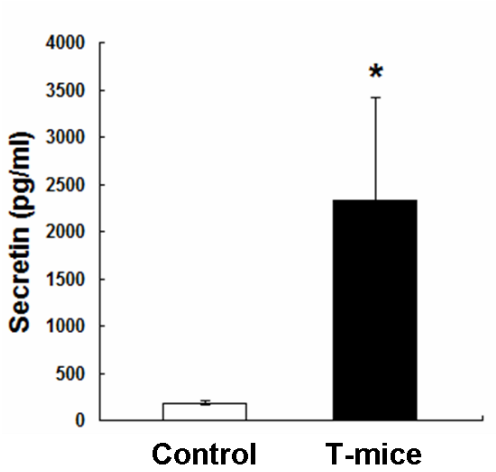

Figure 15. ELISA analysis of secretin level in the plasma of 90-day-old CEA424-SV40 TAg mice and non-transgenic mice. T-mice: CEA424-SV40 TAg transgenic mice; n=4 in each group; * $p<0.05$.

One of the consequences of high secretin level in the blood could be the reduction of acid output of the stomach because secretin functions as a feedback inhibitor of gastric acid secretion. Since the titration of the gastric acid output in mice is highly complicated, we used the number of acid producing cells as a surrogate marker for the acid output. Therefore, the number of H^+-K^+-ATPase positive cells was checked. Stomachs from five normal mice and five CEA424-SV40 TAg transgenic mice were used for H^+-K^+-ATPase staining. For each mouse, twelve 400× magnification fields were randomly selected for H^+-K^+-ATPase positive cell counting. As shown in Figure 16, the number of H^+-K^+-ATPase positive cells in the stomachs of CEA424-SV40 TAg transgenic mice was significantly reduced when compared with normal mice (normal mice: 202.45±5.34; CEA424-SV40 TAg transgenic mice: 164.02±12.95; * $p<0.0005$), which indicated a suppression of acid output in the stomachs of the

transgenic mice.

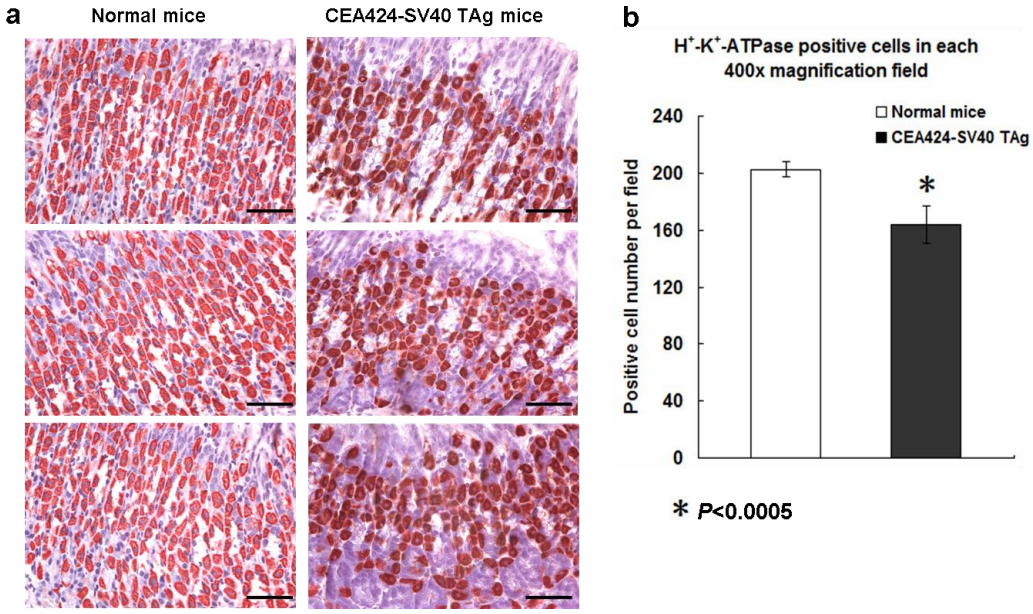

Figure 16. Analysis of H^+-K^+-ATPase expression in CEA424-SV40 TAg transgenic mice. a) Immunohistochemistry for H^+-K^+-ATPase in CEA424-SV40 TAg transgenic mice and normal mice. Scale bars: 50µm. b) Number of H^+-K^+-ATPase positive cells in the stomach of EA424-SV40 TAg transgenic mice and normal mice. n=5 in each group, * p<0.0005

6.1.3.5 Serotonin concentration in the plasma of 90-day-old CEA424-SV40 TAg mice.

Serotonin, also known as 5-hydroxytryptamine (5-HT), is a neurotransmitter. Hypersecretion of serotonin can lead to the carcinoid syndrome. In clinical practice, it is considered as a biomarker for disease mornitoring (NCCN Guidelines Version 1.2011). According to the transcriptome analysis, both the tumor tissue and isolated cell lines highly expressed mRNA for tryptophan hydroxylase 1 (Tph1). As Tph1 is the rate limiting enzyme for the biosynthesis of serotonin, we expected an elevated hormone level for serotonin in the blood. Thus, whole blood was taken from six 90-day-old CEA424-SV40 TAg mice and non transgenic mice. EDTA plasma was used for measuring the hormone concentration by ELISA. As shown in Figure 17, dramatically elevated concentrations of serotonin in the plasma of the transgenic mice

were detected when compared to normal mice (CEA424-SV40 TAg transgenic mice: 505±89 ng/ml, control mice: 27.8±8.9 ng/ml, $p<0.05$). This confirmed that the Tph1 gene was active which led to a high serotonin response.

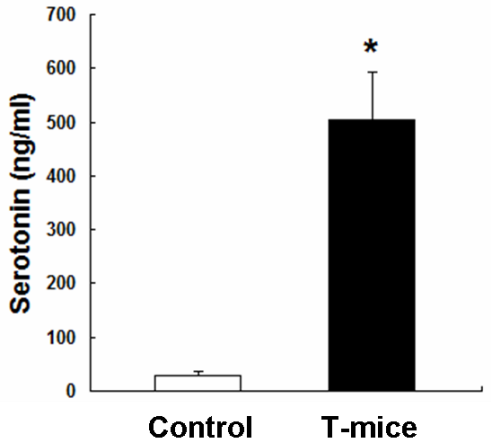

Figure 17. ELISA analysis for serotonin concentration in the plasma of 90 days old CEA424-SV40 TAg mice and non-transgenic mice. T-mice: CEA424-SV40 TAg transgenic mice; n=6 in each group, * $p<0.05$.

6.1.4 Expression analysis of transcription factors with a role in neuroendocrine cell differentiation.

Results presented above gave a clear indication that the CEA424-SV40 TAg transgenic mice develped a neuroendocrine tumor in the antrum with severe consequences. We then asked whether specific transcription factors drive the tumor development. The crucial steps of the neuro/enteroendocrine cell differentiation process are controlled by the sequential expression of three basic helix-loop-helix transcription factors, Math1, Neurogenin3 and NeuroD, according to the current model of neuro/enteroendocrine cell differentiation[135]. While Math1 is an early transcription factor, both NeuroD and Nkx2.2 are believed to play a role in later events in the differentiation which confine the cells to an neuro/enteroendocrine cell fate[135]. In our former microarray analysis, the expression levels of NeuroD and Nkx2.2 were significantly up-regulated in day-90 CEA424-SV40 TAg tumors compared to normal antral tissue. To confirm their overexpression also at protein level, western blot was performed. Protein was isolated from the CEA424-SV40 TAg gastric tumor in the antral region (from a 85 days old mouse) as well as 3 cell lines

(424GC, mGC3, mGC8) derived from the primary tumors. Cell line End3, which is an endothelioma cell line, served as a negative control. As shown in Figure 18, all the three cell lines strongly expressed NeuroD and Nkx2.2. Nkx2.2 was also highly expressed in the tumor tissue. The expression level of NeuroD in the tumor tissue was lower, but still detectable. Thus, important transcription factors were found in tumor tissue and isolated cell lines which can explain the differentiation of the tumor cells.

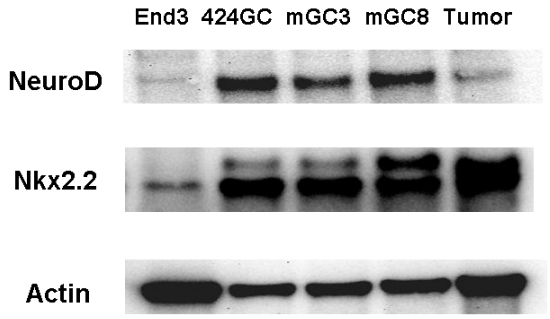

Figure 18. Western blot for transcription factors NeuroD and Nkx2.2 in tumor tissue and cell line 424GC, mGC3, mGC8. Cell line End3 was used as a negative control. NeuroD and Nkx2.2 proteins were detected at 49 kDa and 30 kDa, respectively.

6.1.5 Summary for the characterization of the tumor

Data from this part demonstrate that the CEA424-SV40 TAg transgenic mice develope solid tumors in the antral region of the stomach which are of high proliferative capacity. The CEA424-SV40 TAg gastric tumors express several neuroendocrine markers including chromogranin A, chromogranin B, secretin and glucagon. Dramatically elevated hormone levels of serotonin and secretin in the plasma of the transgenic mice prove that the up-regulated gene expression translates into functional consequences. Furthermore, the CEA424-SV40 TAg gastric tumor and tumor derived cell lines express transcription factors with a role in neuroendocrine cell differentiation. All these information indicate that CEA424-SV40 TAg gastric tumors exhibit a neuroendocrine phenotype which makes the CEA424-SV40 TAg transgenic mouse a clinically relevant model for gastric neuroendocrine tumors.

6.2 Testing of molecularly targeted therapies on CEA424-SV40 TAg transgenic mouse model system

6.2.1 In vitro screening of molecularly targeted therapies for gastric neuroendocrine tumor

For testing novel therapies in vitro, drugs targeting molecular markers for NETs were chosen. mTOR is a serine/threonine protein kinase which is essential for protein translation, cell growth, metabolism and autophagy[55-57]. Aberrant activation of PI3K-Akt-mTOR pathway has been identified as one of the mechanisms for the tumorigenesis of NETs. HSP90 is an ATP-dependent molecular chaperone frequently exploited by tumor cells to overcome environmental perturbations during oncogenic transformation[136]. Recently, it has also been included as a molecular marker for neuroendocrine (carcinoid) tumors[72]. Thus, two mTOR inhibitors RAD001 (everolimus) and NVP-BEZ235 as well as one HSP90 inhibitor NW457 were selected for screening anti-tumor effects.

Besides, drugs that target specific pathways activated by the TAg were also included. Two major targets of the transformation induced by TAg are Rb1 and Trp53 tumor suppressors. Inactivation of Rb1 sets free host E2F transcription factors which leads to the transcriptional activation of E2F-regulated S-phase genes[29]. Mdm2, a cellular antagonist of p53, is responsible for the degradation of p53 and may take an essential role in a trimeric TAg-p53-Mdm2 complex during the transformation[24]. So it makes sense to try agents targeting these two pathways which may take a major role in the tumorigenesis of the CEA424-SV40 TAg gastric tumors. Thus, Nutlin-3, which can stabilize p53 by inhibiting the interaction between Mdm2 and p53, and E2F inhibitor HLM006474 were selected for testing. Besides, the mitotic inhibitor paclitaxel was also used as an agent for traditional chemotherapy.

6.2.1.1 Cell proliferation assay

As a first step, the drugs described above were tested for their ability to inhibit cell proliferation. Three cell lines derived from the primary CEA424-SV40 TAg gastric tumors (424GC, mGC3 and mGC8) were used throughout the experiment. Cells were incubated with normal culture medium and different concentrations of the drugs in 96-well plate for 72 hours. Cell viability was estimated by WST-1 assay. As shown in Figure 19, all the drugs could dose dependently inhibit the proliferation of all the three cell lines. The concentration range for GI_{50} from several experiments was listed in Table 1.

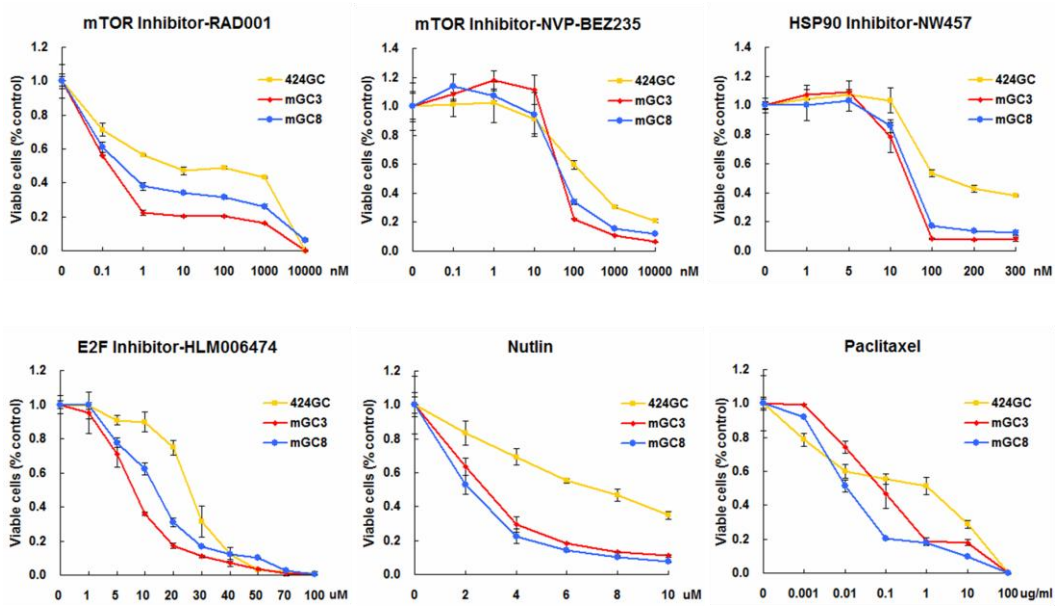

Figure 19. Cell proliferation after 72 hours treatment. WST-1 absorption was tested after 72 hours treatment. The experiments were performed in triplicate.

	RAD001 (nM)	NVP-BEZ23 (nM)	NW457 (nM)	HLM006474 (μM)	Nutlin (μM)	Paclitaxel (μg/ml)
424GC	1-10	100-1000	100-200	20-30	6-8	1-10
mGC3	0.1-1	10-100	10-100	5-10	2-4	0.01-0.1
mGC8	0.1-1	10-100	10-100	10-20	2-4	0.01-0.1

Table 1. The concentration range for GI_{50}. The GI_{50} for each drug tested was shown in concentration range.

6.2.1.2 Colony formation with mTOR inhibitors (RAD001 and NVP-BEZ235) and Paclitaxel

Another way to confirm the inhibitory effect of these drugs on cell proliferation is the colony formation assay. In contrast to the WST-1 assay which showed transient effect of the drugs, colony formation could display a long term effect of the treatment on the cell lines. mTOR inhibitors (RAD001 and NVP-BEZ235) and paclitaxel were selected in this assay. Cell lines were treated with 100 nM RAD001, 100 nM NVP-BEZ235 and 1 μg/ml Paclitaxel for 24 and 72 hours in 12-well plates before being seeded into 6-well plates for colony formation. Cells without any treatment were used as control. After 3 weeks cultivation, colonies formed were fixed by methanol and stained with crystal violet. For all the three drugs, 72 hours treatment could significantly inhibit the ability to form colonies in all the three cell lines. In Figure 20, an example from each group is shown. A significant decrease of the colony number could be observed in the treated group when compared to the control group as shown in Figure 21. This effect could even be observed after a short 24 hours treatment in 424GC and mGC3, while in mGC8, the inhibitory effect from RAD001 was not significant.

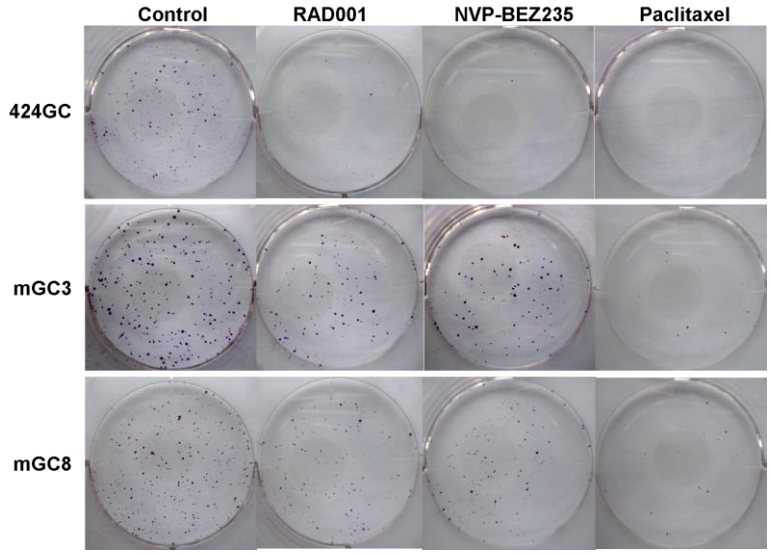

Figure 20. Colony formation assay with cells treated for 72 hours. Colonies stained with crystal violet in 6-well plate are shown for each treated group from the three cell lines 424GC, mGC3, mGC8. A significant reduced colony number could be observed in the treated group.

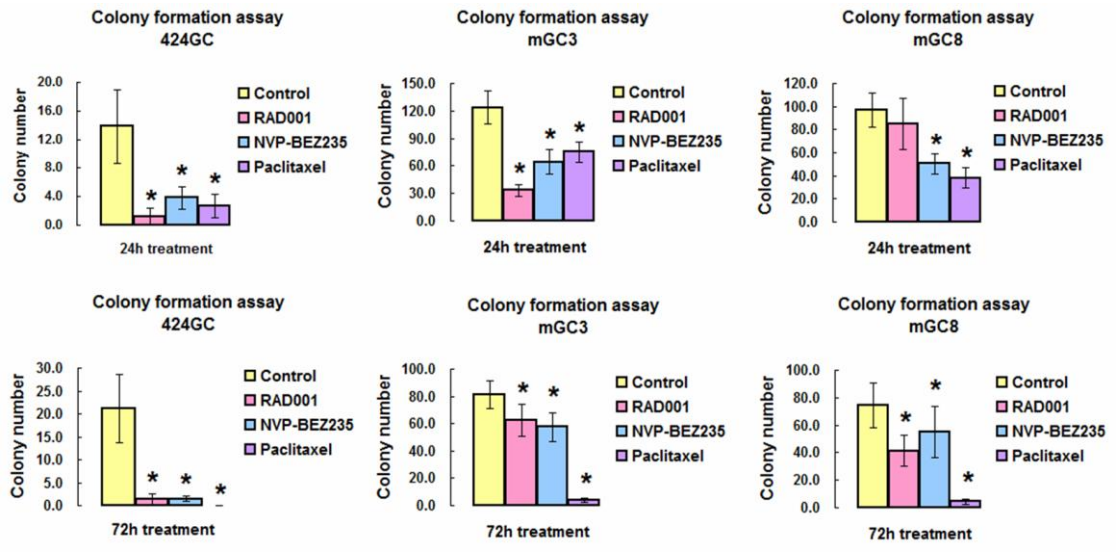

Figure 21. Colonies formed by cells treated for 24 (first row) and 72 hours (second row). Colony numbers from each group are shown. (n= 6 for each group, * p<0.05, treated group compared with control group)

6.2.1.3 Induction of cell apoptosis by mTOR inhibitors RAD001 and NVP-BEZ235

To find out whether the mTOR inhibitors can induce apoptosis in the cell lines, FACS analysis was applied on cells treated with 100 nM RAD001 or 100 nM NVP-BEZ235 for 72 hours with Annexin V-FITC Kit. Cells without treatment were used as control. As shown in Figure 22, treated cells displayed higher early apoptotic rate. The induction of cell apoptosis may be one of the mechanisms involved in the anti-tumor effects of mTOR inhibitors.

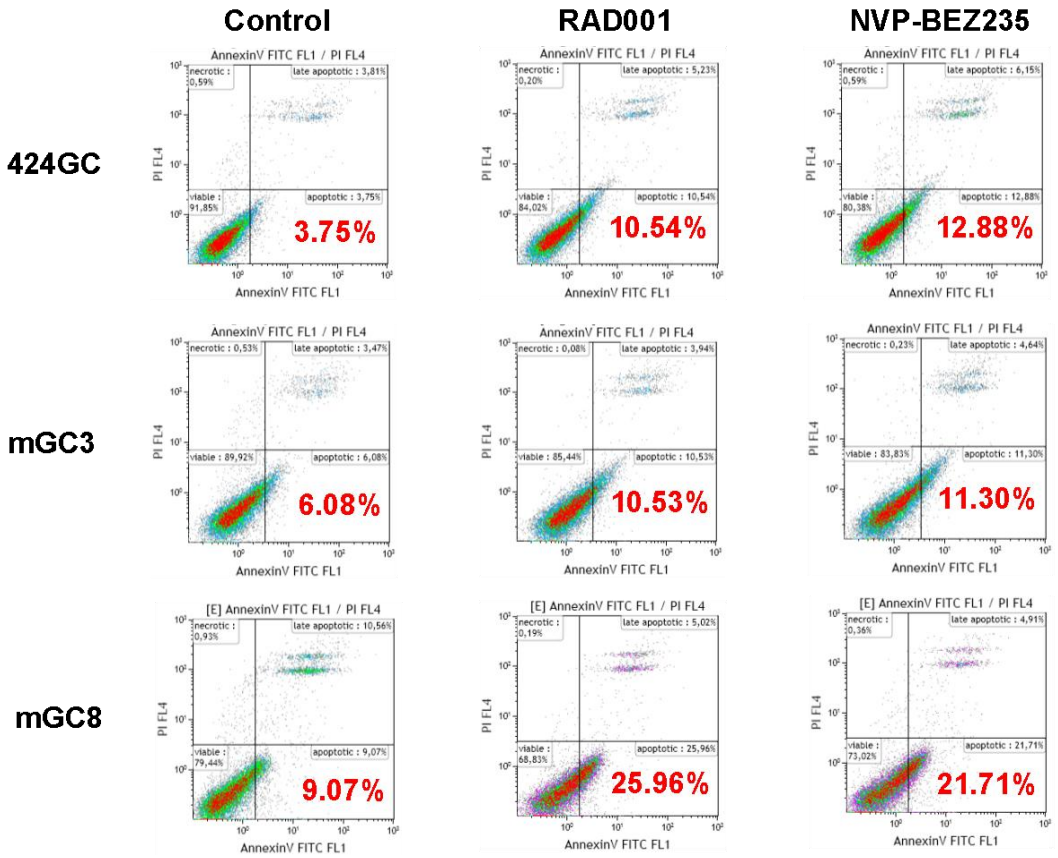

Figure 22. Apoptotic rate analyzed by flow cytometry on cells treated with 100 nM RAD001 or 100 nM NVP-BEZ235 for 72h. Cells without treatment were used as control. Y-axis shows the PI signal, and the X-axis shows the binding of Annexin V-FITC.

6.2.2 In vivo study of molecularly targeted therapy on CEA424-SV40 TAg transgenic mice with mTOR inhibitor RAD001

The in vitro studies above revealed anti-tumor potential of the tested drugs which made them promising candidates for further in vivo experiments. As a first step, the mTOR inhibitor RAD001, with a GI_{50} at 0.1-10 nM, was selected. To test the drug in a clinically relevant form, 50 days old CEA424-SV40 TAg mice were used for the in vivo study. Mice of this age were selected because at this time point, tumor lesions have been well formed in the antrum, which is also in line with the situation in the clinic.

6.2.2.1 Effect of RAD001 treatment on tumor development of the CEA424-SV40 TAg transgenic mice

Since we were interested only in strong effects, a sample size of 4 per group was calculated to be sufficient to give a significant result. Thus, 4 mice were included in both the RAD001 treated group and placebo group. 10 mg/kg RAD001 or placebo was given orally once per day from day 1 to day 5 every week, according to published protocols and suggestions from the company. Weight was monitored daily and the mice were sacrificed when they lost 20% of their peak weight which is a surrogate marker for terminal tumor growth. At the end of the experiment, the average survival time for both groups was evaluated. As shown in Figure 23, mice treated with RAD001 lived much longer than the mice in the control group. The survival time of the RAD001 treated mice was prolonged by 35 days on average (control group: 100±4.97 day; RAD001 group: 135±4.90 day, $p<0.0001$). Compared with the overall survival time of tumor mice (on average 100 days), this is a dramatic increase by 35%. In Figure 23 a, the weight on day 90 was used as the base line because most of the CEA424-SV40 TAg transgenic mice started to lose weight around day 90.

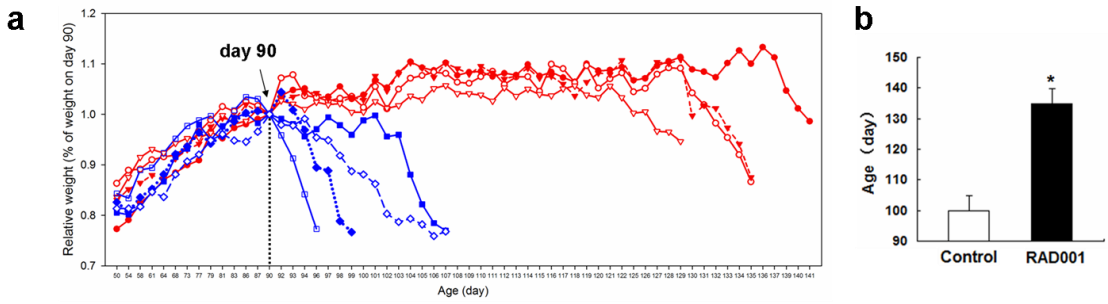

Figure 23. Effect of RAD001 treatment on the survival time of the CEA424-SV40 TAg transgenic mice. a) Weight curves of the CEA424-SV40 TAg transgenic mice. Blue curve: control group; red curve: RAD001 treated group. b) Mean age of the CEA424-SV40 TAg transgenic mice when they lost 20% of the peak weight. * $p<0.0001$: RAD001 treated group compared with control group.

To further analyze the effects of the mTOR inhibitor RAD001, a different set up was chosen. Instead of testing the survival time when all tumors developed a terminal size, a fixed time protocol was chosen. The experiment was stopped when the first control mouse started to lose weight. In another word, instead of being sacrificed when 20% of the peak weight was lost, all the mice in this experiment were ended at the same age (on day 98). Four 50 days old CEA424-SV40 TAg transgenic mice were included in the RAD001 treated group and three of the same age in the placebo group. 10 mg/kg RAD001 or placebo was given orally once per day from day 1 to day 5 every week as before. Weight was monitored daily, as in the first set up.

After 48 days treatment, one of the mice in the control group started to lose weight. At that time, all the mice treated with RAD001 still showed a normal behaviour and no weigh loss could be observed. As shown in Figure 24, mice of both the control group and RAD001 treated group developed tumors in the antral region of the stomach with no visible difference of tumor size and morphology. However, the weight of the tumors in the RAD001 group was significantly lower when compared with the control group (control group: 0.1473 ± 0.0197 g; RAD001 group: 0.1118 ± 0.0114 g, $p<0.05$). This demonstrates that RAD001 treatment suppressed the tumor development in CEA424-SV40 TAg transgenic mice, although this effect was not strong enough to eliminate all the tumor cells and cure the mice. There were still some tumor cell population which could escape from the treatment and eventually led to the death of the host.

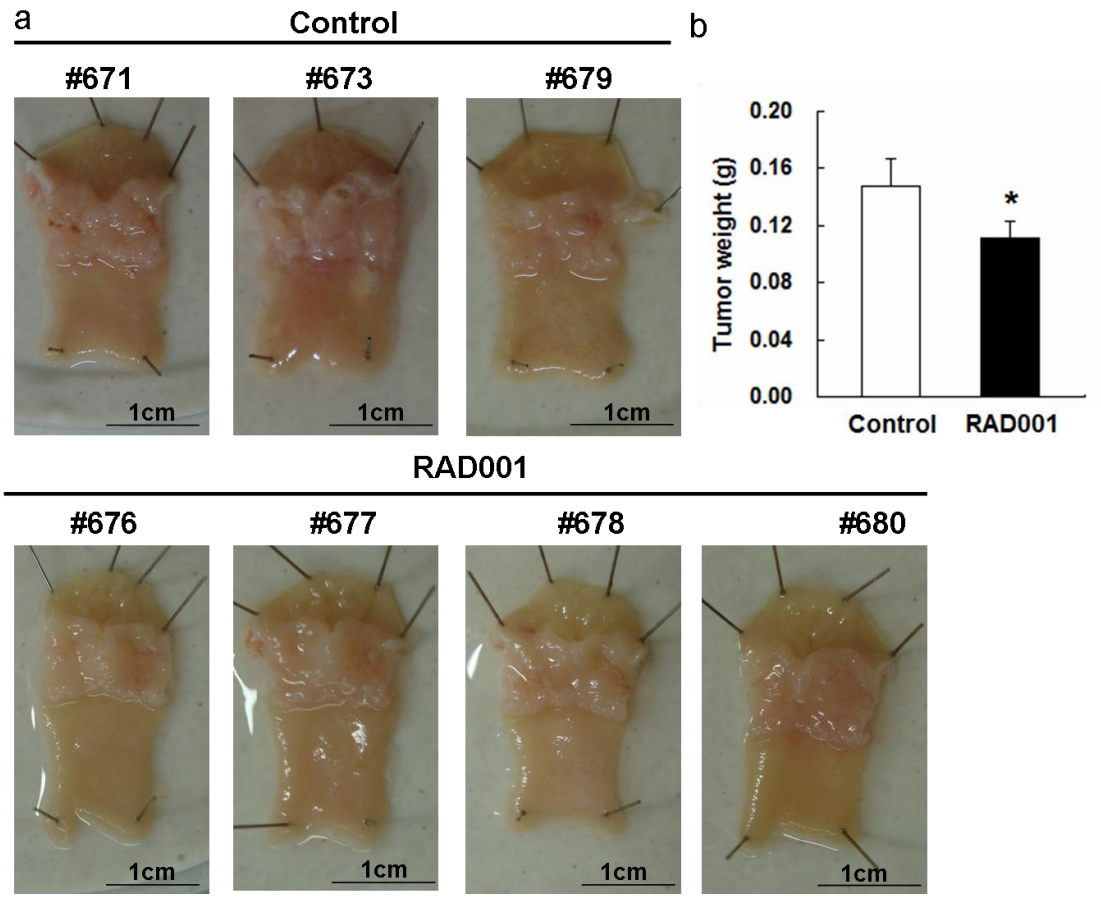

Figure 24. Tumor development in the RAD001 treated CEA424-SV40 TAg transgenic mice. a) Macroscopic pictures of the gastric tumors developed in the RAD001 treated mice and control mice. The numbers represent individual mice. b) Tumor weight of the RAD001 treated mice and control mice. * $p<0.05$.

6.2.2.2 Effect of RAD001 treatment on the proliferative status of the tumor at the time point of terminal tumor growth

To get an idea of how the RAD001 treatment affected the number of proliferating tumor cells at the time point of terminal tumor growth, stomachs of the four RAD001 treated mice and four control mice from the first experiment (experiment A: all the mice were sacrificed when 20% of the peak weight was lost) were analyzed for the expression of proliferation marker Ki-67 by immunohistochemistry. Three 400× magnification fields were selected randomly from each mouse and the percentage of Ki-67 positive cells was evaluated. As shown in Figure 25 and 26, both the control

mice and the RAD001 treated mice developed high proliferative tumors. The average Ki-67 index for RAD001 treated group and the control group was 59.68±12.42% and 55.43±11.07%, respectively (p>0.05). No significant difference of the Ki-67 index was observed between the RAD001 treated group and the control group.

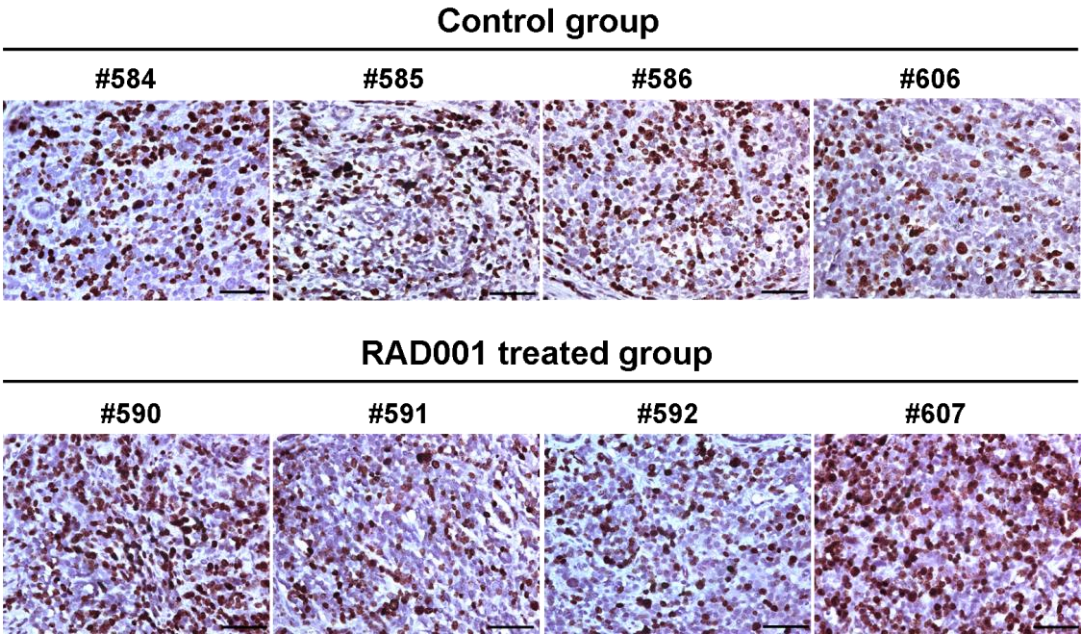

Figure 25. Examples of Ki-67 staining on stomach sections from the RAD001 treated mice and control mice. The numbers represent individual mice. Scale bars: 50 μm.

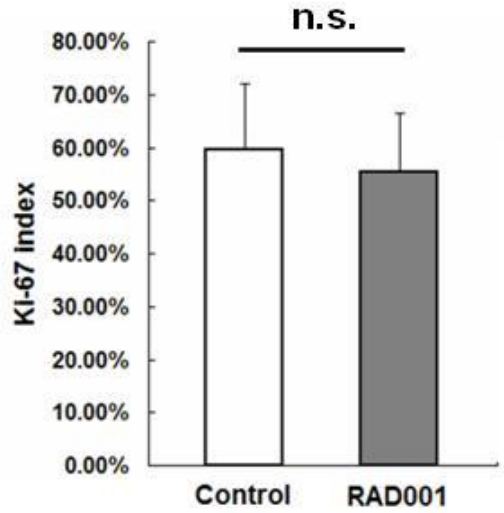

Figure 26. Ki-67 index in the tumors of the RAD001 treated mice and control mice at the time point of terminal tumor growth. No significant difference was observed between the two groups.

6.2.2.3 Effect of the RAD001 treatment on the neuroendocrine phenotype of CEA424-SV40 TAg gastric tumor cells

As shown above, RAD001 treatment did not change the proliferative status of the tumor cell at the time point of terminal tumor growth. To further study what the treatment did to the tumors, we checked if RAD001 affected the neuroendocrine phenotype of the tumor cells.

Glucagon was one of the neuroendocrine tumor markers which were aberrantly expressed in the CEA424-SV40 TAg gastric tumors. To check if its expression was influenced by the RAD001 treatment, immunohistochemical staining for glucagon was applied on stomach sections from the four RAD001 treated mice and four control mice from animal experiment A (all the mice were sacrificed when 20% of the peak weight was lost). Six 400× magnification fields were selected randomly for each mouse and the percentage of glucagon positive cells was evaluated. As shown in Figure 27, a significant decrease of the glucagon positive cell number was observed in the RAD001 treated group when compared with the control group. The average glucagon positive cell number in each 400× magnification field for the control group and RAD001 treated group was 106.71±11.34% and 64.25±12.82%, respectively ($p<0.05$).

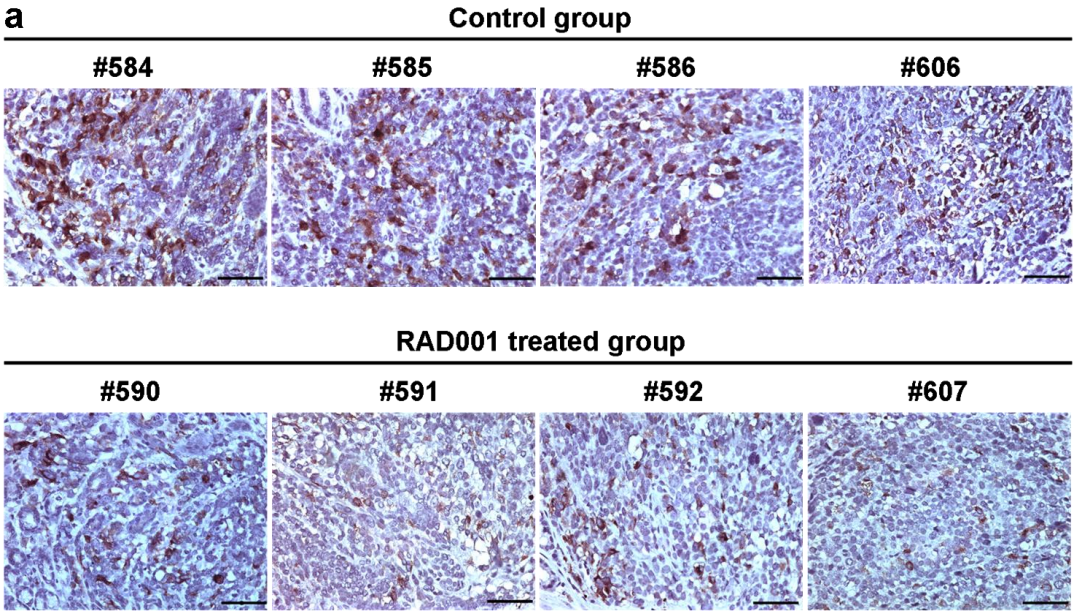

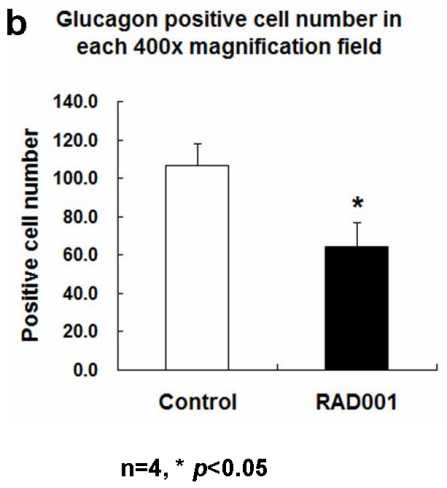

Figure 27. The effect of the RAD001 treatment on glucagon expression in the gastric tumors of CEA424-SV40 TAg transgenic mice. a) Immunohistochemical staining of glucagon on gastric tumors from both the RAD001 treated mice and control mice. The numbers represent individual mice. Scale bars: 50 μm. b) Statistic analysis of the glucagon positive cell numbers in the tumor area. (n=4 for each group, * $p<0.05$)

The down-regulation of the glucagon expression gave a clue that RAD001 treatment may affect the neuroendocrine phenotype of the CEA424-SV40 TAg gastric tumors. We then checked if RAD001 treatment influenced the expression of transcription factors with a role in the neuroendocrine cell differentiation. Protein lysate was obtained strictly from tumors of the mice in the second experiment (experiment B: all the mice were sacrificed at d98, 48 days after the treatment started). Western blot was carried out with primary antibody directed at transcription factor Nkx2.2, which was shown to be expressed in the tumor tissue and the cell lines (Figure 18). As shown in Figure 28, the expression level of Nkx2.2 was lower in all the tumor samples from RAD001 treated mice when compared with control mice.

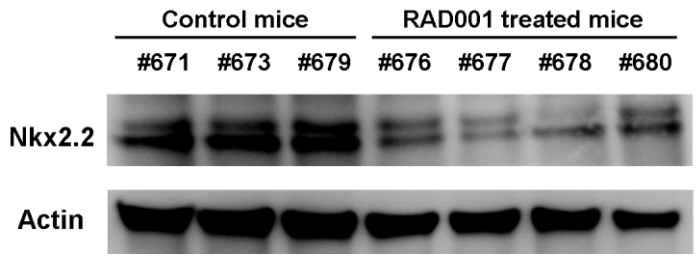

Figure 28. Nkx2.2 expression in the tumor tissue from RAD001 treated mice and control mice. Nkx2.2 protein was detected at 30 kDa. Actin was used as control. The numbers represent individual mice.

These results indicated that the RAD001 treatment had some impact on the neuroendocrine phenotype of CEA424-SV40 TAg gastric tumors.

6.2.3 Possible mechanisms of the anti-tumor effects induced by RAD001 in CEA424-SV40 TAg gastric tumors

As RAD001 treatment in the CEA424-SV40 TAg transgenic mouse model was successful both in vitro and in vivo, possible mechanisms of these anti-tumor effects induced by RAD001 were analyzed. RAD001 is a mTOR inhibitor which specifically targets mTORC1. The p70 ribosomal S6 kinase (p70S6K) and the eukaryotic translation initiation factor 4E (eIF4E)-binding protein (4EBP1) are two well discribed mTORC1 substrates, which are responsible for the regulation of cell growth and proliferation[137]. Thus, the effect of RAD001 treatment on the activation of these two downstream targets of mTOR pathway was tested.

6.2.3.1 Effect on mTOR- p70S6K pathway

6.2.3.1.1 Effect on mTOR- p70S6K pathway in vitro

p70S6 kinase (p70S6K) is a downstream target of the mTOR signaling pathway and its activation is essential to the regulation of cell growth and proliferation[55, 138]. To show the possible mechanism of the anti-proliferation effects induced by the mTOR

inhibitor RAD001, the expression of phosphorylated p70S6K (p-p70S6K), which was considered as the active form, was first analyzed in sample of cell lines treated with 100 nM RAD001 for 2h, 24h and 72h. Cells incubated with culture medium were used as control. As shown in Figure 29, p-p70S6K was expressed in all the three cell lines which proved the activated mTOR-p70S6K signaling in the tumor derived cell lines. In addition, a completely suppressed expression of the p-p70S6K was observed in all the three cell lines after treatment which clearly demonstrated that RAD001 efficiently inhibited this pathway in vitro.

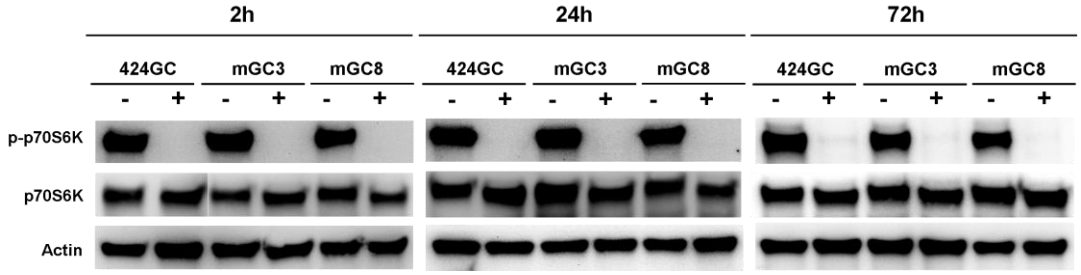

Figure 29. Western blot for phosphorylated p70S6K in cell lines treated with 100 nM RAD001 for 2h, 24h and 72h. First row shows the phosphorylated form of p70S6K. As controls, the unphosphorylated form of p70S6K and Actin are shown. -: control; +: 100 nM RAD001. p70S6K and p-p70S6K proteins were detected at 70 kDa while Actin was detected at 43 kDa.

6.2.3.1.2 Effect on mTOR- p70S6K parthway in vivo

Western blot for p-p70S6K was also carried out on tumor tissue from RAD001 treated mice to see if the mTOR-p70S6K signaling was also inhibited by RAD001 in vivo. As shown in Figure 30, the expression level of p-p70S6K in tumor tissue from RAD001 treated mice was reduced or almost absent.

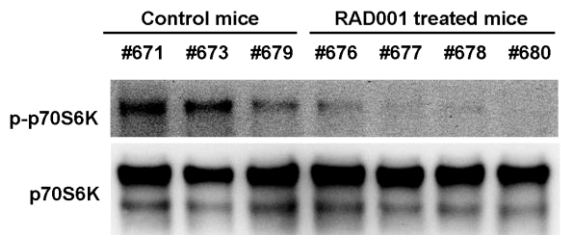

Figure 30. Western blot for p-p70S6K on tumor tissue from RAD001 treated mice and control mice. The numbers represent individual mice. p70S6K and p-p70S6K proteins were detected at 70 kDa.

S6 ribosomal protein is a downstream target of p70S6K, which is involved in the regulation of translation. To see if RAD001 treatment could affect the mTOR-p70S6K pathway further down, immunohistochemistry for phospho-S6 ribosomal protein was carried out on tumor tissue from RAD001 treated mice and control mice. Staining for SV40 TAg, phospho-S6 ribosomal protein (Ser 235/236), and phospho-S6 ribosomal protein (Ser 240/244) were carried out on serial sections from the stomachs of RAD001 treated and control mice. In Figure 31, examples for the staining from two mice of each group are shown. Lower expression levels of phospho-S6 ribosomal protein (Ser 235/236) and phospho-S6 ribosomal protein (Ser 240/244) could be observed in the RAD001 treated group.

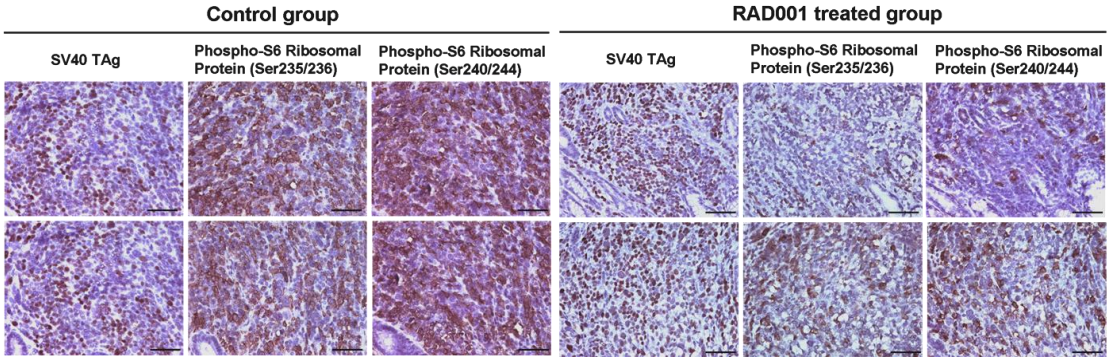

Figure 31. Immunohistochemistry for SV40 TAg and phospho-S6 ribosomal proteins on tumor tissue from RAD001 treated mice and control mice. Stainings from two mice of each group are shown. Scale bars: 50μm.

For statistical analysis, 400× magnification areas where more than 50% nuclei were positively stained with SV40 TAg were randomly selected for counting. As shown in Figure 32, a significant decrease of the phospho-S6 ribosomal protein positive rate (phospho-S6 ribosomal protein positive cell number/total cell number) in the RAD001 treated group was confirmed (Ser235/236: control group: 59.64±9.39%, RAD001 group: 32.82±11.92%, $p<0.05$; Ser240/244: control group: 65.31±4.15%, RAD001 group: 26.88±14.38%, $p<0.05$). These results indicated that the RAD001 treatment in vivo suppressed the activation of S6 ribosomal protein and further confirmed the influence of RAD001 treatment on p70S6K function since the S6 ribosomal protein is

activated by p70S6K.

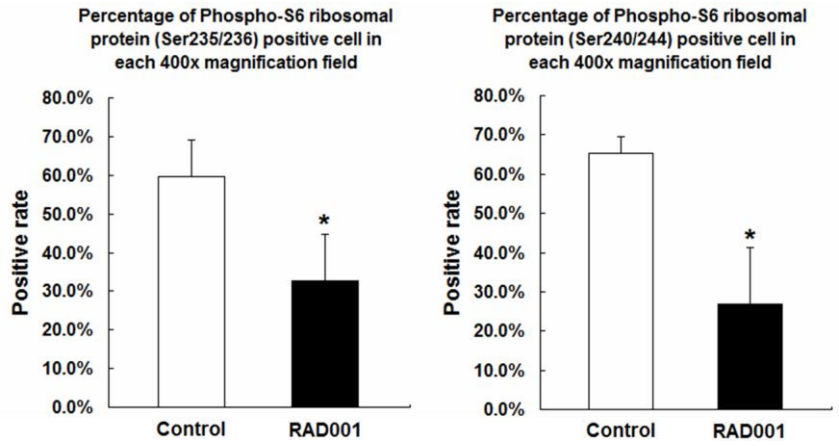

Figure 32. Number of Phospho-S6 ribosomal protein positive cells in tumors from RAD001 treated mice and control mice. Data are shown as positive rate (phospho-S6 ribosomal protein positive cell number/total cell number). n=4, * $p<0.05$: RAD001 treated group compared with control group, nonparametric test.

These results indicated that RAD001 treatment inhibited the activation of mTOR-p70S6K signaling pathway also in vivo, although not completely.

6.2.3.2 Effect on mTOR-4EBP1 pathway

6.2.3.2.1 Effect on mTOR-4EBP1 pathway in vitro

4EBP1 is another mTORC1 substrate responsible for transcription and translation initiation of genes involved in cell growth. Western blots for 4EBP1 and phospho-4EBP1 were applied to the protein samples from the cell lines treated with 100 nM RAD001 for 2h, 24h and 72h. Cells incubated with culture medium were used as control. As shown in Figure 33, although transient treatment of 2h and 24h did not affect the phospho-4EBP1 level apparently, 72h treatment with RAD001 significantly inhibited the phosphorylation of 4EBP1, especially in mGC3 and mGC8.

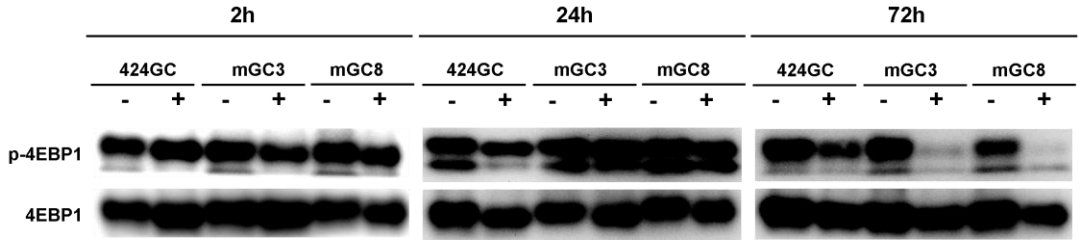

Figure 33. Western blot for 4EBP1 and phospho-4EBP1 (p-4EBP1) on cell lines treated with 100 nM RAD001 for 2h, 24h and 72h. -: control; +: 100 nM RAD001. 4EBP1 and p-4EBP1 proteins were detected at 15-20 kDa.

6.2.3.2.2 Effect on mTOR-4EBP1 pathway in vivo

The effect of RAD001 treatment on the phosphorylation leve of 4EBP1 in vivo was also analyzed. Tumor tissue from the second RAD001 treatment experiment (experiment B, all the mice were treated with 10 mg/kg RAD001 for 48 days and sacrificed on d98) were used for western blot. In contract to the clear effect in vitro, the phosphorylation of 4EBP1 was not affected by the long term treatment of RAD001 in vivo (Figure 34).

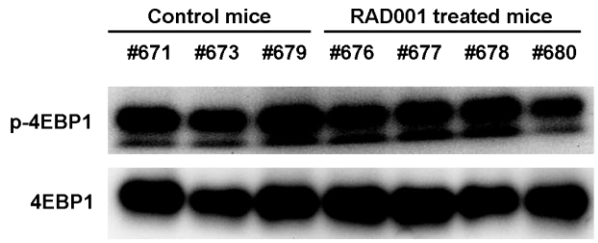

Figure 34. Western blot for 4EBP1 and phospho-4EBP1 on tumor tissue. The numbers represent individual mice. 4EBP1 and p-4EBP1 proteins were detected at 15-20 kDa.

6.2.4 Summary for the molecularly targeted therapies in the CEA424-SV40 TAg transgenic mouse model

In this part, molecularly targeted therapies were tested in the CEA424-SV40 TAg transgenic mouse model system. The mTOR inhibitors RAD001 and NVP-BEZ235, HSP90 inhibitor NW457, p53 stabilizer Nutlin-3, E2F inhibitor HLM006474 and

mitotic inhibitor paclitaxel induced anti-proliferation effect in the preliminary screening. In more detailed analysis in vitro, mTOR inhibitors RAD001 and NVP-BEZ235 showed effects on inhibiting colony formation and inducing cell apoptosis. In the in vivo experiment, RAD001 turned out to be a safe and efficient drug. Treatment with RAD001 was well tolerated, and significantly prolonged the survival time of the tumor bearing mice as well as inhibited the tumor development (reduced tumor weight). RAD001 treatment also had some impact on the neuroendocrine phenotype of CEA424-SV40 TAg gastric tumor cells as the expression levels of neuroendocrine marker glucagon and the transcription factor Nkx2.2, which involved in the differentiation of neuroendocrine lineage, were reduced in the tumor tissue from RAD001 treated mice. The effects of mTOR inhibition could be demonstrated by the suppression of mTOR-p70S6K and mTOR-4EBP1 signaling pathways. In the in vitro experiment, the inhibition of p70S6K activation induced by RAD001 was of high-efficiency because a complete elimination of p70S6K phosphorylation was observed even after 2h treatment. The inhibition of 4EBP1 activation needed longer period of treatment because transient treatment of 2h and 24h did not change the phospho-4EBP1 level apparently and a decreased phospho-4EBP1 expression was achieved after 72h treatment. In the in vivo experiment, mTOR-p70S6K signaling was still efficiently suppressed while an inhibition of mTOR-4EBP1 signaling was not observed after 48 days of RAD001 treatment in vivo. These results not only offered useful insights into the clinical aspects of a molecularly targeted therapy for neuroendocrine tumors, but also verified the practical utility of the CEA424-SV40 TAg transgenic mouse model system as powerful translational tools for human cancer research.

6.3 Possible “escape” mechanisms of tumor cells from RAD001 treatment

The results of the molecularly targeted therapies on CEA424-SV40 TAg transgenic mouse model system, especially the successful experience with mTOR inhibitor RAD001, raised some obvious questions. RAD001 treatment inhibited tumor development and significantly prolonged the survival time. However, the anti-tumor effect achieved was not strong enough to kill all the tumor cells and cure the mice. RAD001 treated mice still developed highly proliferative tumor mass and presented similar behavior when the cancer progressed, like losing weight. Thus, we tried to find possible escape mechanism of tumor cells from RAD001 treatment for even more efficient treatment protocols. Possible hypothesis were the selection of cells by the mTOR inhibition, or the change in differentiation. Besides, the feed back activation of PI3K-Akt pathway was also evaluated because this side effect induced by single RAD001 treatment has been reported on other neuroendocrine cell lines.

6.3.1 The effect of the molecularly targeted therapy with mTOR inhibitors on the expression pattern of epithelial stem cell markers

One possible explanation for the escape of tumor cells from RAD001 treatment could be a selection of a different tumor cell population with a more stem cell like appearance, which led to the final death of the mice. For this question, analysis for the expression level of certain stem cell markers could give some information. As the adult stem cell theory in small intestine was better described, certain markers from both the “crypt base columnar (CBC) cell” model and the “+4” model were used for testing.

6.3.1.1 Revers-transcription analysis for epithelial stem cell marker expression in the cell lines

Cells were analyzed for known epithelial stem cell markers and the influence of the

RAD001 treatment was tested. Reverse transcription RCR (RT-PCR) for the expression of stem cell markers was first applied to cells treated with 100 nM RAD001, 100 nM NVP-BEZ235, or 1 μg/ml paclitaxel for 72 hours. Crypt base columnar (CBC) cell markers Lgr5, Sox9, Olfm4 and Prom1, "+4" cell markers Bmi1, Dclk1, Tert and Ahr were selected for RT-PCR analysis. However, no obvious change was detected after 72 hours treatment. In Figure 35, the results from crypt base columnar (CBC) cell markers Lgr5 and Olfm4 as well as "+4" cell markers Bmi1 and Tert are shown as examples.

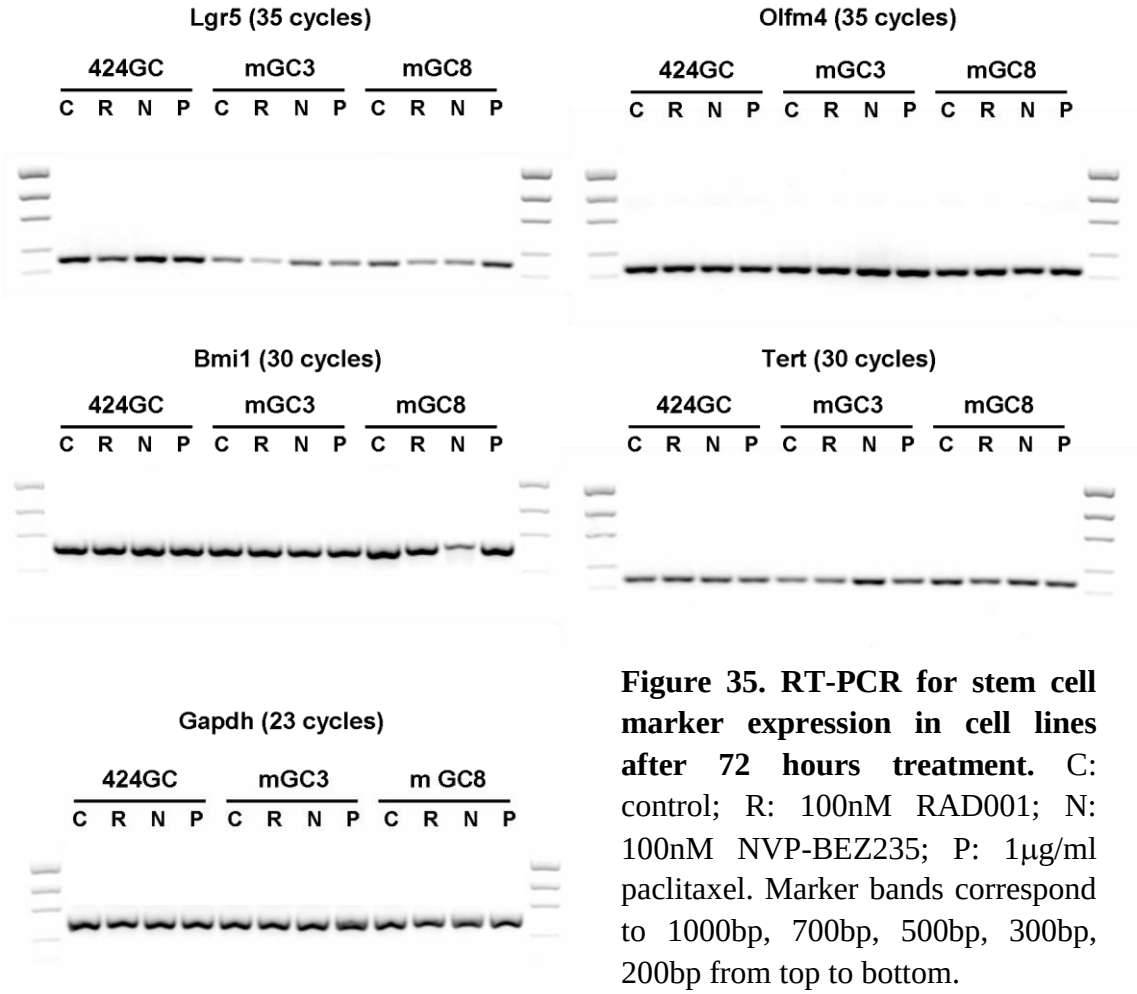

Figure 35. RT-PCR for stem cell marker expression in cell lines after 72 hours treatment. C: control; R: 100nM RAD001; N: 100nM NVP-BEZ235; P: 1μg/ml paclitaxel. Marker bands correspond to 1000bp, 700bp, 500bp, 300bp, 200bp from top to bottom.

As 72 hours treatment did not have a significant effect on the expression of the tested stem cell markers, we asked if a long term selection in vitro could change the expression pattern. For this, RAD001 resistant cell lines were established. 424GC,

mGC3, and mGC8 cell lines were treated by RAD001 with gradually increasing drug concentrations from 10nM to 400nM. Three different cell samples named as RAD-100, RAD-200 and RAD-400 were established during the whole treatment period. As shown in Table 2, cells were first treated with 10nM RAD001 for 3 days, followed with 9 days treatment with 100nM RAD001. Cell sample harvested at this time point was named as RAD-100. RAD-100 cells were then treated with 200nM RAD001 for 14 days (RAD-200) while the RAD-400 cell sample were further kept in culture with 400nM RAD001 for about one month.

Sample name	10nM	100nM	200nM	400nM
RAD-100	3 days	9 days		
RAD-200	3 days	9 days	14 days	
RAD-400	3 days	9 days	14 days	29 days

Table 2. RAD001 treatment for establishing RAD001 resistant cell lines. Cell line 424GC, mGC3, and mGC8 were included in the treatment.

From this selection process, cell lines were established which could grow in the presence of 400nM RAD001. To test whether these cells could still respond to the same RAD001 concentration compared with the parental cells, WST-1 assay was applied to the RAD-400 cell samples with untreated cell lines used as controls. As shown in Figure 36, the selected cell lines (red curves) had much higher GI_{50}s than the control cell lines. Even at high concentration of 1000nM, there were still about 60-80% cells alive.

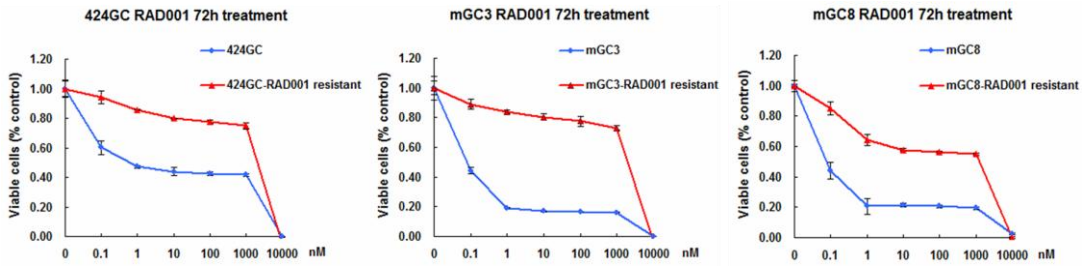

Figure 36. Cell proliferation assay on normally cultured cell lines and RAD001 selected cell lines. Blue curve: control cell line without pretreatment; red curve: RAD-400 cell line. The experiments were performed in triplicate.

Then, we asked if these selected cells are different from the parental cells. For this question, stem cell marker expression screening was applied to RAD-100, RAD-200, RAD400 cell samples to see if a long term selection in vitro could have any influence on the expression of stem cell markers. Epithelial stem cell markers for crypt base columnar (CBC) cells (Lgr5 and Olfm4) and "+4" cells (Bmi1 and Tert) were selected for screening. As shown in Figure 37, only Olfm4 expression was inhibited by the long term treatment of RAD001. There was no remarkable change observed in the expression of other stem cell markers checked.

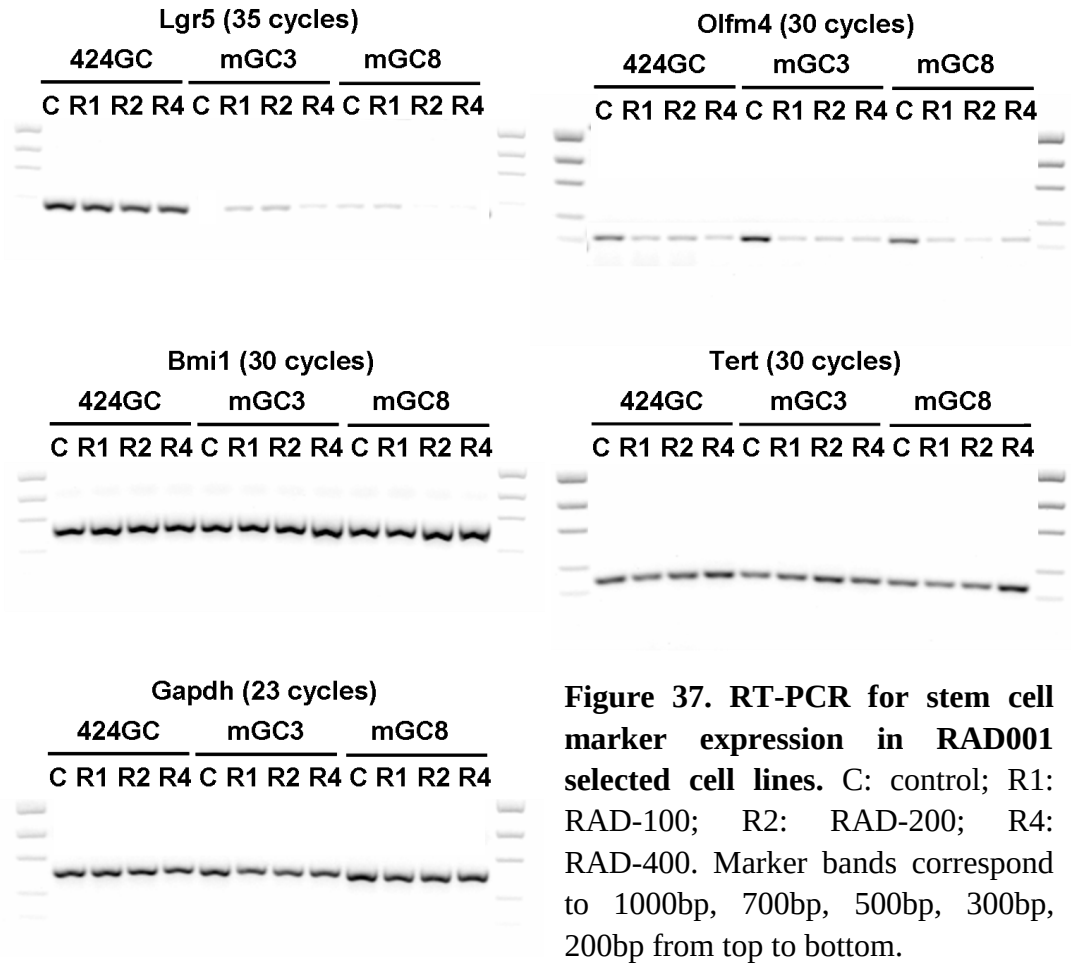

Figure 37. RT-PCR for stem cell marker expression in RAD001 selected cell lines. C: control; R1: RAD-100; R2: RAD-200; R4: RAD-400. Marker bands correspond to 1000bp, 700bp, 500bp, 300bp, 200bp from top to bottom.

The screening was also applied to tumor tissue from mice treated with RAD001 to see if the situation in vivo was similar. The expression of "CBC" markers Lgr5, Olfm4, Prom1, Ascl2 and "+4" markers Bmi1, Tert, Hopx, Dclk1 were checked in tumor

tissue from three control mice and three RAD001 treated mice. As shown in Figure 38, a complete suppression of Ascl2 expression was observed in the RAD001 treated group. The expression levels of all the other markers checked were not significantly affected.

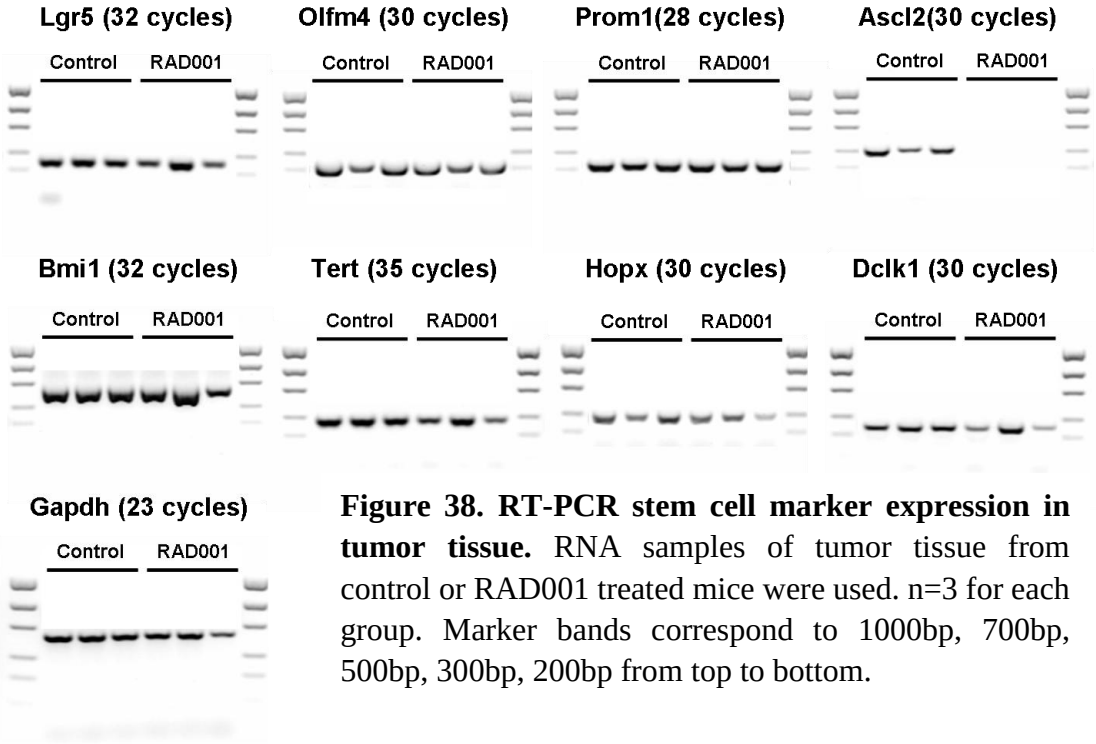

Figure 38. RT-PCR stem cell marker expression in tumor tissue. RNA samples of tumor tissue from control or RAD001 treated mice were used. n=3 for each group. Marker bands correspond to 1000bp, 700bp, 500bp, 300bp, 200bp from top to bottom.

The RT-PCR data showed that RAD001 treatment had no effect on the differentiation of the tumor cells and there was no indication that RAD001 could select for a more "cancer stem cell" like population.

6.3.1.2 Protein analysis for epithelial stem cell marker expression after RAD001 treatment

Data presented above showed that at mRNA level, RAD001 treatment did not induce a strong effect on differentiation of the tumor cells. However, RT-PCR shows only the presence of a certain RNA which may not reflect the protein expression. It still makes

sense to check whether the treatment had an apparent influence on the expression of certain stem cell markers at protein level. Among several epithelial stem cell markers screened in the tumor derived cell lines, the "+4" marker Bmi1 was the most highly expressed. Thus, Bmi1 was selected for protein analysis.

Cell lines treated with 100 nM RAD001 for 2h, 24h, and 72h were analyzed to check if the expression level of Bmi1 was changed. As shown in Figure 39, no significant change of the Bmi1 expression level was detected.

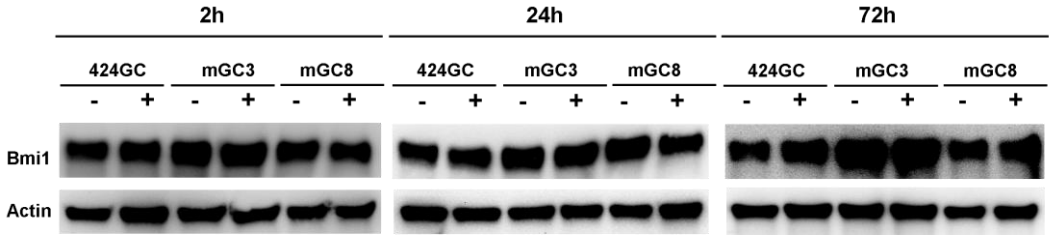

Figure 39. Western blot for Bmi1 expression in cell lines treated with 100 nM RAD001 for 2h, 24h and 72h. -: untreated cells; +: cells treated with 100 nM RAD001. Bmi1 was detected at 41-43 kDa. Actin was detected at 43 kDa.

Then, we asked if the situation was similar after a long term treatment. Cell lines from the long term RAD001 selection (RAD-400) as well as the tumor tissue from the second RAD001 experiment were used to analyze this effect both in vitro and in vivo. As shown in Figure 40, RAD001 resistant cells had the same Bmi1 expression level as the untreated cell line. In fact, the long term selection by RAD001 in vivo (48 days) did not change the Bmi1 expression level either (Figure 40).

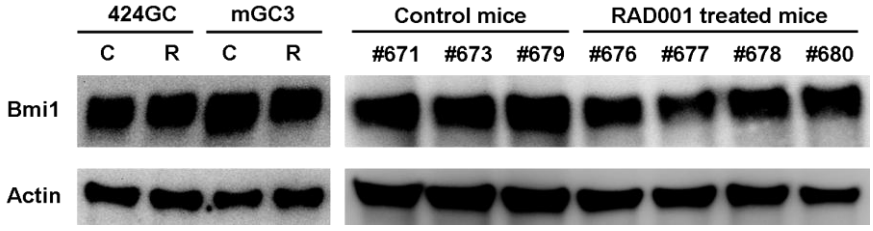

Figure 40. Western blot for Bmi1 expression in RAD001 selected cell lines and tumor tissue from RAD001 treated mice. C: Control (untreated cell lines); R: RAD001 selected cell lines (RAD-400); the numbers represent individual mice. Actin was used as control. Bmi1 protein was detected at 41-43 kDa. Actin protein was detected at 43 kDa.

So the RAD001 treatment had no effect neither in vitro nor in vivo on the differentiation of the tumor cells at least with regard to the Bmi1 expression. So it is obvious that the tumor cells do not change the phenotype and have to develop other machanisms for an escape from mTOR inhibition.

6.3.2 The feedback activation of Akt induced by single RAD001 treatment

Another possible mechanism for the escape of tumor cells from RAD001 treatment could be the loss of p70S6K-mediated negative feedback loop on the PI(3)K–Akt–mTOR pathway induced by single RAD001 treatment[137, 138]. This side effect could attenuate the anti-tumor efficiency of RAD001. To check if this effect also exists in our cell lines, western blot for Akt and phospho-Akt (Thr 308) was applied to the cell lines treated with 100 nM RAD001 for 2h, 24h, and 72h. As shown in Figure 41, after RAD001 treatment, a feed back activation of Akt could be detected.

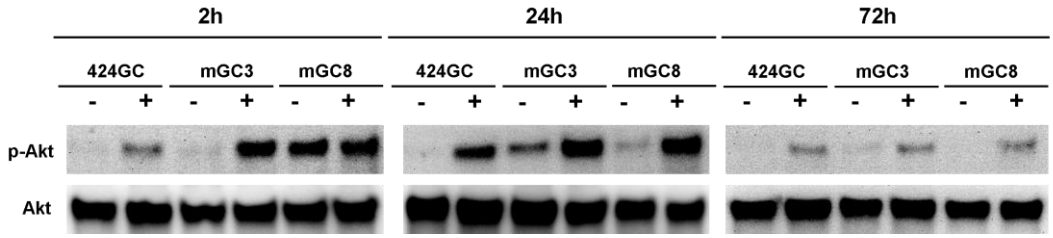

Figure 41. Western blot for phospho-Akt (Thr 308) on cell lines treated with RAD001. -: control; +: 100nM RAD001. Akt and p-Akt protein were detected at 60 kDa.

Since these data reflected only the short term effect of RAD001, it was interesting to check if the effect still existed in the long term RAD001 selected tumor cells. Protein samples from RAD-400 resistant cell lines were used for western blot. As shown in Figure 42, a feed back activation of phospho-Akt could still be observed in RAD001 resistant cell line of 424GC and mGC3, while in mGC8, this effect was not obvious.

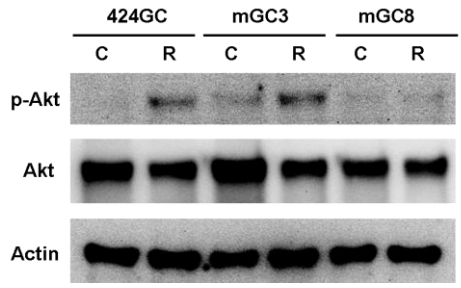

Figure 42. Phospho-Akt (Thr 308) expression in RAD001 selected cell lines. C: control cell lines without pretreatment; R: RAD-400 selected cell lines. Akt and p-Akt proteins were detected at 60 kDa.

However, this effect was not significant after long term RAD001 treatment in vivo. As shown in Figure 43, the phosphorylated Akt protein could be detected in all the tumor samples from the control mice. Tumor tissue from the RAD001 treated by mice displayed similar phospho-Akt expression level as observed in the control mice.

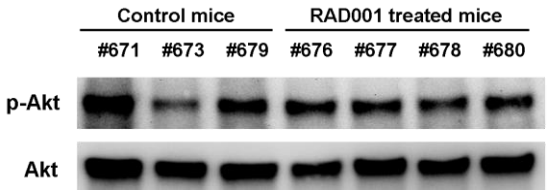

Figure 43. Expression of phospho-Akt (Thr 308) on tumor tissue. The numbers represent individual mice. Akt and p-Akt proteins were detected at 60 kDa.

In summary, single RAD001 treatment in vitro induced a feed back activation of the PI(3)K–Akt–mTOR pathway, although in vivo, this side effect was not significant.

6.3.3 Effect of long term RAD001 treatment on the activation of mTOR downstream target p70S6K

The results presented before showed that short term treatment of RAD001 in vitro could efficiently suppressed the mTOR-p70S6K signaling in the tumor derived cells. We then asked if the tumor cells were still sensitive to RAD001 after a long term selection. Thus, the activation of p70S6K in the RAD001 resistant cell lines was tested. RAD-400 resistant cell lines were used for western blot. Cells without treatment were used as control. As shown in Figure 44, the expression of active form

of p70S6K (p-p70S6K) was completely inhibited in the RAD-400 resistant cell lines. This indicated that the mTOR- p70S6K signaling was still well in control of RAD001 in these suvival tumor cells after long term selection. This pathway was not likely to be invovled in the escape mechanism for the resistant cell lines.

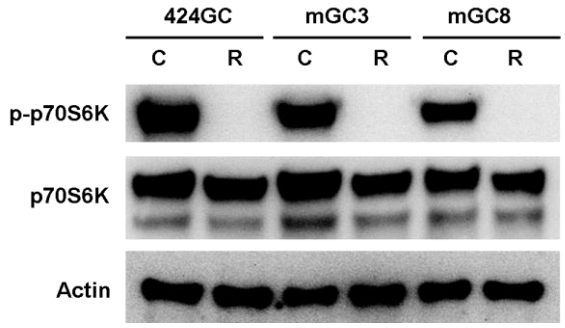

Figure 44. Western blot for phospho-p70S6K on RAD001 selected cell lines. C: control cell lines without pretreatment; R: RAD-400 resistant cell lines. p70S6K and p-p70S6K proteins were detected at 70 kDa.

6.3.4 Summary for the possible escape mechanisms

In looking for the possible escape mechanisms for the tumor cells from RAD001 treatment, the expression of stem cell markers, which was taken as a factor of the differentiation, was screened by RT-PCR. No apparent influence was observed after RAD001 treatment, neither in vitro nor in vivo. This indicated that RAD001 treatment had no influence on the differentiation of the tumor cells. On the other hand, a feed back activation of PI(3)K–Akt–mTOR signaling was observed after RAD001 treatment in vitro. This could be one of the explanations of why the anti-tumor effect of RAD001 was not curable.

6.4 Research on the tumor originating cells

Although the CEA424-SV40 TAg transgenic mouse model was established some years ago, and the gastric tumors developed in these mice have only been recently better characterized, it is still not clear which cell type forms the tumor originating cells. The in vivo experiment for RAD001 showed that although RAD001 could

significantly inhibit tumor development and prolong the survival time of the CEA424-SV40 TAg transgenic mouse, there were still some tumor cells which could escape from the therapy and finally lead to the death of the tumor bearing mice. This means that there might be a subpopulation of the tumor cells that may act like "cancer stem cells". Thus, looking for the tumor originating cells may not only be helpful for a better understanding of the tumorigenesis of neuroendocrine tumor but also important for establishing more targeted and efficient therapies.

The localization of the tumor in the gastric wall provided epithelial as well as mesenchymal stem cells as candidates for the tumor originating cells. Therefore, we looked for markers of these cells by several methods.

6.4.1 Epithelial stem cell markers in the tumor initiating cells of CEA424-SV40 TAg gastric tumor

There are two principal epithelial stem cell pools identified, one representing the crypt base columnar cells (CBCs) and the other the "+4" cells. Lgr5 is a classic marker for crypt base columnar cells. In the microarray analysis for the tumor tissue of 30, 60, 90 days old CEA424-SV40 TAg transgenic mice, the expression of Lgr5 was below the detection limit as shown in Figure 45 (probe sets exhibiting a fluorescence of >100 (RFU) were considered as positive in this assay). In the RT-PCR analysis for tumor derived cell lines, 35 cycles were needed to detect the Lgr5 expression which also indicated a low mRNA level.

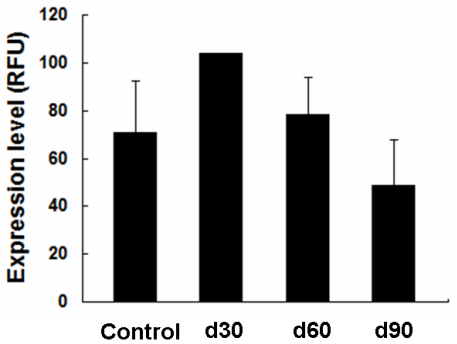

Figure 45. Expression level for Lgr5 in tumor tissue (microarray). RNA samples from antral tissue of normal mice and gastric tumors of 30, 60, 90 days old CEA424-SV40 TAg transgenic mice were used. n=3 for each age group.

Because there is no good anti-Lgr5 antibody available, the CEA424-SV40 TAg transgenic mice were crossed with Lgr5-EGFP-IRES-CreERT2 mice to analyze the Lgr5 expression. Although single Lgr5 positive cells could clearly be shown at the bottom of the gastric units, there was no GFP/TAg double-positive cell observed in the tumor area. Lineage tracing experiment could not provide supportive information for the hypothesis that the $Lgr5^+$ cells might give rise to the tumor either (data from E. Vetter and W. Zimmermann, unpublished results). Thus, the Lrg5 expressing CBC cells seem not to be promising candidates for the tumor originating cells in CEA424-SV40 TAg transgenic mice although they can still not be fully excluded.

Besides $Lgr5^+$ cells, $Bmi1^+$ cells have also been discussed as potential epithelial stem cells. In fact, when we screened the expression levels of many epithelial stem cell markers in cell line 424GC, mGC3 and mGC8 by RT-PCR, Bmi1 was found to be the most highly expressed marker (Figure 46). As shown in the figure, Bmi1 was much higher expressed than Lgr5, which was barely detectable even after 30 cycles' amplification. Thus, Bmi1 expression was further analyzed in CEA424-SV40 TAg gastric tumor in more detail to check if the Bmi1 positive cells could be the candidates for the tumor originating cells in this model system.

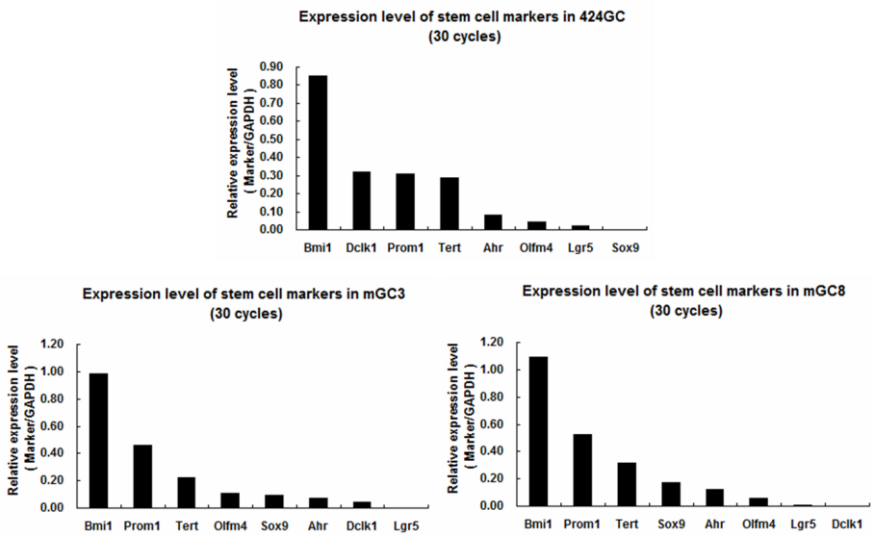

Figure 46. RT-PCR analysis for epithelial stem cell markers in cell lines derived from the tumor. Cell line 424GC, mGC3 and mGC8 were analyzed. OD values were normalized for the GAPDH expression to calculate the relative expression level for each marker.

6.4.1.1 RT-PCR for Bmi1 expression in tumor tissue and cell lines derived from the tumor

RT-PCR was carried out for detecting the Bmi1 expression in mRNA level with RNA samples from tumor tissue of four CEA424-SV40 TAg transgenic mice (day 96-107) and three cell lines derived from the primary tumor. As shown in Figure 47, Bmi1 expression could be detected in both the tumor tissue and the cell lines. Its expression level in the cell lines was even higher than in the tumor tissue, and could already be detected after 25 cycles. This may due to the fact that the cell lines were pure populations while the tumor tissue was mixed with supporting cells around the tumor cells.

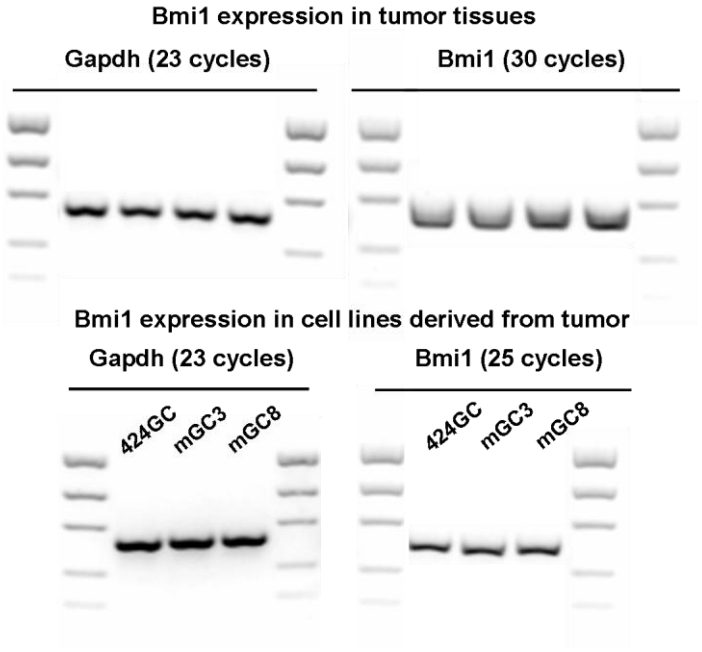

Figure 47. RT-PCR analysis for Bmi1 expression in the tumor tissue and cell lines derived from the tumor. Tumor tissue of four CEA424-SV40 TAg transgenic mice (day 96-107) and three tumor derived cell lines 424GC, mGC3, mGC8 were used. Marker bands correspond to 1000bp, 700bp, 500bp, 300bp, 200bp from top to bottom.

So the tumor samples as well as the cell lines derived from the tumor expressed a high Bmi1 mRNA concentration.

6.4.1.2 Bmi1 protein in tumor tissue and cell lines derived from the tumor

The expression of Bmi1 in CEA424-SV40 TAg gastric tumor was further analyzed by western blotting. Protein samples were obtained from tumor tissue of three 98 days old CEA424-SV40 TAg transgenic mice (#671, #673, #679) and three cell lines derived from the tumor (424GC, mGC3, mGC8). As shown in Figure 48, all the tumor tissue samples and the cell lines highly expressed Bmi1.

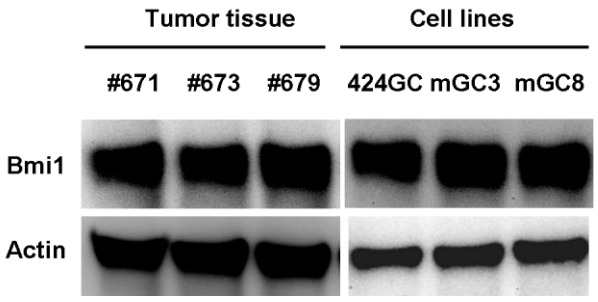

Figure 48. Western blot for Bmi1 expression in both tumor tissue and tumor derived cell lines. The numbers represent individual mice. Cell line 424GC, mGC3 and mGC8 were used. Actin was used as control. Bmi1 protein was detected at 41-43 kDa.

6.4.1.3 Immunostainings for Bmi1 expression in tumor tissue and cell lines derived from the tumor

To prove the correct expression of Bmi1 in tumor tissue, +4 cells, for which Bmi1 is a solid marker, were used as positive control. As shown in Figure 49, "+4" cells could be correctly detected in both stomach and duodenum by immunohistochemistry.

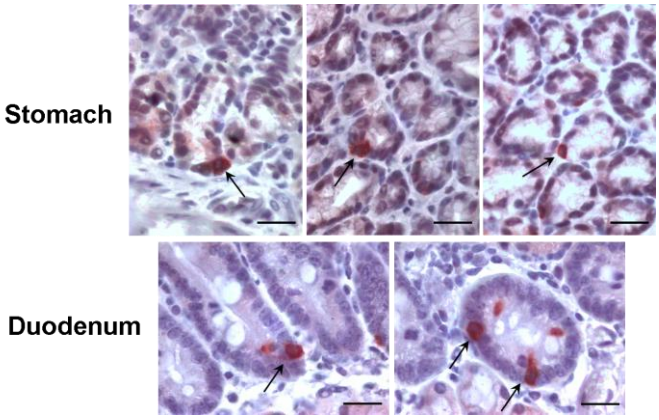

Figure 49. Immunohistochemistry for Bmi1 on normal tissue of stomach and duodenum. Positive cells (arrow) could clearly be detected at "+4" position. Scale bars: 20 μm.

Bmi1 staining was then applied to the tumor tissue from CEA424-SV40 TAg transgenic mice. In Figure 50, Bmi1 expression was detected in small tumor islands, while in Figure 51, numerous Bmi1 positive cells were found in big tumor masses.

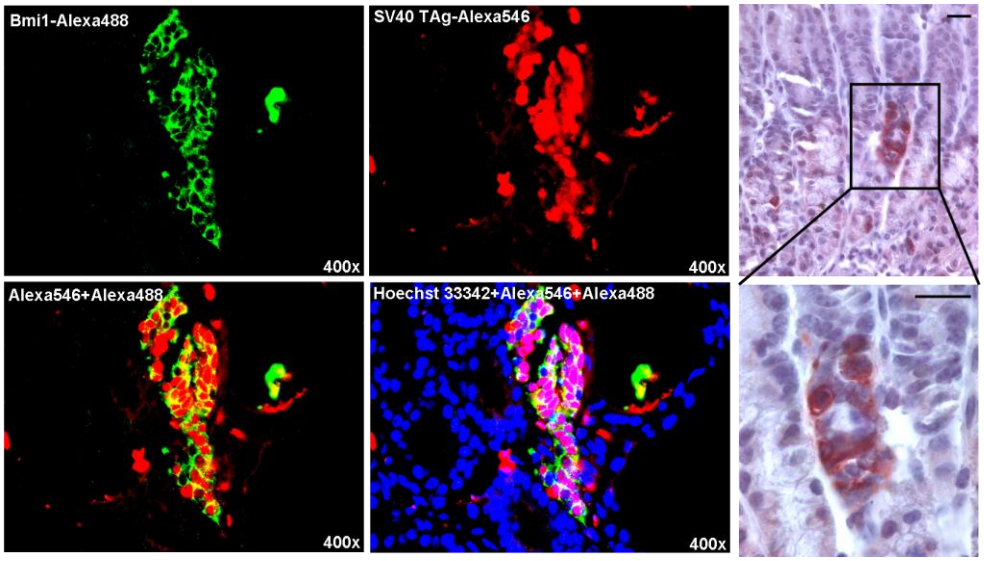

Figure 50. Bmi1 staining in the stomach of 92 days old CEA424-SV40 TAg transgenic mouse. Left: Double immunofluorescent labeling for SV40 TAg and Bmi1 identified small tumor island expressing Bmi1. Bmi1: green (Alexa-488), SV40 TAg: red (Alexa-546), DNA: blue (Hoechst), images of 400× magnifications are shown; Right: immunohistochemical staining for Bmi1 showed a small positive area. Scale bars: 20 μm.

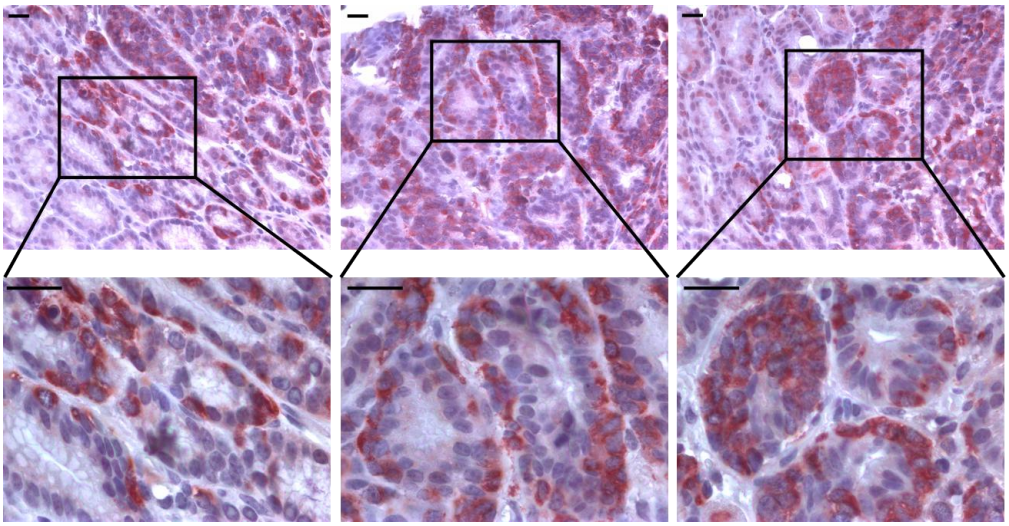

Figure 51. Immunohistochemical staining for Bmi1 in the gastric tumor of a 92 days old CEA424-SV40 TAg transgenic mouse. Scale bars: 20 μm.

Double immunofluorescent staining for SV40 TAg and Bmi1 on stomach sections from 92-107 days old CEA424-SV40 TAg transgenic mice identified Bmi1 and SV40 TAg double positive cells (Figure 52), which clearly shows that these tumor cells expressed Bmi1.

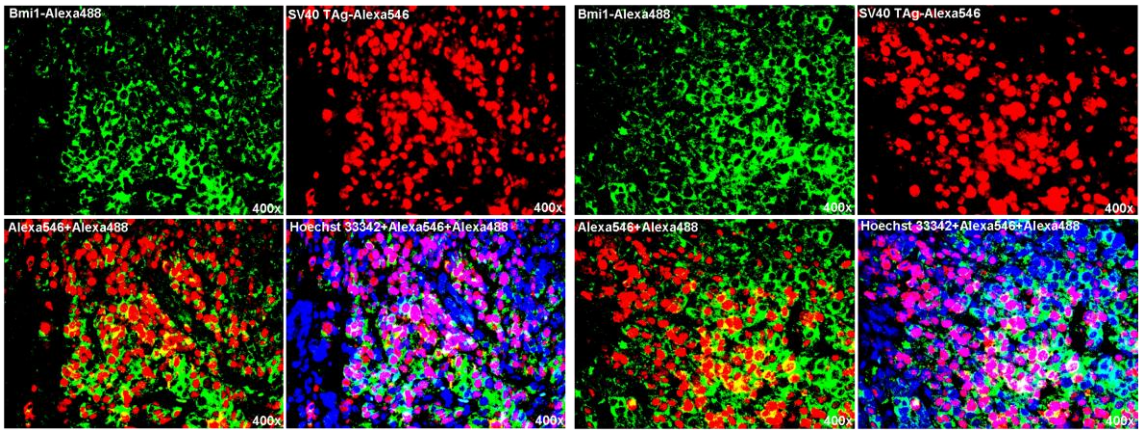

Figure 52. Double immunofluorescent staining for SV40 TAg and Bmi1 in the tumors from a 92 days old CEA424-SV40 TAg transgenic mouse. Two tumor areas are shown here. Bmi1: green (Alexa-488), SV40 TAg: red (Alexa-546); DNA: blue (Hoechst 33342). Images of 400× magnifications are shown.

It is worth pointing out that quite a number of Bmi1 single positive cells were also observed around the tumor area or between two tumor areas (Figure 53-54), which suggests that these Bmi1 positive cells might contribute to the tumorigenic microenvironment.

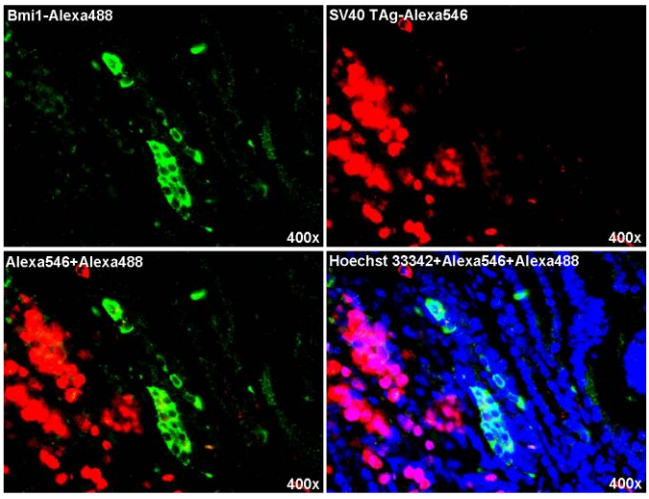

Figure 53. Double immunofluorescent staining for SV40 TAg and Bmi1 in the tumor from a 107 days old CEA424-SV40 TAg transgenic mouse. Bmi1: green (Alexa-488), SV40 TAg: red (Alexa-546), DNA: blue (Hoechst). Images of 400× magnifications are shown.

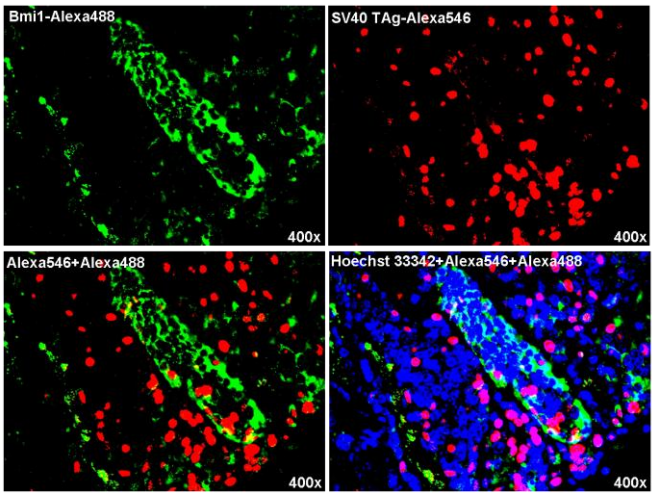

Figure 54. Double immunofluorescent staining for SV40 TAg and Bmi1 in the tumor from a 107 days old CEA424-SV40 TAg transgenic mouse. Bmi1: green (Alexa-488), SV40 TAg: red (Alexa-546), DNA: blue (Hoechst 33342). Images of 400× magnifications are shown.

Besides, Bmi1 staining was also applied to the cell lines derived from the tumor. A strong expression of Bmi1 was found in all the three cell lines as shown in Figure 55. This was a clear nuclear staining with 100% positive rate.

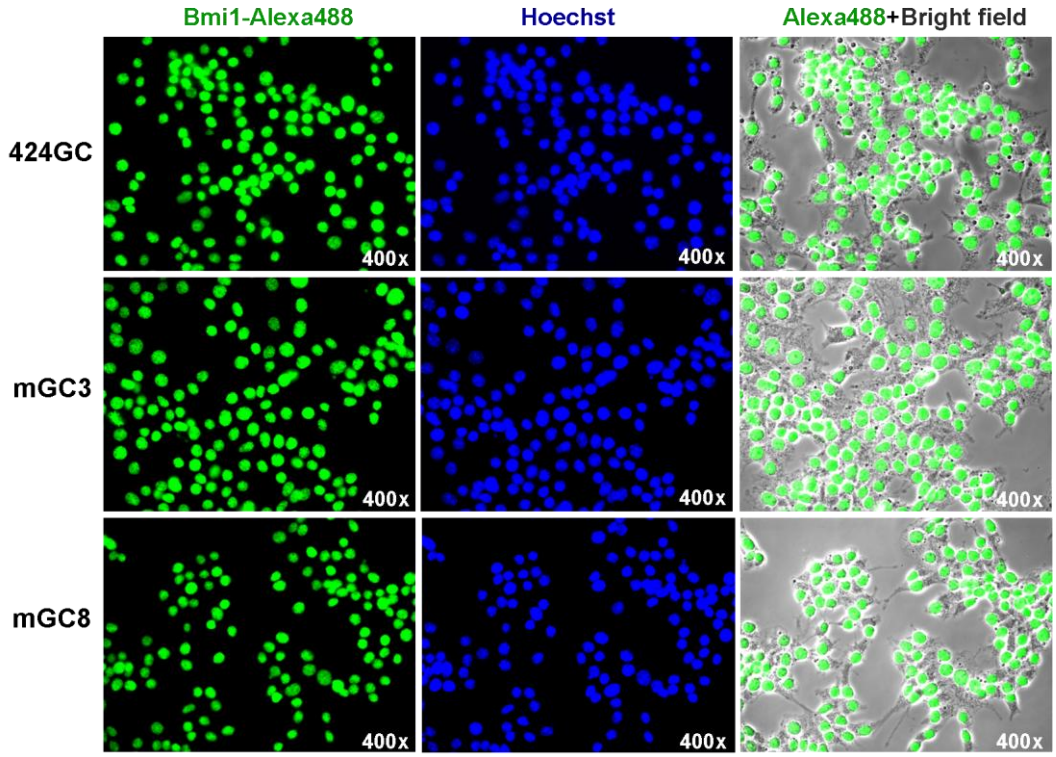

Figure 55. Immunofluorescent staining for Bmi1 on cell line 424GC, mGC3 and mGC8. Bmi1: green (Alexa-488), DNA: blue (Hoechst). Images of 400× magnifications are shown.

So in the tumor tissue an appreciable amount of SV40 TAg positive tumor cells were found to express Bmi1 while in the isolated tumor cell lines a 100% positive rate was observed.

6.4.1.4 Bmi1-TAg interaction

Data presented above showed that Bmi1 was expressed both in the tumor tissue and the cell lines. However, it was not clear whether there is a relationship between Bmi1 expression and the activation of the TAg. To answer this question, cells were transfected with siRNA targeting the TAg. RNA was isolated 72 h after transfection and analyzed by testing the expression of several genes on a cDNA array. As shown in Figure 56, knockdown of TAg significantly decreased the Bmi1 expression level (Control group: 226.77±11.32; TAg siRNA group: 117.32±19.52, $p<0.005$). This suggests that TAg could drive the expression of Bmi1 and Bmi1 positive cells could be the target of the TAg induced transformation.

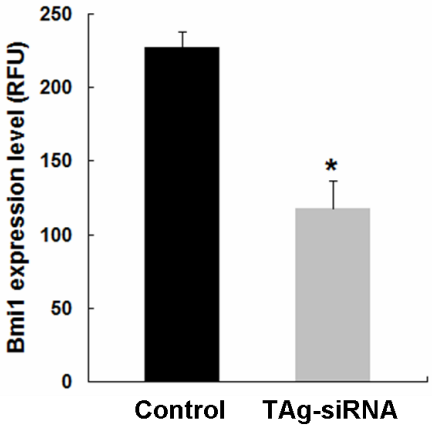

Figure 56. Microarray analysis for Bmi1 expression level in cell line 424GC when TAg was knocked down by siRNA assay. n=3 for each group, *$p<0.005$.

As knocking down TAg could suppress Bmi1 expression, we then asked if this effect also works in the opposite direction. Therefore, the expression of Bmi1 was knocked down by esiRNA assay in cell line 424GC and mGC3. esiRNA is a new method for knocking down specific targets. It is a mixture of several synthetic siRNA targeting the same mRNA sequence and is suggested to be more efficient and with less off-target effects[139]. Cells were treated with different concentrations of Bmi1-esiRNA

(100, 200 or 400 ng/well) for 48 and 96h and harvested for western blotting. As shown in Figure 57, although 48h transfection did not apparently affect the Bmi1 expression, 96h transfection with 200 and 400 ng Bmi1-esiRNA significantly reduced the Bmi1 expression level in both the cell lines. However, the expression of SV40-TAg was not changed in spite of Bmi1 knockdown.

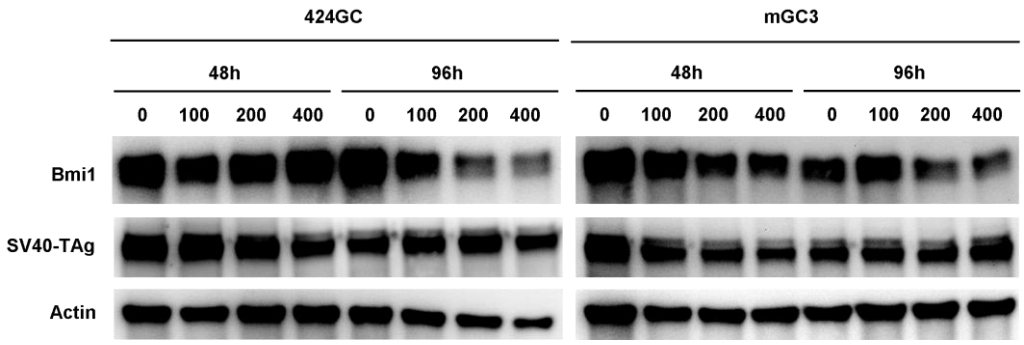

Figure 57. SV40-TAg expression in Bmi1 knocked down cell lines. Protein samples from cell line 424GC and mGC3 were used for western blotting. 0: control; 100, 200 and 400: amount of Bmi1-esiRNA (ng) in each well. Bmi1 and SV40-TAg proteins were detected at 41-43 and 94 kDa, respectively. Actin was used as control.

These results indicate that the Bmi1 expression had no strong effect on the TAg expression. Bmi1 expression is more likely a consequence of the TAg expression.

6.4.2 Mesenchymal stem cell markers in the tumor initiating cells of CEA424-SV40 TAg gastric tumor

Although the results above showed that the tumor cells were clearly Bmi1 positive, it is still intensively debated whether Bmi1 positive "+4" cells represent a true epithelial stem cell population. Bmi1 may be a marker for a more advanced epithelia as well as tumor cell populations. The position of the tumor cells in young mice as well as the screening for stem cell marker expression offered additional candidates for the tumor initiating cells of CEA424-SV40 TAg gastric tumor. One of these candidates is the Etv1 positive mesenchymal stem cell.

6.4.2.1 The distribution of SV40 TAg positive cells observed in the muscularis mucosae of antrum and duodenum

When immunohistochemical staining for SV40 TAg was applied to the stomachs of CEA424-SV40 TAg transgenic mice for the identification of the tumor cells, some SV40 TAg positive cells were also found in the muscularis mucosa layer. In young mice aged 30-60 days, these SV40 TAg positive cells were mostly observed in the muscularis mucosae of the antrum, right below the tumor area. Few single SV40 TAg positive cells were also observed in the muscular layer of the duodenum. When the mice got older, these SV40 TAg positive cells could no longer be found in the muscularis mucosa layer of the antrum region while in the duodenum, especially in the part close to the antrum region where the mucosa of the duodenum was hyperplastic, these SV40 TAg positive cells infiltrated into the mucosa layer (Figure 58).

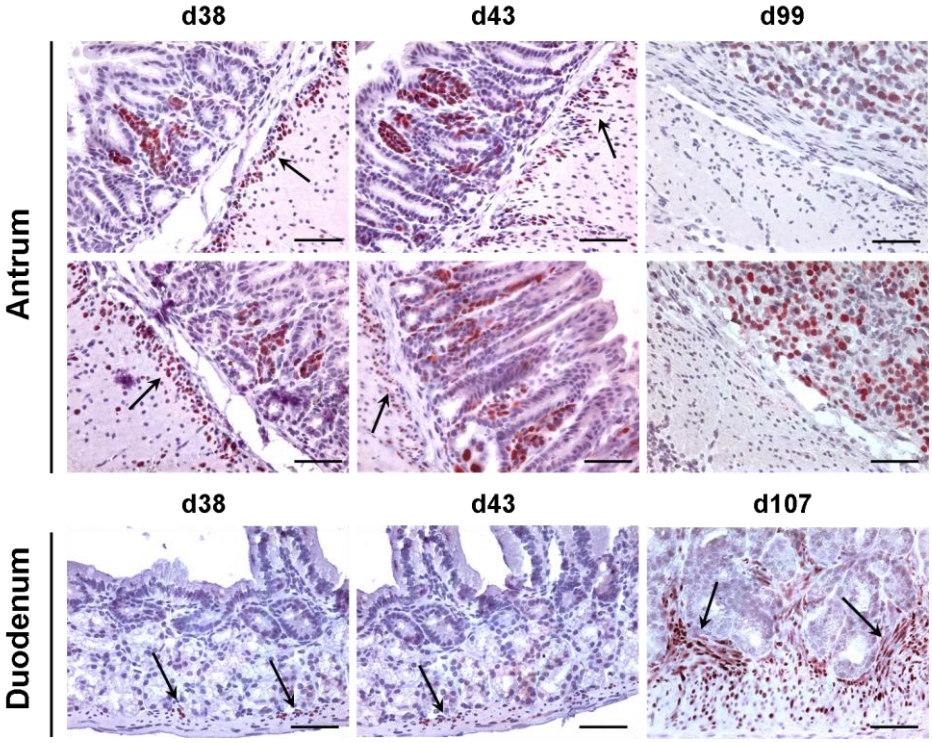

Figure 58. SV40-TAg expression in tissue sections from CEA424-SV40 TAg transgenic mice. SV40 TAg positive cells (arrow) were found in the muscularis mucosa layer of antrum and duodenum. The age of the mice is shown on top of the pictures. Scale bars: 50 µm.

The location of these early tumors in the muscularis mucosa layer forced us to ask whether the tumor cells are of mesenchymal origin. This was further enhanced by the fact that Cajal cells, which are of mesenchymal origin[140], are presumed to be the originating cells for another tumor in this area called gastrointestinal stromal tumour (GIST)[130]. Based on the fact that the SV40 TAg positive cells described above are in the same position as Cajal cells, and are in the neighbourhood of the tumor cells, we suspected that they might be the tumor initiating cells transformed by TAg. So the basic hypothesis was that these cells or a small population of these cells might migrate into the pyloric mucosa, settle down and give rise to the gastric tumors. In fact, c-Kit, a marker for Cajal cell, was expressed in d30, 60, and 90 CEA424-SV40 TAg gastric tumors according to the data from microarray analysis. A significant increase of the c-Kit expression level was observed in d90 gastric tumors when compared with normal antrum tissue (Figure 59). We then tried to stain the CEA424-SV40 TAg gastric tumor with anti-c-Kit antibody. However, neither the tumor cells in the epithelial layer nor the SV40 TAg positive cells in the muscularis mucosa layer were positively stained. So at the moment it is not clear whether this protein is expressed.

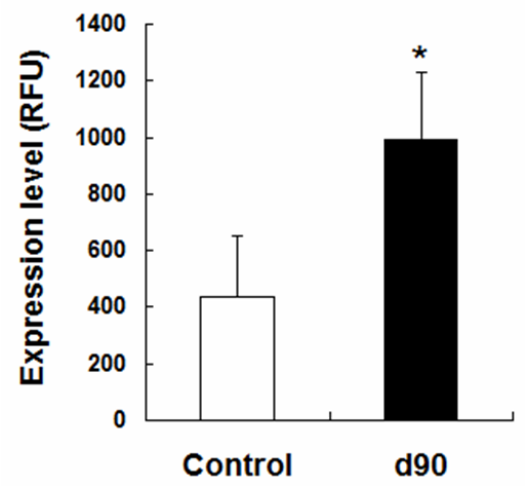

Figure 59. Transcriptome analysis for c-Kit expression. Tumor tissue from d90 CEA424-SV40 TAg transgenic mice and normal antrum tissue from non-transgenic mice were analyzed. n=3 for each group, * $p<0.05$.

6.4.2.2 Etv1 expression in CEA424-SV40 TAg gastric tumor

Although the tumor cells were negative for c-Kit staining, the up-regulated expression of c-Kit in mRNA level in the tumor tissue as well as the appearance of the SV40 TAg positive cells observed in the muscularis mucosa layer of antrum and duodenum, suggested the possibility that other cells of mesenchymal origin may give rise to the CEA424-SV40 TAg gastric tumor.

One newly described mesenchymal stem cell marker Etv1, has been reported as a crucial regulator during the tumorigenesis of GIST in cooperation with Kit[130]. Interestingly, in our transcriptome analysis, Etv1 was present in the tumor tissue over time from d30, d60 and d90 CEA424-SV40 TAg transgenic mice. As shown in Figure 60, the expression level of Etv1 in the tumor tissue increased with the tumor development. A significant increase was observed from d60 on, with an even further rise to day 90.

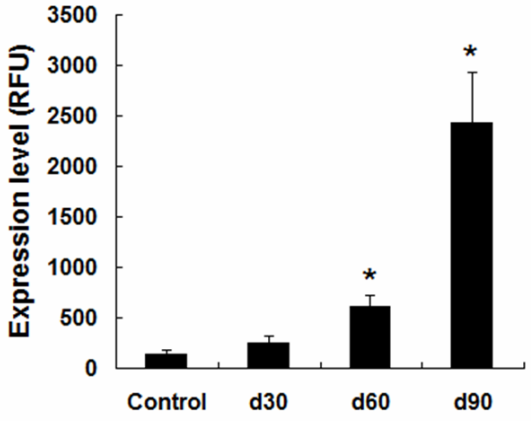

Figure 60. Transcriptome analysis for Etv1 expression. Tumor tissue from d30, 60, 90 CEA424-SV40 TAg transgenic mice and normal antrum tissue from non-transgenic mice were analyzed. n=3 for each time point, * p<0.05, d60, d90 group compared with control group.

Based on an elevated mRNA expression level of Etv1 in the tumor tissue, the analysis of the protein expression was followed. Immunofluorescent staining for Etv1 was applied to tumor tissue from CEA424-SV40 TAg transgenic mice. As shown in Figure 61, Etv1 could be clearly stained in the tumor area. This stainning was defined to the nucleus of the tumor cells, which is characteristic for a transcription factor. In

addition, the same staining could be shown in the cell lines derived from the tumor with 100% positive rate (Figure 62).

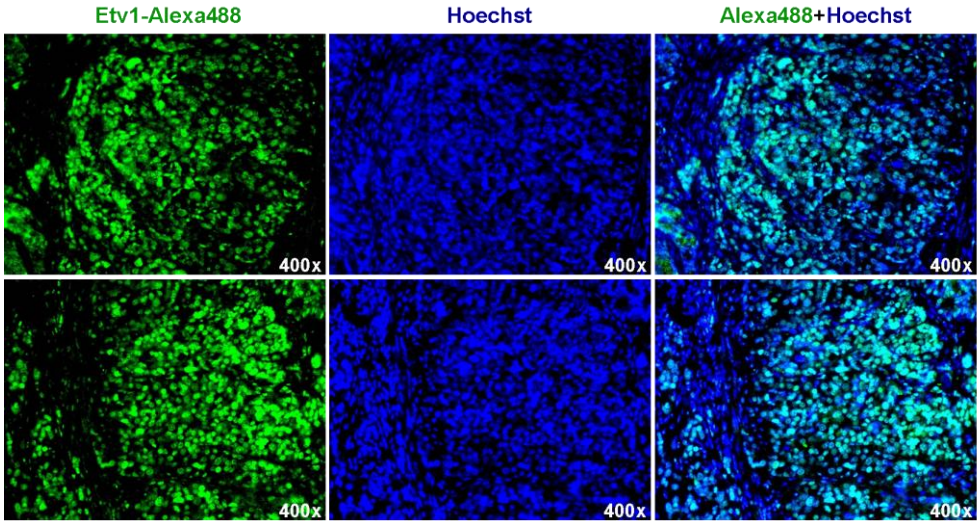

Figure 61. Etv1 staining in gastric tumor from a 92 days old CEA424-SV40 TAg transgenic mouse. Etv1: green (Alexa488); DNA: blue (Hoechst). Images of 400× magnifications are shown.

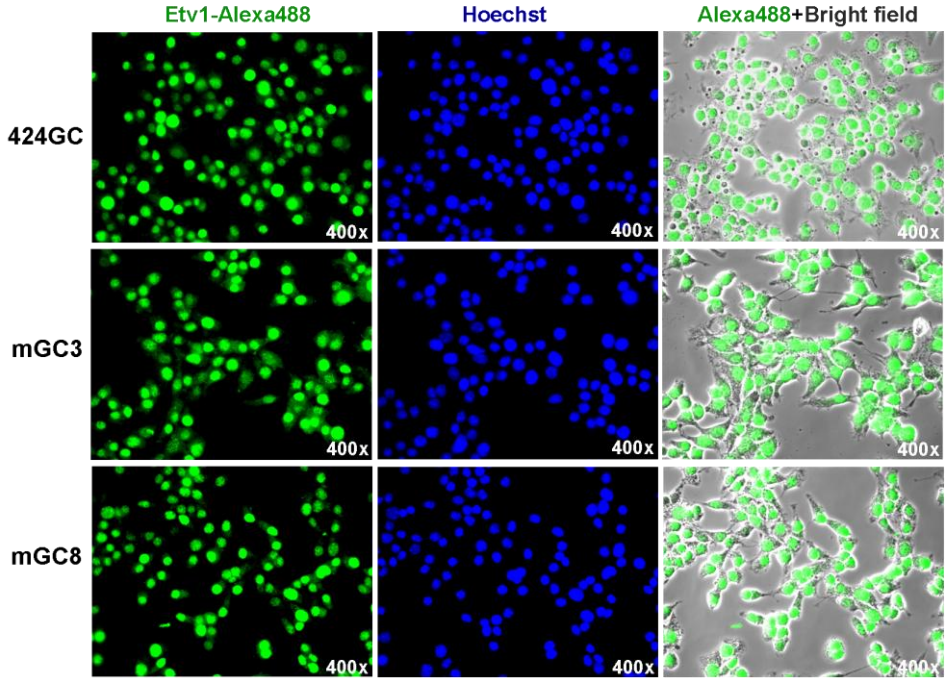

Figure 62. Etv1 staining in three cell lines derived from CEA424-SV40 TAg gastric tumor. Etv1: green (Alexa488); DNA: blue (Hoechst 33342). Images of 400× magnifications are shown.

In summary, the mesenchymal stem cell marker Etv1 was found to be highly expressed in the tumor tissue and isolated tumor cell lines. More interestingly, Etv1 expression level was up-regulated over the time course of the tumor development. From these, Etv1 positive mesenchymal stem cells seem to be a possible candidate for the transformation induced by TAg.

6.4.3 Summary for the tumor originating cells

Here, two hypotheses were presented. In the first part, the "+4" marker Bmi1 was shown to be highly expressed in gastric tumors developed in CEA424-SV40 TAg transgenic mice as well as in the cell lines derived from the primary tumor. Bmi1 expression could also be down-regulated by knockdown of TAg, thus showing the interrelationship. However, there is still an intensive debate on whether Bmi1 positive cells represent a real epithelial stem cell population. On the other hand, the SV40 TAg positive cells observed in the muscularis mucosa layer in the neighbourhood of the tumor cells, as well as the expression of mesenchymal markers in the transcriptome analysis revealed the possibility of mesenchymal stem cells as tumor initiating cells of CEA424-SV40 TAg gastric tumor. Our results showed that the mesenchymal stem cell marker ETV1 was expressed in the tumor tissue and cell lines derived from the tumor. The expression level of ETV1 in the tumor tissue also increased over the time course of the tumor development. Since the CEA-promotor used for the generation of the T-antigen transgenic animals contains Etv1 binding sites, it is tempting to speculate, that this may drive the transcription of the T-antigen. Further studies using e.g. lineage tracing are needed to make this conclusion more solid.

7 DISCUSSION

7.1 In depth characterization of the CEA424-SV40 T Ag transgenic mouse showed a clear neuroendocrine phenotype which made it a clinically relevant model for gastric neuroendocrine tumors

GEP-NETs is a rare disease with an incidence of about 2.5 to 5 cases per 100 000. However, as has been introduced before, the incidence and prevalence of GEP-NETs has increased substantially during the past 30 years. The progress in the management of this disease has been slow and this may to a large extent be due to the limited understanding of the cellular and molecular biology of neuroendocrine cells and the mechanism of tumorigenesis. Thus, neuroendocrine tumor cell lines and animal models are urgently needed for preclinical study. The two most frequently used neuroendocrine cell lines are BON1 and GOT1. BON1 is derived from a human pancreatic carcinoid[141], but it is not a pure neuroendocrine cell line and additional mutations may have been aquired during the in vitro cultivation[3]. GOT1 is derived from a liver metastasis of a human midgut carcinoid and is maintained as a mouse xenograft[3]. Although there are several mouse models which develop tumors with a neuroendocrine phynotype in the pancrease[142, 143] and prostate[50-52, 144, 145], there are very few mouse models for gastrointestinal carcinoids, expecially for gastric neuroendocrine tumors[54]. The shortage of in vitro and animal models is one of the major barrier for research in this area.

SV40 TAg is a potent oncogene that has often been used to generate organ-specific cancers in transgenic mice. The CEA424-SV40 TAg transgenic mouse presented here was established by Thompson et al in 2000. A 424-bp CEA promoter was used to drive the expression of SV40 TAg. One transgenic line (L5496) developed tumors in the pyloric region of the stomach in 100% of the offspring[30]. These gastric tumors were tentatively classified as adenocacinomas in a large part due to the transgenic

CEA and the expression of EpCAM and CEACAM1 in cell lines derived from the primary tumor[31, 37].

In order to characterize these tumors in more detail, genome-wide expression analysis with RNA from tumor-bearing mice and normal littermates were performed. To our surprise, transcriptome analyses revealed an enrichment of typical gene signature for neuroendocrine tumors. Gene expression analysis of 424GC, a cell line derived from the primary tumor, showed similarity to the gene expression profile in the tumor tissue from 90-day-old CEA424-SV40 TAg-transgenic mice, which reflects the neuroendocrine phenotype of the parental tumor. Furthermore, when SV40 T antigen expression was knocked down by siRNA, a down-regulation of neuroendocrine gene expression in this cell line was observed[37].

These previous studies inspired the work presented in this thesis. The CEA424-SV40 TAg gastric tumor was further analyzed for the expression of neuroendocrine markers, the proliferation status which is important for the grading, and its ability to cause aberrant physical signs like hormone levels. Data from the first part of the result section demonstrated that the CEA424-SV40 TAg transgenic mice developed solid tumors in the antral region of the stomach which are of high proliferative capacity. These gastric tumors expressed several neuroendocrine markers including chromogranin A, chromogranin B, secretin and glucagon. Overexpression of secretin and Tph1 as observed in the transcriptome microarray analysis led to elevated hormone levels of secretin and serotonin as shown in the ELISA experiment. One of the consequences of high secretin secretion is the suppression of gastric acid out put. As it is quite difficult to measure the pH in the stomach directly, the expression of a key component of the acid production, H^+-K^+-ATPase, was evaluated. As expected, a decreased H^+-K^+-ATPase positive cell number was observed in the CEA424-SV40 TAg transgenic mice comparing to the non-transgenic mice. Thus, the tumor shows strong hormone activity. Furthermore, the CEA424-SV40 TAg gastric tumor and tumor derived cell lines express transcription factors with crucial roles in neuroendocrine cell differentiation. All these information indicate that the

CEA424-SV40 TAg gastric tumors exhibit a neuroendocrine phenotype which make the CEA424-SV40 TAg transgenic mouse a clinically relevant model for gastric neuroendocrine tumors.

7.2 Possible connection between SV40 TAg transforming ability and the neuroendocrine features of the mouse tumor model

The reason why CEA424-SV40 TAg gastric tumor turns out to be a neuroendocrine carcinoma is not well understood. It is not likely that the very short CEA promoter used in this mouse model takes a leading role in the development of the neuroendocrine features because CEA is a tumor marker widely used for adenocarcinomas[30]. Then, the question was whether the neuroendocrine phenotype is a result from the specific effects of the TAg.

The transforming ability of SV40 TAg is in large part due to its involvment in inactivating cellular tumor suppressors like p53 and retinoblastoma (RB) proteins. There have been reports that abnormalities of the p53 and RB pathway are frequently detectable in neuroendocrine tumors. Tang et al tested 92 cases of well-differentiated Pan-NETs, and found that 68% of the samples were positive for phospho-RB. They were also able to show that RB phosphorylation coincided with high expression of Cdk4, which is responsible for phosphorylating RB[146]. As regard to the poorly differentiated neuroendocrine carcinomas (NECs) of the pancreas, the study from Yachida et al showed high frequences of abnormal immunolabeling patterns of p53 and RB (95% and 74%, respectively). This observation correlated with the intragenic mutations of TP53 and RB1 genes[147]. Another tumor with a neuroendocrine phenotype is the small cell lung carcinoma (SCLC). It is the most aggressive type of lung cancers with poor prognosis. Numerous investigations have shown that dysfunction of both the RB1 and TP53 gene are crucial for the carcinogenesis of SCLC[148, 149]. By inactivating both p53 and Rb1 gene, Zhou et al successfully

developed mouse prostate tumor models with carcinomas showing both luminal epithelial and neuroendocrine differentiation[150]. As p53 and retinoblastoma (RB) proteins are among the major targets of SV40 TAg, their roles in the tumorigenesis of these neuroendocrine tumors may explain why SV40 TAg is capable of inducing neuroendocrine tumors in transgenic mouse models.

This hypothesis can also get some supportive informations from our CEA424-SV40 TAg transgenic mouse model system. Former transcriptome microarray analysis showed that Cdk4, which is responsible for the phosphorylation of Rb1, is highly expressed in the tumor tissue and cell lines from the tumor. More interestingly, Cdk4 expression level went down after TAg was blocked by siRNA in the cell line 424GC. The kockdown of TAg expression also contributed to a reduced expression level of genes considered to be typically active in neuroendocrine tumors[37]. These information indicate that there is an obvious connection between the TAg expression and the neuroendocrine phenotype.

However, the hypothesis given above might not apply in general because loss of Rb1 function not always results in a neuroendocrine phenotype. For example, Hill et al showed that inactivation of the Rb1 family proteins (Rb/p107/p130) in genetically engineered mice led to prostate adenocarcinomas with no evidence of neuroendocrine tumors[151]. One possible explanation for this is that the chance for a neuroendocrine feature might be bigger when both p53 and Rb1 are suppressed, which is the case for SV40 TAg induced transformation. Therefore it seems quite plausible that the changes by the expression of the SV40 TAg in the model presented here heavily contributes to the neuroendocrine phenotype.

7.3 Testing of molecularly targeted therapy on CEA424-SV40 TAg transgenic mouse model offered promising candidates for the treatment of neuroendocrine tumors

The CEA424-SV40 TAg transgenic mice develop spontaneous tumors in the stomach. This mirrors the pathophysiology of the tumor disease probably much better than the xenograft models. In addition, several cell lines derived from the tumor were also well established which is another advantage. These in vitro and in vivo systems offered the opportunity to test new targeted treatment protocols for gastric neuroendocrine tumors in a preclinical setting.

To choose reasonable targets for testing novel therapies, agents belonging to the following two families were taken into consideration: agents targeting molecular markers for NET (like mTOR inhibitors and HSP90 inhibitors) and agents targeting certain signaling pathways aberrantly regulated by SV40 TAg (like E2F inhibitors and the p53 stabilizer Nutlin-3). These selected agents induced anti-proliferation effects in vitro which revealed their potential for in vivo study.

The majority of the in vivo experiments included in this thesis focused on the use of mTOR inhibitors. The crucial role taken by the PI(3)K–Akt–mTOR pathway has been implicated in the tumorigenesis of many malignancies. Former studies have also revealed the link between aberrant PI(3)K–Akt–mTOR signaling and neuroendocrine tumors[72, 152-155]. The PI(3)K–Akt–mTOR pathway is also shown to be active in the CEA424-SV40 TAg gastric tumor cells as all the tumor derived cell lines tested displayed a high expression level of the phosphorylated p70S6K, which is a hallmark of TOR-activation. In the in vitro study, the mTOR inhibitors RAD001 and NVP-BEZ235 (Novartis) suppressed cell proliferation and induced cell apoptosis in all the three cell lines at clinically relevant low concentrations. All these information provided a rationale for testing their anti-tumor efficiency in vivo.

Two different experimental setting were used for the RAD001 in vivo studies. In the

first set up (experiment A), mice were sacrificed when they lost 20% of their peak weight. This was the end point according to the legal restrictions by animal rights. From this setting, the effect of the treatment on survival time could be learned. In the second set up (experiment B), the experiment was stopped when the mice reached the same age (d98, this was when the first control mouse started to lose weight) for a timely more precise analysis of the molecular biological changes of the tumor cells. Daily feeding the CEA424-SV40 TAg transgenic mice with 10 mg/kg RAD001 significantly prolonged the survival time of the tumor bearing mice by 35 days on average. Significantly decreased tumor weights were observed in the second experiment with a 48-day treatment. RAD001 treatment in vivo had a slight influence on the neuroendocrine phenotype of the tumor as the expression levels of glucagon and Nkx2.2 were reduced.

To dig into the mechanism of how RAD001 induced the anti-tumor effects both in vitro and in vivo, the active state of two major mTORC1 substrates, the eukaryotic translation initiation factor 4E (eIF4E)-binding protein(4EBP1) and p70 ribosomal S6 kinase (p70S6K)[137, 138], was checked. In the in vitro study, a suppressed phospho-4EBP1 expression was observed 72 hours after RAD001 treatment while a complete elimination of phosphorylation of p70S6K could already be achieved even after 2 hours treatment. This clearly shows that the treatment of RAD001 was efficient in vitro. In the in vivo experiment, daily RAD001 treatment also significantly decreased the expression of the active form of p70S6K (p-p70S6K). The active p70S6K promotes translation and growth by phosphorylating cellular substrates, such as S6. A significantly decreased number of phospho-S6 positive cells in the tumor areas were observed in the RAD001 treated mice when compared with the control mice, which indicates a suppressed S6 ribosomal protein function. As both p70S6K and 4EBP1 are essential for regulating cell growth and proliferation, their suppression can explain the therapeutic effects induced by RAD001 both in vitro and in vivo. On the other hand, not all of these substrates were suppressed in vivo. The mTOR-4EBP1 and mTOR-p70S6K pathway were still active in some tumor cells. This observation

showed either that the local concentration was too low or single cells escape from the active drug.

7.4 Possible escape mechanism for the tumor cells under RAD001 treatment

In the in vivo experiment, the RAD001 treatment did not eliminate all the tumor cells and the RAD001 treated mice still developed highly proliferative tumors which eventually led to the death of these mice. This is similar to the situation in the clinic. Although the treatment with everolimus prolonged the progression-free survival of the patients[62], the patients were not cured.

There were several possibilities for the incomplete elimination of tumor cells in the in vivo experiment. First, the concentration used in the in vivo experiment may not be high enough. RAD001 could kill 100% of the tumor cells in vitro at a concentration of 10μM. An estimate of the serum concentration after total absorption clearly gave a concentration higher than 10μM. In the complex in situ environment, however, the real drug concentration may be too low to cause a lethal effect, especially when the tumor cells were under the protection of supportive cells around them. In addition, the metabolic process may reduce the drug activity. To answer this question, tumor tissue as well as other organs like liver and kidney were taken from the RAD001 treated mice and analyzed by MALDI Imaging technique to see if RAD001 could be detected in these tissues. The signal for RAD001, however, was quite low in the tested tissue (data not shown). Another form of escape mechanism is the loss of the p70S6K-mediated negative feedback loop on the PI(3)K–Akt–mTOR pathway. IRS-1 can activate the PI(3)K–Akt signaling through IGF-1. By phosphorylating IRS-1, S6K1 destabilizes IRS-1 and blocks its effect on the PI(3)K–Akt signaling[138]. An increase of phospho-Akt expression could clearly been shown in the RAD001 treated tumor cells which indicates that single RAD001 treatment induced the feedback

activation of PI(3)K–Akt–mTOR signaling and this may explain why the elimination of tumor cells was not complete. This effect has also been reported in other neuroendocrine tumor cell lines which may attenuate the anti-tumor efficacy of the drug[137].

However, the most likely explanation for ongoing tumor growth in the RAD001 treated mice could be the induction of drug resistance in the tumor cells. The treatment may select a certain population of the primary tumor cells which successfully escape the treatment. Long term RAD001 selection may either enrich potential "cancer stem cells" in this population or induce further transformation of the tumor cells to overcome the tough anti-tumor environment. To answer this question, RAD001 resistant cell lines were established and the expression of several stem cell markers, some of which were also considered as "cancer stem cell" markers, was screened. Epithelial stem cell markers from the "CBC" model (Lgr5, Olfm4), and the "+4" model (Bmi1, Tert) were included. From the markers selected, a down-regulated expression level was only observed for Olfm4 in the RAD001 selected cell lines. The expression of all the other markers was not affected by the long term RAD001 treatment. Similar experiments were applied to the tumor tissue from the second RAD001 in vivo experiment to see if a long term selection in vivo could have some effect on the expression of certain markers. Except for Ascl2, which was suppressed after RAD001 treatment, all the other markers checked were not significantly affected. Thus, these studies showed that the RAD001 treatment had no strong effect on the expression of stem cell markers and therefore not induce dedifferentiation of the tumor cells. It is hard to see if the treatment enriched a "cancer stem cell" like population. However, these results were from single experiment and the RT-PCR itself may not be sensitive enough to detect these effects. In fact, our microarray analysis with RNA from tumor tissue of RAD001 treated mice and control mice revealed a series of genes significantly up or down regulated by RAD001 treatment in vivo (data not shown), including genes of neuroendocrine lineage (Chga, Cck, Nkx2.2, Tph1), epithelial stem cell markers (Olfm4, Sox9) and mesenchymal stem cell

markers (c-Kit, Etv1), although more detailed analysis on the array data is needed to obtain a deeper insight into this issue.

7.5 Possible candidates for the tumor originating cells in CEA424-SV40 TAg transgenic mouse

The origin of the cells from which GEP-NETs arise is poorly understood. The transformation may take place either on precursor/stem cells or terminally differentiated neuroendocrine cells. There is a theory which describes the transformative events in the development of GEP-NETs. It postulates that the earlier the damage is, the poorer the prognosis is. In other word, damages occuring at a committed neuroendocrine precursor stage are more likely to induce well-differentiated NETs (NET-G1) while damages occuring early in stem cell progress may probably lead to the development of high grade or poorly differentiated neuroendocrine carcinomas (NECs)[42].

Based on the mophology and the Ki-67 index, the gastric tumors developed in the CEA424-SV40 TAg transgenic mice were defined as neuroendocrine carcinomas. According to the theory described above, the tumor initiating cells may be the neuroendocrine precursor/stem cells. In addition, the tumor cells express multiple neuroendocrine markers and could produce several peptide, which further indicates that the transformation may have taken place in an early stage.

Gut neuroendocrine cells exist throughout the length of the gut and are the largest population of hormone-producing cells in the body[3]. At present, there have been at least 17 different neuroendocrine cells identified in the gastrointestinal tract including the pancreas which derive from local multipotent gastrointestinal stem cells, although in the past they are thought to migrate from the neural crest[42, 156]. Therefor, the newly described stem cell models in the gastrointestinal system may give some indications

where the tumor cells in the CEA424-SV40 TAg transgenic mouse model come from.

Nick Barker et al described a population of Lgr5^{+ve} cells, which are predominantly restricted to the base of adult pyloric glands, as multi-potent, self-renewing stem cells responsible for the long-term renewal of the gastric epithelium[84]. And it has been reported that Lgr5 positive cells can give rise to chromogranin A expressing cells[123]. To see if these Lgr5^{+ve} cells might be the tumor initiating cells targeted by TAg, CEA424-SV40 TAg×Lgr5-EGFP-IRES-CreERT2 double transgenic mouse line was generated. However, there was no GFP/TAg double-positive cells observed in the gastric mucosa or in gastric tumors even in young mice. Lineage tracing experiment could not provide supportive information for the hypothesis that the Lgr5^{+ve} cells may give rise to the tumor either (data from E. Vetter and W. Zimmermann, unpublished results). It seems unlikely that Lgr5^{+ve} cells in the stomach could be the primary target of TAg.

Both the stomach and the small intestine are of common endodermal origin and have a constantly renewing epithelium. Moreover, the gastric units are somehow similar to the crypts in the small intestine with “stem cell zone” at the bottom. Since the stem cell theories for stomach and small intestine share some common ground and the stem cell markers of small intestine are better described, the stem cell models for the small intestine were used for reference. There are currently two epithelial stem cell pools described in the small intestine, the crypt base columnar (CBC) cells pool and the “+4” cell pool. As the typical “CBC” marker Lgr5 is not likely to be expressed in the tumor originating cells of the CEA424-SV40 TAg gastric tumor, the “+4” cell pool was taken into consideration. Bmi1 is the most prominent marker for the “+4” cells and is the most highly expressed epithelial stem cell marker tested in the cell lines derived from the CEA424-SV40 TAg gastric tumors. The tumor cell lines derived from the tumor showed a high expression of Bmi1 in RT-PCR and cDNA expression array. This could be further substantiated by western-blotting and immunohistochemistry. Consequently, Bmi1 message could also be found in the growing tumors by RT-PCR and cDNA expression array. Immunohistologic staining

for Bmi1 revealed TAg and Bmi1 double positive cells in the tumor tissue while a 100% positive rate was observed in the isolated cell lines. In addition, when SV40-TAg expression was knocked down by siRNA assay, the expression level of Bmi1 in cell line 424GC also went down, thus showing the interrelationship.

These observations indicate that these Bmi1 positive cells may be one target of the transformation induced by TAg. In fact, when we take a close look at Bmi1 function and the signaling pathway in which it is involved, more supportive information came up. Bmi1 is a component of polycomb group (PcG) multiprotein PRC1-like complex[157]. There have been studies which characterized the role of Bmi1 in multiple biological processes. For example, Bmi1 is involved in the self-renewal, maintenance and differentiation of normal stem cells in intestine[95], lung[158], liver[159], prostate[160], pancreas[161], as well as in neural and hemopoietic system[162, 163]. It is found to be frequently up-regulated in various types of human cancers, including bladder cancer[164], breast cancer[165], gastric cancer[166-169], liver cancer[170], lymphoma[171], prostate cancer[160, 172] and skin cancer[173], and is responsible for chemoresistance[157, 174-178] . Except for contributing to epithelial-mesenchymal transition (EMT)[179-181] and senescence regulation[182], Bmi1 also takes part in the maintenance of "cancer stem cell" in some tumor types[159, 183-186]. Bmi1 performs these functions by regulating $p16^{Ink4a}$ and $p19^{Arf}$ genes. $p16^{Ink4a}$ regulates the formation of cyclin D/Cdk4/6 complex. This complex can phosphorylate RB1, thus promoting transcriptional activation of E2F1-regulated S-phase genes. On the other hand, $p19^{Arf}$ helps to maintain a certain level of p53 through inhibiting MDM2-mediated p53 degradation[182]. By controlling the activation of $p16^{Ink4a}$ and $p19^{Arf}$, Bmi1 plays an essential role in cell cycle progression and DNA synthesis. It is worth noting that through these two pathways Bmi1 has an impact on RB1 and p53 indirectly, which are two major targets of TAg. This may indicate a closer internal relationship between Bmi1 and the CEA424-SV40 TAg gastric tumor. Our data clearly show that Bmi1 declines after inhibition of the TAg expression. So in the model presented here, TAg drives the expression of Bmi1 which may lead to a further enhancement of the TAg effects on RB1 and p53. On the

other hand, we observed that the TAg expression was not strongly affected by the knockdown of Bmi1. Therefore, the Bmi1 expression is more likely a consequence of TAg expression rather than the other way around.

In addition to epithelial stem cells, the possibility of mesenchymal stem cells as tumor originating cell in the CEA424-SV40 TAg transgenic mouse model was also presented in this thesis. The observation of the TAg positive cells in the muscularis mucosae of antrum and duodenum in young mice suggested a possible mesenchymal origin of the tumor. The expression of Etv1 in both the cell lines and the tumor tissue added more supportive information for this hypothesis. The more interesting observation was that, Etv1 expression level in the tumor tissue increased over the time course of the tumor development, while no significant difference of Bmi1 expression was observed between different age groups. Since the CEA-promoter, which controled the expression of TAg in the transgenic mice, contains Etv1 binding sites ($_{A/C}GGAA_{G}$), it is tempting to speculate that this may drive the transcription of the TAg.

8 PERSPECTIVES

So far, the neuroendocrine phenotype developed in the CEA424-SV40 TAg transgenic mouse model has been confirmed. Testing of molecularly targeted therapies like the studies on mTOR inhibitors achieved promising anti-tumor effects. Analysis on the expression patterns of epithelial and mesenchymal stem cell markers offered some clues for the originating cells of the CEA424-SV40 TAg gastric tumor. However, there are still several questions to be answered:

- Except for inactivating pRB and p53, are there other important tumorigenesis mechanisms for the transformation induced by the TAg in the CEA424-SV40 TAg transgenic mouse? Is the TAg directly involved in the development of the neuroendocrine phenotype and how is this achieved?
- Will other molecularly targeted agents, like the ones targeting angiogenesis and growth factors, have efficient anti-tumor effects in CEA424-SV40 TAg transgenic mouse as well? What about combination strategies?
- Is there a specific cell type which is first transformed by the TAg?

It would be fascinating to continue research based on these questions with this mouse model system. Thus, this model could be of great value not only for further studies on the mechanisms of how SV40 TAg induces neuroendocrine tumors but also for testing new treatment protocols in a preclinical setting.

9 CONCLUSIONS

The main goal of this thesis was to characterize the CEA424-SV40 TAg transgenic mouse model in more detail including the identification of the tumor originating cells in this model system and to test novel molecularly targeted therapies for gastric neuroendocrine tumors. Specifically, the following results were obtained:

- The CEA424-SV40 TAg gastric tumors exhibit a typical neuroendocrine phenotype and the tumors were classified as neuroendocrine carcinomas.
- Testing of the molecularly targeted therapy both in vitro and in vivo offered promising candidates for further clinical evaluation to improve current management of neuroendocrine tumors.
- Bmi1 is highly expressed in the CEA424-SV40 TAg gastric tumor as well as the tumor derived cell lines. Instead of being involved in the tumor initiating issue, Bmi1 expression is more likely a result of the TAg expression.
- Etv1 expressing mesenchymal stem cells may be the tumor originating cells of the CEA424-SV40 TAg transgenic mouse model.

10 EQUIPMENT AND CONSUMABLES

10.1 General materials

Equipment and consumables	**Manufacturers**
Ice machine	ZIEGRA, Isernhagen, Germany
Autoclave	MMM, Munich, Germany
Freezer -80 ℃	Hettich, Germany
Freezer -20 ℃	Siemens, Germany
Freezer 4 ℃	Liebherr, Germany
microplate ELISA reader	Tecan, Crailsheim, Germany
Micropipettor	Eppendorf, Germany
Vortex mix	IKA, Wilmington, USA
Heating plate	IKA-Werke, Germany
Centrifuge	Eppendorf, Germany

10.2 Cell culture

Equipment and consumables	**Manufacturers**
Flow Cytometer	Beckman Coulter, Germany
Sterile tissue culture plastic flasks	NUNC, Roskilde, Denmark
Centrifuge tubes 15 mL	Greiner Bio-One, Germany
50ml Polypropylene Conical Tube	BD, NJ, USA

6-well culture plates	Corning, NY, USA
12-well culture plates	Corning, NY, USA
96-well culture plates	NUNC, Roskilde, Denmark
100 mm Cell Culture Dish	BD Falcon, USA
Cryotube (1.0 ml)	NUNC, Roskilde, Denmark
Corning® Costar® Stripette® serological pipettes (2.0 mL, 5.0ml, 10ml, 25ml)	Corning, NY, USA
Pipetboy Pipet Controller	IBS Integra, Swiss
Hemacytometer and cover-slip	Optik Labor, Germany
CO_2 incubator	BINDER, Germany
Microscope	Leitz, Germany
Biological safety cabinet	Heraeus, Germany
Water bath	B. Braun, USA
Stericup® Filter Unit	Millipore
Burner	Schütt Labortechnik, Germany
Vaccum gas pump	VWR, France
Parafilm	American National Can Company, USA

10.3 Animal experiments

Equipment and consumables	**Manufacturers**
INTRAMEDIC polyethylene tube (ID:	Clay Adams, USA

0.76mm; OD: 1.22mm)	
Syringe	BD Plastipak™, Madrid, Spain
Injection needle	BD Microlance™, Spain
Electronic scales	Waagendienst Winkler GmbH, Munich, Germany
Forceps	Dosch GmbH, Heidelberg, Germany
Scissors, sharp / blunt	Dosch GmbH, Heidelberg, Germany
Cryotube (1ml)	NUNC, Roskilde, Denmark

10.4 RNA isolation and reverse transcription PCR

Equipments/consumables	Manufacturers
Tissue grind machine	Heidolph, Germany
Electrophoresis power supply	MWG Biotech, Germany
Heating plate	IKA-Werke, Germany
Electrophoresis chamber	PEQLAB Biotechnologie, Germany
Vortexer	IKA-Werke, Germany
PCR soft tubes	Biozym Biotech Trading, Wien, Austria
Stratagene Robocycler Gradient 40	Stratagene, USA
DNA Thermal Cycler	Perkin Elmer, USA

10.5 Immunohistochemistry and immunofluorescence

Equipment and consumables	**Manufacturers**
Microscope	Carl Zeiss, Germany
Microtome	Leica, Germany
Microtome blade	Feather, Japan
Forceps/brush	Leica, Germany
Water bath	GFL, Germany
Oven	Heraeus, Germany
Coverplate chamber	Thermo Shandon, Pittsburgh, USA
Superfrost® Plus microscope slides	Thermo Scientific Gerhard Menzel, Braunschweig, Germany
Coverslip	Thermo Scientific Gerhard Menzel, Braunschweig, Germany
24 well plate	Corning, NY, USA
Cover glass	Thermo Scientific, Germany
PH meter	WTW, Germany

10.6 Western blot

Equipment and consumables	**Manufacturers**
Electrophoresis chamber	Pharmacia Biotech, USA
Power supply	SERVA, Germany

Electrophoresis transfer unit	LKB, Sweden
Shaker	GFL, Germany
Hamamatsu aequoria imaging system	Hamamatsu Photonics, Herrsching, Germany
Cooling centrifuge	Eppendorf, Germany
Protran™ nitrocellulose (NC) membranes	Whatman, Germany
Gel Transfer filter paper	Whatman, Germany
8-16% Precise Protein Gels	Thermo Scientific, USA
96-well-plates	NUNC, Roskilde, Denmark

11 ABBREVIATIONS

4EBP1, Eukaryotic translation initiation factor 4E-binding protein 1

5-FU, 5-fluorouracil

AEC, 3-Amino-9-Ethylcarbazole

Ascl2, Achaete-scute complex homolog 2

Bmi1, B lymphoma Mo-MLV insertion region 1 homolog

BSA, Bovine serum albumin

C57BL/6, C57 black 6 mouse

CBCs, crypt base columnar cells

CEA, Carcinoembryonic antigen

DAB, 3,3'-Diaminobenzidine

DCAMKL-1, doublecortin-like kinase 1

DMSO, Dimethyl sulfoxide

dNTP, PCR Nucleotide Mix

EDTA, Ethylenediaminetetraacetic acid

EGFR, Epidermal growth factor receptor

ELISA, Enzyme-linked immunosorbent assay

EMR, Endoscopic mucosal resection

EMT, Epithelial-mesenchymal transition

Etv1, ETS translocation variant 1

GAPDH, Glyceraldehyde 3-phosphate dehydrogenase

GEP-NETs, Gastroenteropancreatic neuroendocrine tumors

HEPES, 4-(2-hydroxyethyl)-1-piperazineethanesulfonic acid

Hopx, Homeodomain-only protein

HRP, Horseradish peroxidase

HSP, Heat shock protein

IFN, Interferon

IGF-1, Insulin-like growth factor 1

IL-6, Interleukin-6

ISCs, Intestinal stem cells

Lgr5, Leucine-rich repeat-containing G-protein coupled receptor 5

Lrig1, Leucine-rich repeats and immunoglobulin-like domains protein 1

MEN1, neoplasia type 1

$MgCl_2$, Magnesium chloride

Msi1, Musashi homolog 1

mTOR, mammalian target of rapamycin

NCCN, National Comprehensive Cancer Network

NECs, neuroendocrine carcinomas

NF-1, neurofibromatosis-1

Olfm4, Olfactomedin 4

PCR, polymerase chain reaction

PDGF, platelet-derived growth factor

PFS, Progression-free survival

PI3K, Phosphatidylinositol 3-kinase

Prom1, Prominin 1

PRRT, Peptide receptor radionuclide therapy

PTEN, Phosphatase and tensin homolog

PVDF, Polyvinylidene Fluoride

Tris, Tris hydroxymethyl aminomethane

SDS, Sodium dodecyl sulfate

SEER, The Surveillance, Epidemiology, and End Results database

sFRP5, Secreted frizzled-related protein 5

SSAs, Somastostatin analogues

SOX, SRY-related HMG-box

STAT3, Signal transducer and activator of transcription 3

STZ, streptozotocin

SV40 TAg, Simian Vacuolating Virus 40 large T antigen

TERT, Telomerase reverse transcriptase

TSC2, tuberous sclerosis 2

VEGF, vascular endothelial growth factor

VEGFR-1, Vascular endothelial growth factor receptor-1

VHL, von Hippel-Lindau disease

12 REFERENCES

1. DePinho RA, Jacks T: Introduction. The laboratory mouse in cancer research, Semin Cancer Biol 2001, 11:175-176
2. Hanahan D, Wagner EF, Palmiter RD: The origins of oncomice: a history of the first transgenic mice genetically engineered to develop cancer, Genes Dev 2007, 21:2258-2270
3. Modlin IM, Oberg K, Chung DC, Jensen RT, de Herder WW, Thakker RV, Caplin M, Delle Fave G, Kaltsas GA, Krenning EP, Moss SF, Nilsson O, Rindi G, Salazar R, Ruszniewski P, Sundin A: Gastroenteropancreatic neuroendocrine tumours, Lancet Oncol 2008, 9:61-72
4. Jones KB, Haldar M, Schiffman JD, Cannon-Albright L, Lessnick SL, Sharma S, Capecchi MR, Randall RL: Of mice and men: opportunities to use genetically engineered mouse models of synovial sarcoma for preclinical cancer therapeutic evaluation, Cancer Control 2011, 18:196-203
5. Olive KP, Tuveson DA: The use of targeted mouse models for preclinical testing of novel cancer therapeutics, Clin Cancer Res 2006, 12:5277-5287
6. Singh M, Johnson L: Using genetically engineered mouse models of cancer to aid drug development: an industry perspective, Clin Cancer Res 2006, 12:5312-5328
7. Johnson JI, Decker S, Zaharevitz D, Rubinstein LV, Venditti JM, Schepartz S, Kalyandrug S, Christian M, Arbuck S, Hollingshead M, Sausville EA: Relationships between drug activity in NCI preclinical in vitro and in vivo models and early clinical trials, Br J Cancer 2001, 84:1424-1431
8. Carver BS, Pandolfi PP: Mouse modeling in oncologic preclinical and translational research, Clin Cancer Res 2006, 12:5305-5311
9. Abate-Shen C: A new generation of mouse models of cancer for translational research, Clin Cancer Res 2006, 12:5274-5276
10. Rathi AV, Cantalupo PG, Sarkar SN, Pipas JM: Induction of interferon-stimulated genes by Simian virus 40 T antigens, Virology 2010, 406:202-211
11. Tseng-Rogenski SS, Arredouani MS, Escara-Wilke JF, Neeley YC, Imperiale MJ, Sanda MG: A safety-modified SV40 Tag developed for human cancer immunotherapy, Drug Des Devel Ther 2009, 2:17-24
12. David H, Mendoza S, Konishi T, Miller CW: Simian virus 40 is present in human lymphomas and normal blood, Cancer Lett 2001, 162:57-64
13. Shivapurkar N, Harada K, Reddy J, Scheuermann RH, Xu Y, McKenna RW, Milchgrub S, Kroft SH, Feng Z, Gazdar AF: Presence of simian virus 40 DNA sequences in human lymphomas, Lancet 2002, 359:851-852
14. Jasani B, Cristaudo A, Emri SA, Gazdar AF, Gibbs A, Krynska B, Miller C, Mutti L, Radu C, Tognon M, Procopio A: Association of SV40 with human tumours, Semin Cancer Biol 2001, 11:49-61
15. Klein G, Powers A, Croce C: Association of SV40 with human tumors, Oncogene 2002, 21:1141-1149

16. Garcea RL, Imperiale MJ: Simian virus 40 infection of humans, J Virol 2003, 77:5039-5045
17. Cuesta I, Nunez-Ramirez R, Scheres SH, Gai D, Chen XS, Fanning E, Carazo JM: Conformational rearrangements of SV40 large T antigen during early replication events, J Mol Biol 2010, 397:1276-1286
18. Ahuja D, Saenz-Robles MT, Pipas JM: SV40 large T antigen targets multiple cellular pathways to elicit cellular transformation, Oncogene 2005, 24:7729-7745
19. Shah KV: Does SV40 infection contribute to the development of human cancers?, Rev Med Virol 2000, 10:31-43
20. Ali SH, DeCaprio JA: Cellular transformation by SV40 large T antigen: interaction with host proteins, Semin Cancer Biol 2001, 11:15-23
21. Kierstead TD, Tevethia MJ: Association of p53 binding and immortalization of primary C57BL/6 mouse embryo fibroblasts by using simian virus 40 T-antigen mutants bearing internal overlapping deletion mutations, J Virol 1993, 67:1817-1829
22. Pipas JM, Levine AJ: Role of T antigen interactions with p53 in tumorigenesis, Semin Cancer Biol 2001, 11:23-30
23. Oren M, Maltzman W, Levine AJ: Post-translational regulation of the 54K cellular tumor antigen in normal and transformed cells, Mol Cell Biol 1981, 1:101-110
24. Henning W, Rohaly G, Kolzau T, Knippschild U, Maacke H, Deppert W: MDM2 is a target of simian virus 40 in cellular transformation and during lytic infection, J Virol 1997, 71:7609-7618
25. DeCaprio JA, Ludlow JW, Figge J, Shew JY, Huang CM, Lee WH, Marsilio E, Paucha E, Livingston DM: SV40 large tumor antigen forms a specific complex with the product of the retinoblastoma susceptibility gene, Cell 1988, 54:275-283
26. Sullivan CS, Gilbert SP, Pipas JM: ATP-dependent simian virus 40 T-antigen-Hsc70 complex formation, J Virol 2001, 75:1601-1610
27. Johnson JL, Pillai S, Pernazza D, Sebti SM, Lawrence NJ, Chellappan SP: Regulation of matrix metalloproteinase genes by E2F transcription factors: Rb-Raf-1 interaction as a novel target for metastatic disease, Cancer Res 2012, 72:516-526
28. Gordon GM, Du W: Conserved RB functions in development and tumor suppression, Protein Cell 2011, 2:864-878
29. Munro S, Carr SM, La Thangue NB: Diversity within the pRb pathway: is there a code of conduct?, Oncogene 2012,
30. Thompson J, Epting T, Schwarzkopf G, Singhofen A, Eades-Perner AM, van Der Putten H, Zimmermann W: A transgenic mouse line that develops early-onset invasive gastric carcinoma provides a model for carcinoembryonic antigen-targeted tumor therapy, Int J Cancer 2000, 86:863-869
31. Nockel J, van den Engel NK, Winter H, Hatz RA, Zimmermann W, Kammerer R: Characterization of gastric adenocarcinoma cell lines established from CEA424/SV40 T antigen-transgenic mice with or without a human CEA transgene, BMC Cancer 2006, 6:57
32. Regel I, Merkl L, Friedrich T, Burgermeister E, Zimmermann W, Einwachter H, Herrmann K, Langer R, Rocken C, Hofheinz R, Schmid R, Ebert MP: Pan-histone

deacetylase inhibitor panobinostat sensitizes gastric cancer cells to anthracyclines via induction of CITED2, Gastroenterology 2012, 143:99-109 e110
33. Yuan G, Regel I, Lian F, Friedrich T, Hitkova I, Hofheinz RD, Strobel P, Langer R, Keller G, Rocken C, Zimmermann W, Schmid RM, Ebert MP, Burgermeister E: WNT6 is a novel target gene of caveolin-1 promoting chemoresistance to epirubicin in human gastric cancer cells, Oncogene 2012,
34. van den Engel NK, Ruttinger D, Rusan M, Kammerer R, Zimmermann W, Hatz RA, Winter H: Combination immunotherapy and active-specific tumor cell vaccination augments anti-cancer immunity in a mouse model of gastric cancer, J Transl Med 2011, 9:140
35. Bourquin C, von der Borch P, Zoglmeier C, Anz D, Sandholzer N, Suhartha N, Wurzenberger C, Denzel A, Kammerer R, Zimmermann W, Endres S: Efficient eradication of subcutaneous but not of autochthonous gastric tumors by adoptive T cell transfer in an SV40 T antigen mouse model, J Immunol 2010, 185:2580-2588
36. Ballesta AM, Molina R, Filella X, Jo J, Gimenez N: Carcinoembryonic antigen in staging and follow-up of patients with solid tumors, Tumour Biol 1995, 16:32-41
37. Ihler F, Vetter EV, Pan J, Kammerer R, Debey-Pascher S, Schultze JL, Zimmermann W, Enders G: Expression of a neuroendocrine gene signature in gastric tumor cells from CEA 424-SV40 large T antigen-transgenic mice depends on SV40 large T antigen, PLoS One 2012, 7:e29846
38. Yao JC, Hassan M, Phan A, Dagohoy C, Leary C, Mares JE, Abdalla EK, Fleming JB, Vauthey JN, Rashid A, Evans DB: One hundred years after "carcinoid": epidemiology of and prognostic factors for neuroendocrine tumors in 35,825 cases in the United States, J Clin Oncol 2008, 26:3063-3072
39. Buchanan KD, Johnston CF, O'Hare MM, Ardill JE, Shaw C, Collins JS, Watson RG, Atkinson AB, Hadden DR, Kennedy TL, et al.: Neuroendocrine tumors. A European view, Am J Med 1986, 81:14-22
40. Hemminki K, Li X: Incidence trends and risk factors of carcinoid tumors: a nationwide epidemiologic study from Sweden, Cancer 2001, 92:2204-2210
41. Levi F, Te VC, Randimbison L, Rindi G, La Vecchia C: Epidemiology of carcinoid neoplasms in Vaud, Switzerland, 1974-97, Br J Cancer 2000, 83:952-955
42. Schimmack S, Svejda B, Lawrence B, Kidd M, Modlin IM: The diversity and commonalities of gastroenteropancreatic neuroendocrine tumors, Langenbecks Arch Surg 2011, 396:273-298
43. Delle Fave G, Kwekkeboom DJ, Van Cutsem E, Rindi G, Kos-Kudla B, Knigge U, Sasano H, Tomassetti P, Salazar R, Ruszniewski P: ENETS Consensus Guidelines for the management of patients with gastroduodenal neoplasms, Neuroendocrinology 2012, 95:74-87
44. Ramage JK, Davies AH, Ardill J, Bax N, Caplin M, Grossman A, Hawkins R, McNicol AM, Reed N, Sutton R, Thakker R, Aylwin S, Breen D, Britton K, Buchanan K, Corrie P, Gillams A, Lewington V, McCance D, Meeran K, Watkinson A: Guidelines for the management of gastroenteropancreatic neuroendocrine (including carcinoid) tumours, Gut 2005, 54 Suppl 4:iv1-16
45. Modlin IM, Lye KD, Kidd M: A 5-decade analysis of 13,715 carcinoid tumors,

Cancer 2003, 97:934-959
46. Modlin IM, Gustafsson BI, Moss SF, Pavel M, Tsolakis AV, Kidd M: Chromogranin A--biological function and clinical utility in neuro endocrine tumor disease, Ann Surg Oncol 2010, 17:2427-2443
47. Modlin IM, Moss SF, Chung DC, Jensen RT, Snyderwine E: Priorities for improving the management of gastroenteropancreatic neuroendocrine tumors, J Natl Cancer Inst 2008, 100:1282-1289
48. Hanahan D: Heritable formation of pancreatic beta-cell tumours in transgenic mice expressing recombinant insulin/simian virus 40 oncogenes, Nature 1985, 315:115-122
49. Rane SG, Dubus P, Mettus RV, Galbreath EJ, Boden G, Reddy EP, Barbacid M: Loss of Cdk4 expression causes insulin-deficient diabetes and Cdk4 activation results in beta-islet cell hyperplasia, Nat Genet 1999, 22:44-52
50. Garabedian EM, Humphrey PA, Gordon JI: A transgenic mouse model of metastatic prostate cancer originating from neuroendocrine cells, Proc Natl Acad Sci U S A 1998, 95:15382-15387
51. Chiaverotti T, Couto SS, Donjacour A, Mao JH, Nagase H, Cardiff RD, Cunha GR, Balmain A: Dissociation of epithelial and neuroendocrine carcinoma lineages in the transgenic adenocarcinoma of mouse prostate model of prostate cancer, Am J Pathol 2008, 172:236-246
52. Masumori N, Thomas TZ, Chaurand P, Case T, Paul M, Kasper S, Caprioli RM, Tsukamoto T, Shappell SB, Matusik RJ: A probasin-large T antigen transgenic mouse line develops prostate adenocarcinoma and neuroendocrine carcinoma with metastatic potential, Cancer Res 2001, 61:2239-2249
53. Czeh M, Loddenkemper C, Shalapour S, Schon C, Robine S, Goldscheid E, Stein H, Schuler T, Willimsky G, Blankenstein T: The immune response to sporadic colorectal cancer in a novel mouse model, Oncogene 2010, 29:6591-6602
54. Syder AJ, Karam SM, Mills JC, Ippolito JE, Ansari HR, Farook V, Gordon JI: A transgenic mouse model of metastatic carcinoma involving transdifferentiation of a gastric epithelial lineage progenitor to a neuroendocrine phenotype, Proc Natl Acad Sci U S A 2004, 101:4471-4476
55. Yang Q, Guan KL: Expanding mTOR signaling, Cell Res 2007, 17:666-681
56. Capdevila J, Salazar R, Halperin I, Abad A, Yao JC: Innovations therapy: mammalian target of rapamycin (mTOR) inhibitors for the treatment of neuroendocrine tumors, Cancer Metastasis Rev 2011, 30 Suppl 1:27-34
57. Wullschleger S, Loewith R, Hall MN: TOR signaling in growth and metabolism, Cell 2006, 124:471-484
58. Pavel M: Translation of Molecular Pathways into Clinical Trials of Neuroendocrine Tumors, Neuroendocrinology 2012,
59. Chiu CW, Nozawa H, Hanahan D: Survival benefit with proapoptotic molecular and pathologic responses from dual targeting of mammalian target of rapamycin and epidermal growth factor receptor in a preclinical model of pancreatic neuroendocrine carcinogenesis, J Clin Oncol 2010, 28:4425-4433
60. Jiao Y, Shi C, Edil BH, de Wilde RF, Klimstra DS, Maitra A, Schulick RD, Tang

LH, Wolfgang CL, Choti MA, Velculescu VE, Diaz LA, Jr., Vogelstein B, Kinzler KW, Hruban RH, Papadopoulos N: DAXX/ATRX, MEN1, and mTOR pathway genes are frequently altered in pancreatic neuroendocrine tumors, Science 2011, 331:1199-1203
61. Strimpakos AS, Syrigos KN, Saif MW: Pancreatic neuroendocrine tumors: role of novel agents. Highlights from the "2011 ASCO Gastrointestinal Cancers Symposium". San Francisco, CA, USA. January 20-22, 2011, JOP 2011, 12:117-119
62. Yao JC, Shah MH, Ito T, Bohas CL, Wolin EM, Van Cutsem E, Hobday TJ, Okusaka T, Capdevila J, de Vries EG, Tomassetti P, Pavel ME, Hoosen S, Haas T, Lincy J, Lebwohl D, Oberg K: Everolimus for advanced pancreatic neuroendocrine tumors, N Engl J Med 2011, 364:514-523
63. de Gramont A, Van Cutsem E: Investigating the potential of bevacizumab in other indications: metastatic renal cell, non-small cell lung, pancreatic and breast cancer, Oncology 2005, 69 Suppl 3:46-56
64. Duran I, Salazar R, Casanovas O, Arrazubi V, Vilar E, Siu LL, Yao J, Tabernero J: New drug development in digestive neuroendocrine tumors, Ann Oncol 2007, 18:1307-1313
65. Zhang J, Jia Z, Li Q, Wang L, Rashid A, Zhu Z, Evans DB, Vauthey JN, Xie K, Yao JC: Elevated expression of vascular endothelial growth factor correlates with increased angiogenesis and decreased progression-free survival among patients with low-grade neuroendocrine tumors, Cancer 2007, 109:1478-1486
66. Knosel T, Chen Y, Altendorf-Hofmann A, Danielczok C, Freesmeyer M, Settmacher U, Wurst C, Schulz S, Yang LL, Petersen I: High KIT and PDGFRA are associated with shorter patients survival in gastroenteropancreatic neuroendocrine tumors, but mutations are a rare event, J Cancer Res Clin Oncol 2012, 138:397-403
67. Grande E, Diez JJ, Pachon V, Carrato A: Advances in the therapy of gastroenteropancreatic-neuroendocrine tumours (GEP-NETs), Clin Transl Oncol 2010, 12:481-492
68. Yao JC, Phan A, Hoff PM, Chen HX, Charnsangavej C, Yeung SC, Hess K, Ng C, Abbruzzese JL, Ajani JA: Targeting vascular endothelial growth factor in advanced carcinoid tumor: a random assignment phase II study of depot octreotide with bevacizumab and pegylated interferon alpha-2b, J Clin Oncol 2008, 26:1316-1323
69. Raymond E, Dahan L, Raoul JL, Bang YJ, Borbath I, Lombard-Bohas C, Valle J, Metrakos P, Smith D, Vinik A, Chen JS, Horsch D, Hammel P, Wiedenmann B, Van Cutsem E, Patyna S, Lu DR, Blanckmeister C, Chao R, Ruszniewski P: Sunitinib malate for the treatment of pancreatic neuroendocrine tumors, N Engl J Med 2011, 364:501-513
70. Welin S, Fjallskog ML, Saras J, Eriksson B, Janson ET: Expression of tyrosine kinase receptors in malignant midgut carcinoid tumors, Neuroendocrinology 2006, 84:42-48
71. Wulbrand U, Wied M, Zofel P, Goke B, Arnold R, Fehmann H: Growth factor receptor expression in human gastroenteropancreatic neuroendocrine tumours, Eur J Clin Invest 1998, 28:1038-1049
72. Gilbert JA, Adhikari LJ, Lloyd RV, Rubin J, Haluska P, Carboni JM, Gottardis

MM, Ames MM: Molecular markers for novel therapies in neuroendocrine (carcinoid) tumors, Endocr Relat Cancer 2010, 17:623-636
73. Papouchado B, Erickson LA, Rohlinger AL, Hobday TJ, Erlichman C, Ames MM, Lloyd RV: Epidermal growth factor receptor and activated epidermal growth factor receptor expression in gastrointestinal carcinoids and pancreatic endocrine carcinomas, Mod Pathol 2005, 18:1329-1335
74. Bergmann F, Breinig M, Hopfner M, Rieker RJ, Fischer L, Kohler C, Esposito I, Kleeff J, Herpel E, Ehemann V, Friess H, Schirmacher P, Kern MA: Expression pattern and functional relevance of epidermal growth factor receptor and cyclooxygenase-2: novel chemotherapeutic targets in pancreatic endocrine tumors?, Am J Gastroenterol 2009, 104:171-181
75. Srirajaskanthan R, Shah T, Watkins J, Marelli L, Khan K, Caplin ME: Expression of the HER-1-4 family of receptor tyrosine kinases in neuroendocrine tumours, Oncol Rep 2010, 23:909-915
76. Bago-Horvath Z, Sieghart W, Grusch M, Lackner A, Hayden H, Pirker C, Komina O, Wesierska-Gadek J, Haitel A, Filipits M, Berger W, Schmid K: Synergistic Effects of Erlotinib and Everolimus on Bronchial Carcinoids and Large-Cell Neuroendocrine Carcinomas with Activated EGFR/AKT/mTOR Pathway, Neuroendocrinology 2012,
77. Kaltsas GA, Cunningham JL, Falkmer SE, Grimelius L, Tsolakis AV: Expression of connective tissue growth factor and IGF1 in normal and neoplastic gastrointestinal neuroendocrine cells and their clinico-pathological significance, Endocr Relat Cancer 2011, 18:61-71
78. von Wichert G, Jehle PM, Hoeflich A, Koschnick S, Dralle H, Wolf E, Wiedenmann B, Boehm BO, Adler G, Seufferlein T: Insulin-like growth factor-I is an autocrine regulator of chromogranin A secretion and growth in human neuroendocrine tumor cells, Cancer Res 2000, 60:4573-4581
79. Tolcher AW, Sarantopoulos J, Patnaik A, Papadopoulos K, Lin CC, Rodon J, Murphy B, Roth B, McCaffery I, Gorski KS, Kaiser B, Zhu M, Deng H, Friberg G, Puzanov I: Phase I, pharmacokinetic, and pharmacodynamic study of AMG 479, a fully human monoclonal antibody to insulin-like growth factor receptor 1, J Clin Oncol 2009, 27:5800-5807
80. Reidy-Lagunes DL, Vakiani E, Segal MF, Hollywood EM, Tang LH, Solit DB, Pietanza MC, Capanu M, Saltz LB: A phase 2 study of the insulin-like growth factor-1 receptor inhibitor MK-0646 in patients with metastatic, well-differentiated neuroendocrine tumors, Cancer 2012,
81. Barker N, Bartfeld S, Clevers H: Tissue-resident adult stem cell populations of rapidly self-renewing organs, Cell Stem Cell 2010, 7:656-670
82. Bjerknes M, Cheng H: Multipotential stem cells in adult mouse gastric epithelium, Am J Physiol Gastrointest Liver Physiol 2002, 283:G767-777
83. McDonald SA, Greaves LC, Gutierrez-Gonzalez L, Rodriguez-Justo M, Deheragoda M, Leedham SJ, Taylor RW, Lee CY, Preston SL, Lovell M, Hunt T, Elia G, Oukrif D, Harrison R, Novelli MR, Mitchell I, Stoker DL, Turnbull DM, Jankowski JA, Wright NA: Mechanisms of field cancerization in the human stomach:

the expansion and spread of mutated gastric stem cells, Gastroenterology 2008, 134:500-510
84. Barker N, Huch M, Kujala P, van de Wetering M, Snippert HJ, van Es JH, Sato T, Stange DE, Begthel H, van den Born M, Danenberg E, van den Brink S, Korving J, Abo A, Peters PJ, Wright N, Poulsom R, Clevers H: Lgr5(+ve) stem cells drive self-renewal in the stomach and build long-lived gastric units in vitro, Cell Stem Cell 2010, 6:25-36
85. Hattori T, Fujita S: Tritiated thymidine autoradiographic study on cellular migration in the gastric gland of the golden hamster, Cell Tissue Res 1976, 172:171-184
86. Karam SM, Leblond CP: Dynamics of epithelial cells in the corpus of the mouse stomach. I. Identification of proliferative cell types and pinpointing of the stem cell, Anat Rec 1993, 236:259-279
87. Karam SM, Leblond CP: Dynamics of epithelial cells in the corpus of the mouse stomach. V. Behavior of entero-endocrine and caveolated cells: general conclusions on cell kinetics in the oxyntic epithelium, Anat Rec 1993, 236:333-340
88. Karam SM, Leblond CP: Dynamics of epithelial cells in the corpus of the mouse stomach. III. Inward migration of neck cells followed by progressive transformation into zymogenic cells, Anat Rec 1993, 236:297-313
89. Karam SM, Leblond CP: Dynamics of epithelial cells in the corpus of the mouse stomach. II. Outward migration of pit cells, Anat Rec 1993, 236:280-296
90. Barker N, Clevers H: Leucine-rich repeat-containing G-protein-coupled receptors as markers of adult stem cells, Gastroenterology 2010, 138:1681-1696
91. Bjerknes M, Cheng H: Clonal analysis of mouse intestinal epithelial progenitors, Gastroenterology 1999, 116:7-14
92. Hermiston ML, Green RP, Gordon JI: Chimeric-transgenic mice represent a powerful tool for studying how the proliferation and differentiation programs of intestinal epithelial cell lineages are regulated, Proc Natl Acad Sci U S A 1993, 90:8866-8870
93. Cairnie AB, Lamerton LF, Steel GG: Cell proliferation studies in the intestinal epithelium of the rat. I. Determination of the kinetic parameters, Exp Cell Res 1965, 39:528-538
94. Potten CS: Extreme sensitivity of some intestinal crypt cells to X and gamma irradiation, Nature 1977, 269:518-521
95. Sangiorgi E, Capecchi MR: Bmi1 is expressed in vivo in intestinal stem cells, Nat Genet 2008, 40:915-920
96. Tian H, Biehs B, Warming S, Leong KG, Rangell L, Klein OD, de Sauvage FJ: A reserve stem cell population in small intestine renders Lgr5-positive cells dispensable, Nature 2011, 478:255-259
97. Montgomery RK, Carlone DL, Richmond CA, Farilla L, Kranendonk ME, Henderson DE, Baffour-Awuah NY, Ambruzs DM, Fogli LK, Algra S, Breault DT: Mouse telomerase reverse transcriptase (mTert) expression marks slowly cycling intestinal stem cells, Proc Natl Acad Sci U S A 2011, 108:179-184
98. Breault DT, Min IM, Carlone DL, Farilla LG, Ambruzs DM, Henderson DE,

Algra S, Montgomery RK, Wagers AJ, Hole N: Generation of mTert-GFP mice as a model to identify and study tissue progenitor cells, Proc Natl Acad Sci U S A 2008, 105:10420-10425
99. Takeda N, Jain R, LeBoeuf MR, Wang Q, Lu MM, Epstein JA: Interconversion between intestinal stem cell populations in distinct niches, Science 2011, 334:1420-1424
100. Powell AE, Wang Y, Li Y, Poulin EJ, Means AL, Washington MK, Higginbotham JN, Juchheim A, Prasad N, Levy SE, Guo Y, Shyr Y, Aronow BJ, Haigis KM, Franklin JL, Coffey RJ: The pan-ErbB negative regulator Lrig1 is an intestinal stem cell marker that functions as a tumor suppressor, Cell 2012, 149:146-158
101. Van der Flier LG, Sabates-Bellver J, Oving I, Haegebarth A, De Palo M, Anti M, Van Gijn ME, Suijkerbuijk S, Van de Wetering M, Marra G, Clevers H: The Intestinal Wnt/TCF Signature, Gastroenterology 2007, 132:628-632
102. Gregorieff A, Pinto D, Begthel H, Destree O, Kielman M, Clevers H: Expression pattern of Wnt signaling components in the adult intestine, Gastroenterology 2005, 129:626-638
103. Gregorieff A, Clevers H: Wnt signaling in the intestinal epithelium: from endoderm to cancer, Genes Dev 2005, 19:877-890
104. Giannakis M, Stappenbeck TS, Mills JC, Leip DG, Lovett M, Clifton SW, Ippolito JE, Glasscock JI, Arumugam M, Brent MR, Gordon JI: Molecular properties of adult mouse gastric and intestinal epithelial progenitors in their niches, J Biol Chem 2006, 281:11292-11300
105. May R, Riehl TE, Hunt C, Sureban SM, Anant S, Houchen CW: Identification of a novel putative gastrointestinal stem cell and adenoma stem cell marker, doublecortin and CaM kinase-like-1, following radiation injury and in adenomatous polyposis coli/multiple intestinal neoplasia mice, Stem Cells 2008, 26:630-637
106. Gerbe F, Brulin B, Makrini L, Legraverend C, Jay P: DCAMKL-1 expression identifies Tuft cells rather than stem cells in the adult mouse intestinal epithelium, Gastroenterology 2009, 137:2179-2180; author reply 2180-2171
107. Bezencon C, Furholz A, Raymond F, Mansourian R, Metairon S, Le Coutre J, Damak S: Murine intestinal cells expressing Trpm5 are mostly brush cells and express markers of neuronal and inflammatory cells, J Comp Neurol 2008, 509:514-525
108. Cheng H, Leblond CP: Origin, differentiation and renewal of the four main epithelial cell types in the mouse small intestine. V. Unitarian Theory of the origin of the four epithelial cell types, Am J Anat 1974, 141:537-561
109. Barker N, van Es JH, Kuipers J, Kujala P, van den Born M, Cozijnsen M, Haegebarth A, Korving J, Begthel H, Peters PJ, Clevers H: Identification of stem cells in small intestine and colon by marker gene Lgr5, Nature 2007, 449:1003-1007
110. dos Santos CM, Hilgert JB, Padilha DM, Hugo FN: Denture stomatitis and its risk indicators in south Brazilian older adults, Gerodontology 2010, 27:134-140
111. Snippert HJ, van der Flier LG, Sato T, van Es JH, van den Born M, Kroon-Veenboer C, Barker N, Klein AM, van Rheenen J, Simons BD, Clevers H:

Intestinal crypt homeostasis results from neutral competition between symmetrically dividing Lgr5 stem cells, Cell 2010, 143:134-144
112. Sato T, Vries RG, Snippert HJ, van de Wetering M, Barker N, Stange DE, van Es JH, Abo A, Kujala P, Peters PJ, Clevers H: Single Lgr5 stem cells build crypt-villus structures in vitro without a mesenchymal niche, Nature 2009, 459:262-265
113. Zhu L, Gibson P, Currle DS, Tong Y, Richardson RJ, Bayazitov IT, Poppleton H, Zakharenko S, Ellison DW, Gilbertson RJ: Prominin 1 marks intestinal stem cells that are susceptible to neoplastic transformation, Nature 2009, 457:603-607
114. Snippert HJ, van Es JH, van den Born M, Begthel H, Stange DE, Barker N, Clevers H: Prominin-1/CD133 marks stem cells and early progenitors in mouse small intestine, Gastroenterology 2009, 136:2187-2194 e2181
115. van der Flier LG, Haegebarth A, Stange DE, van de Wetering M, Clevers H: OLFM4 is a robust marker for stem cells in human intestine and marks a subset of colorectal cancer cells, Gastroenterology 2009, 137:15-17
116. Formeister EJ, Sionas AL, Lorance DK, Barkley CL, Lee GH, Magness ST: Distinct SOX9 levels differentially mark stem/progenitor populations and enteroendocrine cells of the small intestine epithelium, Am J Physiol Gastrointest Liver Physiol 2009, 296:G1108-1118
117. Mori-Akiyama Y, van den Born M, van Es JH, Hamilton SR, Adams HP, Zhang J, Clevers H, de Crombrugghe B: SOX9 is required for the differentiation of paneth cells in the intestinal epithelium, Gastroenterology 2007, 133:539-546
118. van der Flier LG, van Gijn ME, Hatzis P, Kujala P, Haegebarth A, Stange DE, Begthel H, van den Born M, Guryev V, Oving I, van Es JH, Barker N, Peters PJ, van de Wetering M, Clevers H: Transcription factor achaete scute-like 2 controls intestinal stem cell fate, Cell 2009, 136:903-912
119. Barker N, Ridgway RA, van Es JH, van de Wetering M, Begthel H, van den Born M, Danenberg E, Clarke AR, Sansom OJ, Clevers H: Crypt stem cells as the cells-of-origin of intestinal cancer, Nature 2009, 457:608-611
120. Munoz J, Stange DE, Schepers AG, van de Wetering M, Koo BK, Itzkovitz S, Volckmann R, Kung KS, Koster J, Radulescu S, Myant K, Versteeg R, Sansom OJ, van Es JH, Barker N, van Oudenaarden A, Mohammed S, Heck AJ, Clevers H: The Lgr5 intestinal stem cell signature: robust expression of proposed quiescent '+4' cell markers, EMBO J 2012, 31:3079-3091
121. Wong VW, Stange DE, Page ME, Buczacki S, Wabik A, Itami S, van de Wetering M, Poulsom R, Wright NA, Trotter MW, Watt FM, Winton DJ, Clevers H, Jensen KB: Lrig1 controls intestinal stem-cell homeostasis by negative regulation of ErbB signalling, Nat Cell Biol 2012, 14:401-408
122. Li L, Clevers H: Coexistence of quiescent and active adult stem cells in mammals, Science 2010, 327:542-545
123. Sato T, van Es JH, Snippert HJ, Stange DE, Vries RG, van den Born M, Barker N, Shroyer NF, van de Wetering M, Clevers H: Paneth cells constitute the niche for Lgr5 stem cells in intestinal crypts, Nature 2011, 469:415-418
124. Le Blanc K, Mougiakakos D: Multipotent mesenchymal stromal cells and the

innate immune system, Nat Rev Immunol 2012, 12:383-396
125. Uccelli A, Moretta L, Pistoia V: Mesenchymal stem cells in health and disease, Nat Rev Immunol 2008, 8:726-736
126. Petersen BE, Bowen WC, Patrene KD, Mars WM, Sullivan AK, Murase N, Boggs SS, Greenberger JS, Goff JP: Bone marrow as a potential source of hepatic oval cells, Science 1999, 284:1168-1170
127. Oh S, Shin S, Janknecht R: ETV1, 4 and 5: An oncogenic subfamily of ETS transcription factors, Biochim Biophys Acta 2012, 1826:1-12
128. Kubo H, Shimizu M, Taya Y, Kawamoto T, Michida M, Kaneko E, Igarashi A, Nishimura M, Segoshi K, Shimazu Y, Tsuji K, Aoba T, Kato Y: Identification of mesenchymal stem cell (MSC)-transcription factors by microarray and knockdown analyses, and signature molecule-marked MSC in bone marrow by immunohistochemistry, Genes Cells 2009, 14:407-424
129. Rubin BP: Bioinformatic mining of gene expression datasets identifies ETV1 as a critical regulator of oncogenesis in gastrointestinal stromal tumors, Cancer Cell 2010, 18:407-408
130. Chi P, Chen Y, Zhang L, Guo X, Wongvipat J, Shamu T, Fletcher JA, Dewell S, Maki RG, Zheng D, Antonescu CR, Allis CD, Sawyers CL: ETV1 is a lineage survival factor that cooperates with KIT in gastrointestinal stromal tumours, Nature 2010, 467:849-853
131. Taupenot L, Harper KL, O'Connor DT: The chromogranin-secretogranin family, N Engl J Med 2003, 348:1134-1149
132. Banks P, Helle K: The release of protein from the stimulated adrenal medulla, Biochem J 1965, 97:40C-41C
133. Helle KB: Some chemical and physical properties of the soluble protein fraction of bovine adrenal chromaffin granules, Mol Pharmacol 1966, 2:298-310
134. Taupenot L, Harper KL, O'Connor DT: Role of H+-ATPase-mediated acidification in sorting and release of the regulated secretory protein chromogranin A: evidence for a vesiculogenic function, J Biol Chem 2005, 280:3885-3897
135. Li HJ, Ray SK, Singh NK, Johnston B, Leiter AB: Basic helix-loop-helix transcription factors and enteroendocrine cell differentiation, Diabetes Obes Metab 2011, 13 Suppl 1:5-12
136. Neckers L, Workman P: Hsp90 molecular chaperone inhibitors: are we there yet?, Clin Cancer Res 2012, 18:64-76
137. Zitzmann K, Ruden J, Brand S, Goke B, Lichtl J, Spottl G, Auernhammer CJ: Compensatory activation of Akt in response to mTOR and Raf inhibitors - a rationale for dual-targeted therapy approaches in neuroendocrine tumor disease, Cancer Lett 2010, 295:100-109
138. Dancey J: mTOR signaling and drug development in cancer, Nat Rev Clin Oncol 2010, 7:209-219
139. Kittler R, Putz G, Pelletier L, Poser I, Heninger AK, Drechsel D, Fischer S, Konstantinova I, Habermann B, Grabner H, Yaspo ML, Himmelbauer H, Korn B, Neugebauer K, Pisabarro MT, Buchholz F: An endoribonuclease-prepared siRNA screen in human cells identifies genes essential for cell division, Nature 2004,

432:1036-1040
140. Young HM: Embryological origin of interstitial cells of Cajal, Microsc Res Tech 1999, 47:303-308
141. Parekh D, Ishizuka J, Townsend CM, Jr., Haber B, Beauchamp RD, Karp G, Kim SW, Rajaraman S, Greeley G, Jr., Thompson JC: Characterization of a human pancreatic carcinoid in vitro: morphology, amine and peptide storage, and secretion, Pancreas 1994, 9:83-90
142. Asa SL, Lee YC, Drucker DJ: Development of colonic and pancreatic endocrine tumours in mice expressing a glucagon-SV40 T antigen transgene, Virchows Arch 1996, 427:595-606
143. Franklin DS, Godfrey VL, O'Brien DA, Deng C, Xiong Y: Functional collaboration between different cyclin-dependent kinase inhibitors suppresses tumor growth with distinct tissue specificity, Mol Cell Biol 2000, 20:6147-6158
144. Djokovic D, Trindade A, Gigante J, Badenes M, Silva L, Liu R, Li X, Gong M, Krasnoperov V, Gill PS, Duarte A: Combination of Dll4/Notch and Ephrin-B2/EphB4 targeted therapy is highly effective in disrupting tumor angiogenesis, BMC Cancer 2010, 10:641
145. Perez-Stable C, Altman NH, Mehta PP, Deftos LJ, Roos BA: Prostate cancer progression, metastasis, and gene expression in transgenic mice, Cancer Res 1997, 57:900-906
146. Tang LH, Contractor T, Clausen R, Klimstra DS, Du YC, Allen PJ, Brennan MF, Levine AJ, Harris CR: Attenuation of the retinoblastoma pathway in pancreatic neuroendocrine tumors due to increased cdk4/cdk6, Clin Cancer Res 2012, 18:4612-4620
147. Yachida S, Vakiani E, White CM, Zhong Y, Saunders T, Morgan R, de Wilde RF, Maitra A, Hicks J, Demarzo AM, Shi C, Sharma R, Laheru D, Edil BH, Wolfgang CL, Schulick RD, Hruban RH, Tang LH, Klimstra DS, Iacobuzio-Donahue CA: Small cell and large cell neuroendocrine carcinomas of the pancreas are genetically similar and distinct from well-differentiated pancreatic neuroendocrine tumors, Am J Surg Pathol 2012, 36:173-184
148. Kitamura H, Yazawa T, Sato H, Okudela K, Shimoyamada H: Small cell lung cancer: significance of RB alterations and TTF-1 expression in its carcinogenesis, phenotype, and biology, Endocr Pathol 2009, 20:101-107
149. Swarts DR, Ramaekers FC, Speel EJ: Molecular and cellular biology of neuroendocrine lung tumors: Evidence for separate biological entities, Biochim Biophys Acta 2012, 1826:255-271
150. Zhou Z, Flesken-Nikitin A, Corney DC, Wang W, Goodrich DW, Roy-Burman P, Nikitin AY: Synergy of p53 and Rb deficiency in a conditional mouse model for metastatic prostate cancer, Cancer Res 2006, 66:7889-7898
151. Hill R, Song Y, Cardiff RD, Van Dyke T: Heterogeneous tumor evolution initiated by loss of pRb function in a preclinical prostate cancer model, Cancer Res 2005, 65:10243-10254
152. Shah T, Hochhauser D, Frow R, Quaglia A, Dhillon AP, Caplin ME: Epidermal growth factor receptor expression and activation in neuroendocrine

tumours, J Neuroendocrinol 2006, 18:355-360
153. Zitzmann K, De Toni EN, Brand S, Goke B, Meinecke J, Spottl G, Meyer HH, Auernhammer CJ: The novel mTOR inhibitor RAD001 (everolimus) induces antiproliferative effects in human pancreatic neuroendocrine tumor cells, Neuroendocrinology 2007, 85:54-60
154. Grozinsky-Glasberg S, Franchi G, Teng M, Leontiou CA, Ribeiro de Oliveira A, Jr., Dalino P, Salahuddin N, Korbonits M, Grossman AB: Octreotide and the mTOR inhibitor RAD001 (everolimus) block proliferation and interact with the Akt-mTOR-p70S6K pathway in a neuro-endocrine tumour cell Line, Neuroendocrinology 2008, 87:168-181
155. Yao JC, Phan AT, Chang DZ, Wolff RA, Hess K, Gupta S, Jacobs C, Mares JE, Landgraf AN, Rashid A, Meric-Bernstam F: Efficacy of RAD001 (everolimus) and octreotide LAR in advanced low- to intermediate-grade neuroendocrine tumors: results of a phase II study, J Clin Oncol 2008, 26:4311-4318
156. Pearse AG: The cytochemistry and ultrastructure of polypeptide hormone-producing cells of the APUD series and the embryologic, physiologic and pathologic implications of the concept, J Histochem Cytochem 1969, 17:303-313
157. Siddique HR, Saleem M: Role of BMI1, a stem cell factor, in cancer recurrence and chemoresistance: preclinical and clinical evidences, Stem Cells 2012, 30:372-378
158. Zacharek SJ, Fillmore CM, Lau AN, Gludish DW, Chou A, Ho JW, Zamponi R, Gazit R, Bock C, Jager N, Smith ZD, Kim TM, Saunders AH, Wong J, Lee JH, Roach RR, Rossi DJ, Meissner A, Gimelbrant AA, Park PJ, Kim CF: Lung stem cell self-renewal relies on BMI1-dependent control of expression at imprinted loci, Cell Stem Cell 2011, 9:272-281
159. Lessard J, Sauvageau G: Bmi-1 determines the proliferative capacity of normal and leukaemic stem cells, Nature 2003, 423:255-260
160. Lukacs RU, Memarzadeh S, Wu H, Witte ON: Bmi-1 is a crucial regulator of prostate stem cell self-renewal and malignant transformation, Cell Stem Cell 2010, 7:682-693
161. Fukuda A, Morris JPt, Hebrok M: Bmi1 is required for regeneration of the exocrine pancreas in mice, Gastroenterology 2012, 143:821-831 e822
162. Molofsky AV, He S, Bydon M, Morrison SJ, Pardal R: Bmi-1 promotes neural stem cell self-renewal and neural development but not mouse growth and survival by repressing the p16Ink4a and p19Arf senescence pathways, Genes Dev 2005, 19:1432-1437
163. Hosen N, Yamane T, Muijtjens M, Pham K, Clarke MF, Weissman IL: Bmi-1-green fluorescent protein-knock-in mice reveal the dynamic regulation of bmi-1 expression in normal and leukemic hematopoietic cells, Stem Cells 2007, 25:1635-1644
164. Zhang Y, Wang Z, Yu J, Shi J, Wang C, Fu W, Chen Z, Yang J: Cancer stem-like cells contribute to cisplatin resistance and progression in bladder cancer, Cancer Lett 2012, 322:70-77
165. Glinsky GV: Stem cell origin of death-from-cancer phenotypes of human

prostate and breast cancers, Stem Cell Rev 2007, 3:79-93
166. Zhang XW, Sheng YP, Li Q, Qin W, Lu YW, Cheng YF, Liu BY, Zhang FC, Li J, Dimri GP, Guo WJ: BMI1 and Mel-18 oppositely regulate carcinogenesis and progression of gastric cancer, Mol Cancer 2010, 9:40
167. Lu YW, Li J, Guo WJ: Expression and clinicopathological significance of Mel-18 and Bmi-1 mRNA in gastric carcinoma, J Exp Clin Cancer Res 2010, 29:143
168. Li W, Li Y, Tan Y, Ma K, Cui J: Bmi-1 is critical for the proliferation and invasiveness of gastric carcinoma cells, J Gastroenterol Hepatol 2010, 25:568-575
169. Yang DD, Cui BB, Sun LY, Zheng HQ, Huang Q, Tong JX, Zhang QF: The co-expression of USP22 and BMI-1 may promote cancer progression and predict therapy failure in gastric carcinoma, Cell Biochem Biophys 2011, 61:703-710
170. Marquardt JU, Factor VM, Thorgeirsson SS: Epigenetic regulation of cancer stem cells in liver cancer: current concepts and clinical implications, J Hepatol 2010, 53:568-577
171. Jares P, Campo E: Advances in the understanding of mantle cell lymphoma, Br J Haematol 2008, 142:149-165
172. Cooper CS, Foster CS: Concepts of epigenetics in prostate cancer development, Br J Cancer 2009, 100:240-245
173. Balasubramanian S, Lee K, Adhikary G, Gopalakrishnan R, Rorke EA, Eckert RL: The Bmi-1 polycomb group gene in skin cancer: regulation of function by (-)-epigallocatechin-3-gallate, Nutr Rev 2008, 66 Suppl 1:S65-68
174. Bhattacharyya J, Mihara K, Ohtsubo M, Yasunaga S, Takei Y, Yanagihara K, Sakai A, Hoshi M, Takihara Y, Kimura A: Overexpression of BMI-1 correlates with drug resistance in B-cell lymphoma cells through the stabilization of survivin expression, Cancer Sci 2012, 103:34-41
175. Zhu Y, Yu F, Jiao Y, Feng J, Tang W, Yao H, Gong C, Chen J, Su F, Zhang Y, Song E: Reduced miR-128 in breast tumor-initiating cells induces chemotherapeutic resistance via Bmi-1 and ABCC5, Clin Cancer Res 2011, 17:7105-7115
176. Sun L, Yao Y, Liu B, Lin Z, Lin L, Yang M, Zhang W, Chen W, Pan C, Liu Q, Song E, Li J: MiR-200b and miR-15b regulate chemotherapy-induced epithelial-mesenchymal transition in human tongue cancer cells by targeting BMI1, Oncogene 2012, 31:432-445
177. Choijamts B, Jimi S, Kondo T, Naganuma Y, Matsumoto T, Kuroki M, Iwasaki H, Emoto M: CD133+ cancer stem cell-like cells derived from uterine carcinosarcoma (malignant mixed Mullerian tumor), Stem Cells 2011, 29:1485-1495
178. Wang E, Bhattacharyya S, Szabolcs A, Rodriguez-Aguayo C, Jennings NB, Lopez-Berestein G, Mukherjee P, Sood AK, Bhattacharya R: Enhancing chemotherapy response with Bmi-1 silencing in ovarian cancer, PLoS One 2011, 6:e17918
179. Yang MH, Hsu DS, Wang HW, Wang HJ, Lan HY, Yang WH, Huang CH, Kao SY, Tzeng CH, Tai SK, Chang SY, Lee OK, Wu KJ: Bmi1 is essential in Twist1-induced epithelial-mesenchymal transition, Nat Cell Biol 2010, 12:982-992
180. Song LB, Li J, Liao WT, Feng Y, Yu CP, Hu LJ, Kong QL, Xu LH, Zhang X,

Liu WL, Li MZ, Zhang L, Kang TB, Fu LW, Huang WL, Xia YF, Tsao SW, Li M, Band V, Band H, Shi QH, Zeng YX, Zeng MS: The polycomb group protein Bmi-1 represses the tumor suppressor PTEN and induces epithelial-mesenchymal transition in human nasopharyngeal epithelial cells, J Clin Invest 2009, 119:3626-3636
181. Martin A, Cano A: Tumorigenesis: Twist1 links EMT to self-renewal, Nat Cell Biol 2010, 12:924-925
182. Park IK, Morrison SJ, Clarke MF: Bmi1, stem cells, and senescence regulation, J Clin Invest 2004, 113:175-179
183. Oishi N, Wang XW: Novel therapeutic strategies for targeting liver cancer stem cells, Int J Biol Sci 2011, 7:517-535
184. Zhang S, Balch C, Chan MW, Lai HC, Matei D, Schilder JM, Yan PS, Huang TH, Nephew KP: Identification and characterization of ovarian cancer-initiating cells from primary human tumors, Cancer Res 2008, 68:4311-4320
185. Cui H, Hu B, Li T, Ma J, Alam G, Gunning WT, Ding HF: Bmi-1 is essential for the tumorigenicity of neuroblastoma cells, Am J Pathol 2007, 170:1370-1378
186. Wiederschain D, Chen L, Johnson B, Bettano K, Jackson D, Taraszka J, Wang YK, Jones MD, Morrissey M, Deeds J, Mosher R, Fordjour P, Lengauer C, Benson JD: Contribution of polycomb homologues Bmi-1 and Mel-18 to medulloblastoma pathogenesis, Mol Cell Biol 2007, 27:4968-4979

13 ACKNOWLEDGEMENTS

First of all, I would like to express my sincere gratitude to my supervisor -- Prof. Dr. med. Georg Enders, for his continuous support and encouragement of my doctoral study and research, for his patience, motivation, enthusiasm, inspiration and immense knowledge. From the initial study to the final thesis, he provided nice guidance, sound advice, good teaching, big support and creative ideas. He made great efforts to explain things clearly and simply, which helped me develop an understanding of the subject and fall in love with scientific research. Without his help, this thesis could not be finished. I would also like to thank him for his kind support on my life in Munich.

I would like to thank Prof. Dr. rer. nat. Wolfgang Zimmermann, for his great support on my doctoral program. He is always available for a nice discussion and is never hesitate to offer help. His creativeness, open mind and precise attitude helped me to get fresh ideas and be more critical to my work. I would also like to thank him for including me as a group member in their weekly lab meetings and yearly out going. I also appreciated the support from him and Dr. Christoph J. Auernhammer on my pre-examination.

I am grateful to our group members—Bärbel Lorenz and Claudia Fahney, for their great technical assistance. Thanks for their patience and enthusiasm whenever I had questions or got into difficulties. It was really a wonderful experience to be with you for the past three years.

I would like to thank all the other lab members, for all the help and support which I can not list all down but will never forget.

I would also like to thank the colleagues and students from Prof. Dr. rer. nat. Wolfgang Zimmermann's group for their help and kindness.

I would like to thank Chinese Scholarship Council to provide the economic support. I

would like to thank Prof. Dr. Ulrich Pohl for his support for the CSC-LMU program. I would like to thank Prof. Dr. Alexender Baethmann, who helped our CSC students with great efforts before and after we came here. I would like to thank Dr. Matthias Hadesbeck, Ms. Munique Esnof and all the other members from the International Office, LMU to give the orientation course and living assistance. I would like to thank Mr. Jiqiang Dai from Chinese Consulate Munich for the help on my overseas issues.

Last but not least, I wish to thank my parents – Jianxin Pan and Hao Zhou. They bore me, raised me, and loved me. In particular, I would like to express heartfelt thanks to my mother, who provided understanding and support on my way pursuing my dream. I would also like to thank my husband – Qi Bao. To them I dedicate this thesis.